#2

412

A DIGITAL SPECTRAL ANALYSIS TECHNIQUE AND ITS APPLICATION TO RADIO ASTRONOMY

SANDER WEINREB

TECHNICAL REPORT 412

AUGUST 30, 1963

MASSACHUSETTS INSTITUTE OF TECHNOLOGY
RESEARCH LABORATORY OF ELECTRONICS
CAMBRIDGE, MASSACHUSETTS

The Research Laboratory of Electronics is an interdepartmental laboratory in which faculty members and graduate students from numerous academic departments conduct research.

The research reported in this document was made possible in part by support extended the Massachusetts Institute of Technology, Research Laboratory of Electronics, jointly by the U.S. Army (Signal Corps), the U.S. Navy (Office of Naval Research), and the U.S. Air Force (Office of Scientific Research) under Signal Corps Contract DA36-039-sc-78108, Department of the Army Task 3-99-25-001-08; and in part by Signal Corps Grant DA-SIG-36-039-61-G14; additional support was received from the National Science Foundation (Grant G-13904).

MASSACHUSETTS INSTITUTE OF TECHNOLOGY

RESEARCH LABORATORY OF ELECTRONICS

Technical Report 412 August 30, 1963

A DIGITAL SPECTRAL ANALYSIS TECHNIQUE AND ITS APPLICATION TO RADIO ASTRONOMY

Sander Weinreb

Submitted to the Department of Electrical Engineering, M.I.T., February 1963, in partial fulfillment of the requirements for the degree of Doctor of Philosophy.

(Manuscript received May 23, 1963)

Abstract

An efficient, digital technique for the measurement of the autocorrelation function and power spectrum of Gaussian random signals is described. As is well known, the power spectrum of a signal can be obtained by a Fourier transformation of its autocorrelation function. This report presents an indirect method of computing the autocorrelation function of a signal having Gaussian statistics which greatly reduces the amount of digital processing that is required.

The signal, x(t), is first "infinitely clipped"; that is, a signal, y(t), where y(t) = 1 when x(t) > 0, and y(t) = −1 when x(t) < 0, is produced. The normalized autocorrelation function, $\rho_y(\tau)$, of the clipped signal is then calculated digitally. Since y(t) can be coded into one-bit samples, the autocorrelation processing (delay, storage, multiplication, and summation) can be easily performed in real time by a special-purpose digital machine — a one-bit correlator. The resulting $\rho_y(\tau)$ can then be corrected to give the normalized autocorrelation function, $\rho_x(\tau)$, of the original signal. The relation is due to Van Vleck and is $\rho_x(\tau) = \sin[\pi\rho_y(\tau)/2]$.

A review of the measurement of power spectra through the autocorrelation function method is given. The one-bit technique of computing the autocorrelation function is presented; in particular, the mean and variance of the resulting spectral estimate have been investigated.

These results are then applied to the problem of the measurement of spectral lines in radio astronomy. A complete radio-astronomy system is described. The advantages of this system are: 1) It is a multichannel system; that is, many points are determined on the spectrum during one time interval; and 2) since digital techniques are used, the system is very accurate and highly versatile. This system was built for the purpose of attempting to detect the galactic deuterium line. Results of tests of this system, the attempt to detect the deuterium line, and an attempt to measure Zeeman splitting of the 21-cm hydrogen line are described.

TABLE OF CONTENTS

CONTENTS

CONTENTS

GLOSSARY

Symbol	Definition
	Time Functions
$x(t)$	A stationary, ergodic, random time function having Gaussian statistics.
$y(t)$	The function formed by infinite clipping of $x(t)$. That is, $y(t) = 1$ when $x(t) > 0$, and $y(t) = -1$ when $x(t) < 0$.
	Frequency and Time
	Because of their standard usage in both communication theory and radio astronomy, the symbols T and τ symbolize different quantities in different sections of this report. In Sections I-III, T is a time interval and τ is the autocorrelation function delay variable. In Sections IV-VIII, T is temperature, and τ is either optical depth or observation time. Some other frequency and time variables are the following:
$\Delta t, k, K, f_t$	The time function sampling interval is Δt. A sample of the time function $x(t)$ is $x(k\Delta t)$, where k is an integer. The total number of samples is K. The sampling frequency is $f_t = 1/\Delta t$. In most cases Δt and f_t will be chosen equal to $\Delta\tau$ and f_s, respectively.
$\Delta\tau, n, N, f_s$	The autocorrelation function sampling interval is $\Delta\tau$. The samples of the autocorrelation function are $R(n\Delta\tau)$, where n is an integer going from 0 to N-1. The reciprocal of $\Delta\tau$ is f_s.
Δf	The frequency resolution of a spectral measurement (see section 1.3). It is approximately equal to $1/N\Delta\tau$.
B_1, B_{20}	The 1-db and 20-db bandwidths of a radiometer. The spectrum is analyzed with resolution Δf in the band B_1. The sampling frequencies f_t and f_s are often chosen equal to $2B_{20}$.
f_o	A known combination of local oscillator frequencies.
	Autocorrelation Functions
$R(\tau)$	The true autocorrelation function of $x(t)$.
$R''(\tau)$	A statistical estimate of $R(\tau)$ based upon unquantized or many-bit samples of $x(t)$.

Symbol	Definition
$\rho(\tau)$ or $\rho_x(\tau)$	The true normalized autocorrelation function; $\rho(\tau) = R(\tau)/R(0)$.
$\rho''(\tau)$	A statistical estimate of $\rho(\tau)$ based upon unquantized or many-bit samples of x(t).
$\rho'(\tau)$ or $\rho'_x(\tau)$	A statistical estimate of $\rho(\tau)$ based upon one-bit samples of y(t).
$\rho_y(\tau)$	The true normalized autocorrelation function of y(t).
$\rho'_y(\tau)$	A statistical estimate of $\rho_y(\tau)$ based upon one-bit samples of y(t).

Power Spectra

The power spectrum is defined in section 1.2.

P(f)	The true power spectrum of x(t).
P''(f)	A statistical estimate of P(f) based upon unquantized or many-bit samples of x(t).
$P^*(f)$	The expected value of P''(f).
p(f)	The true normalized power spectrum; p(f) = P(f)/R(0).
p''(f)	A statistical estimate of p(f) based upon many-bit or unquantized samples of x(t).
p'(f)	A statistical estimate of p(f) based upon one-bit samples of y(t).
$p^*(f)$	The expected value of p'(f) and p''(f).
$p'_c(f)$	The normalized spectral estimate produced by a one-bit autocorrelation radiometer when its input is connected to a comparison noise source.
$p'_o(f)$	A normalized estimate of the receiver power transfer function, G(f). It is the spectral estimate produced by a one-bit autocorrelation radiometer when the input spectrum and receiver noise spectrum are white.
$\delta p'(f)$	The estimate of the difference spectrum that is determined by a switched radiometer; $\delta p'(f) = p'(f) - p'_c(f)$.

Symbol	Definition
	Temperature
$T_a(f)$	The power spectrum available at the antenna terminals expressed in degrees Kelvin.
$T_r(f)$	The receiver noise-temperature spectrum.
$T(f)$	The total temperature spectrum referred to the receiver input. $T(f) = T_a(f) + T_r(f)$.
$T_c(f)$	The spectrum of the comparison noise source.
T_{av}	The frequency-averaged value of $T(f)$. The average is weighted with respect to the receiver power-transfer function, $G(f)$.
$T_{a\ av}$	The frequency-averaged value of $T_a(f)$.
$T_{c\ av}$	The frequency-averaged value of $T_c(f) + T_r(f)$.
$T_{r\ av}$	The frequency-averaged value of $T_r(f)$.
δT_{av}	The unbalance temperature; $\delta T_{av} = T_{av} - T_{c\ av}$.
	RMS Deviations

A σ with two subscripts will be used to denote an rms deviation of a statistical estimate. The first subscript will be a P, R, p or ρ, and indicates the variable to which the rms deviation pertains. The second subscript will be a 1 or an m, and indicates whether the statistical estimate is based upon one-bit or many-bit samples. Thus, for example, σ_{p1} is the rms deviation of $p'(f)$, the one-bit estimate of $p(f)$. Statistical estimates of rms deviations will have a single subscript and a prime or double prime to indicate whether one-bit or many-bit samples are referred to. For example, $\sigma'_p(f)$ is a statistical estimate of $\sigma_{p1}(f)$.

	Other Functions
$w(\tau)$	The function that is used to weight the autocorrelation function (see section 2.2).
$W(f)$	The spectral scanning or smoothing function. It is the Fourier transform of $w(\tau)$ (see Fig. 9).
$G(f+f_o)$	The receiver power-transfer function. The spectrum at the clipper input, $P(f)$, is equal to $G(f+f_o)$ times the input temperature spectrum, $T(f+f_o)$.

Symbol	Definition
	Special Symbols
$\overline{x(t)}$	A line over a variable indicates that the statistical average is taken (see Eq. 1).
$P^{*}(f)$	An asterisk on a spectrum indicates that it has been smoothed and is repeated about integer multiples of the sampling frequency. This operation is discussed in section 2.2.
$T^{\dagger}(f)$	The one-bit autocorrelation radiometer produces a statistical estimate of an input temperature spectrum such as T(f). The statistical average or expected value of this estimate is equal to $T^{\dagger}(f)$. The relationship between T(f) and $T^{\dagger}(f)$ is discussed in section 4.2a. Under proper conditions such as a sufficiently fast sampling rate, $T^{\dagger}(f)$ is simply a smoothed version of T(f).

I. INTRODUCTION

This report has three main divisions which will be outlined briefly.

1. In Sections I-III, a technique for the measurement of the power spectrum and autocorrelation function of a Gaussian random process is presented. This technique, which will be referred to as "the one-bit autocorrelation method," has the property that it is easily performed digitally; hence the accuracy and flexibility associated with digital instrumentation is achieved. The technique is a multichannel one; that is, many points on the spectrum and autocorrelation function can be determined at one time. A limitation is that the analyzed bandwidth must be less than 10 mc for operation with present-day digital logic elements.

2. The above-mentioned technique is applied, in Sections IV and V, to the problem of the measurement of spectral lines in radio astronomy. In Section IV the composition and theoretical performance of a practical radio astronomy system utilizing the one-bit digital autocorrelation technique is presented. The design of components of this system is discussed in Section V.

3. The system was constructed and extensive experimental results are given in Sections VI-VIII. These results are from laboratory tests of the system, an attempt to detect the galactic deuterium line, and an attempt to measure Zeeman splitting of the 21-cm hydrogen line.

The reader who is interested in the radio astronomy aspects of this report may wish to skip Sections II and III; the results are summarized in radio astronomy terms in Section IV.

We shall now give some background material, a comparison of filter and autocorrelation methods of spectral measurement, a classification of spectral measurement problems, and finally, a brief description of the one-bit autocorrelation method.

1.1 STATISTICAL PRELIMINARIES

A brief presentation of some of the statistical techniques and terminology used in this report will now be given. Some assumptions will be stated regarding the statistical nature of the signals of interest. For an introduction to statistical communication theory techniques, the reader is referred to Davenport and Root,[1] or Bendat.[2]

The type of signal that is of interest here is the random time function; that is, a signal whose sources are so numerous, complicated, and unknown that exact prediction or description of the time function is impossible. Our interest is in the study of averages of functions of the signal, in particular, the power spectrum, which is defined in section 1.2.

A random variable, x, is the outcome of an experiment that (at least theoretically) can be repeated many times and has a result that cannot be exactly predicted. The flipping of a coin or the measurement of a noise signal at a given time are two such experiments. The outcome of a particular experiment is called a sample of the random

variable; it is implied that there is a large number of samples (although many samples may have the same value).

The random variable is described by a probability density function, p(x). The statistical average (this will sometimes be called the "mean") of a random variable is denoted by a bar over the quantity that is being averaged such as $\overline{x}$. In terms of the probability density function, the statistical average of x is given by

$$\overline{x} = \int_{-\infty}^{\infty} x\, p(x)\, dx. \tag{1}$$

In most signal-analysis cases the random variable is a function of a parameter, such as frequency or time. Thus, there is an infinite number of random variables, one for each value of the parameter. For each random variable there is a large number of samples. This two-dimensional array of sample functions is called a random process.

The concept of a random process with time as the parameter is shown in Fig. 1. For each value of time a random variable, x_{t_o}, is defined. Each random variable has an infinite number of samples, $x_{t_o}^{(1)}, x_{t_o}^{(2)}, \ldots, x_{t_o}^{(\infty)}$. The random process can also be described as having an infinite number of sample functions, $x^{(1)}(t)$, $x^{(2)}(t)$, $\ldots$, $x^{(\infty)}(t)$. (The superscripts will be dropped when they are not needed for clarity.)

Statistical averages, such as $\overline{x_{t_o}}$, are taken vertically through the random-process array, and may or may not be a function of time. Time averages such as

$$\frac{1}{T}\int_0^T x(t)\, dt$$

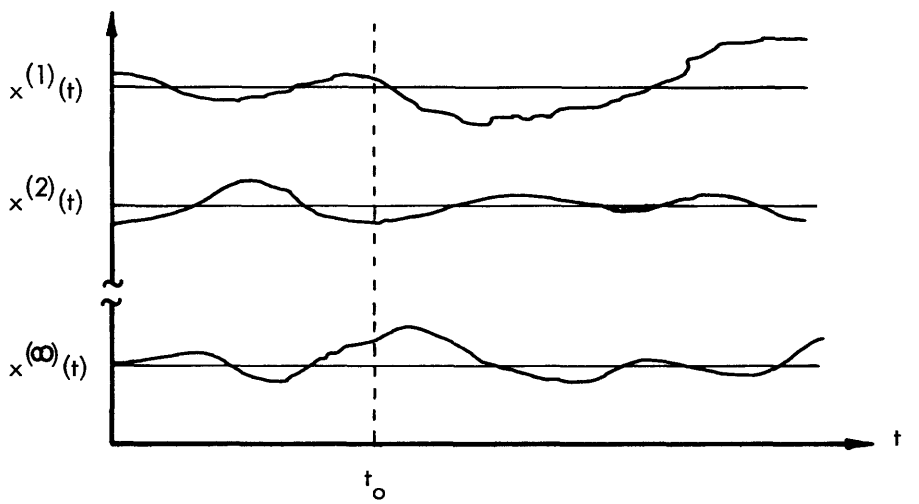

Fig. 1. A random process.

are taken across the array, and may or may not depend on the sample function chosen.

It will be assumed that signals whose power spectra we wish to measure are stationary and ergodic. By this it is meant that statistical averages such as $\overline{x_{t_o}}$, $\overline{x^2_{t_o}}$, and $\overline{x_{t_o} x_{t_o+\tau}}$ are independent of the time, t_o, and are equal to the infinite time averages, which, in turn, are independent of the particular sample function. That is,

$$\overline{x_{t_o}} = \lim_{T\to\infty} \frac{1}{2T} \int_{-T}^{T} x(t)\, dt \tag{2}$$

$$\overline{x^2_{t_o}} = \lim_{T\to\infty} \frac{1}{2T} \int_{-T}^{T} x^2(t)\, dt \tag{3}$$

$$\overline{x_{t_o} x_{t_o+\tau}} = \lim_{T\to\infty} \frac{1}{2T} \int_{-T}^{T} x(t)\, x(t+\tau)\, dt. \tag{4}$$

These assumptions imply that the power spectrum does not vary with time (at least over the period of time during which measurements are made). This is the usual situation in radio astronomy except in the case of solar noise.

Under the stationary and ergodic assumptions, the sample functions of the random process have a convenient interpretation, each sample function is a "record" or length of data obtained during different time intervals. The statistical average then is interpreted as the average result of an operation repeated on many records.

The quantity, $\overline{x_{t_o} x_{t_o+\tau}}$, is called the autocorrelation function of the signal. From Eq. 4 we see that under the stationary and ergodic assumption the autocorrelation function can also be expressed as an infinite time average. Because of the stationary assumption, $\overline{x_{t_o} x_{t_o+\tau}}$ is not a function of t_o, and the notation $R_x(\tau)$ or $R(\tau)$ will be used to signify the autocorrelation function.

In greater detail, the autocorrelation function is the (statistical or infinite time) average of the signal multiplied by a delayed replica of itself. $R_x(0)$ is simply the mean square, $\overline{x^2}$, of the signal, while $R_x(\infty)$ is equal to the square of the mean, $\overline{x}^2$. It is easily shown that $R_x(0) \geq R_x(\tau) = R_x(-\tau)$. The normalized autocorrelation function, $\rho_x(\tau)$, is equal to $R_x(\tau)/R_x(0)$ and is always less than or equal to unity.

The variance, σ_x^2, of a random variable is a measure of its dispersion from its mean. It is defined as

$$\sigma_x^2 \equiv \overline{(x-\overline{x})^2} \tag{5}$$

$$= \overline{x^2} - \overline{x}^2. \tag{6}$$

The positive square root of the variance is the rms deviation, σ_x. The statistical

uncertainty, Δ_x, of a random variable is the rms deviation divided by the mean,

$$\Delta_x = \frac{\sigma_x}{\overline{x}}. \tag{7}$$

As is often the case in the analysis of random signals, it will be assumed that the signal has Gaussian statistics in the sense that the joint probability density function, $p(x_t, x_{t+\tau})$, is the bivariate Gaussian distribution,

$$p(x_t, x_{t+\tau}) = \frac{1}{2\pi R_x(0) \left[1-\rho_x^2(\tau)\right]^{1/2}} \exp\left\{\frac{x_t^2 - 2\rho_x(\tau)\, x_t x_{t+\tau} + x_{t+\tau}^2}{-2R_x(0)\left[1-\rho_x^2(\tau)\right]}\right\}. \tag{8}$$

This assumption is often justified by the central limit theorem (see Bendat[2]) which states that a random variable will have a Gaussian distribution if it is formed as the sum of a large number of random variables of arbitrary probability distribution. This is usually true in the mechanism that gives rise to the signals observed in radio astronomy.

1.2 DEFINITION OF THE POWER SPECTRUM

The power spectrum is defined in many ways that are dependent on: (a) the mathematical rigor necessary in the context of the literature and application in which it is discussed; (b) whether one wishes to have a single-sided or double-sided power spectrum (positive and negative frequencies, with $P(-f) = P(f)$); (c) whether one wishes $P(f)\,\Delta f$ or $2P(f)\,\Delta f$ to be the power in the narrow bandwidth, Δf.

In this report, the double-sided power spectrum will be used because it simplifies some of the mathematical equations that are involved. The negative-frequency side of the power spectrum is the mirror image of the positive-frequency side; in most cases it need not be considered. In accordance with common use by radio astronomers and physicists, $P(f)\,\Delta f$ (or $P(-f)\,\Delta f$) will be taken to be the time-average power in the bandwidth, Δf, in the limit $\Delta f \to 0$ and the averaging time, $T \to \infty$. Thus, the total average power, P_T, is given by

$$P_T = \int_0^\infty P(f)\, df \tag{9}$$

or

$$P_T = \frac{1}{2}\int_{-\infty}^{\infty} P(f)\, df. \tag{10}$$

(If an impulse occurs at $f = 0$, half of its area should be considered to be at $f > 0$ for evaluation of Eq. 9.)

The statements above are not a sufficiently precise definition of the power spectrum because: (a) the relationship of $P(f)$ to the time function, $x(t)$, is not clear; (b) the two

limiting processes ($\Delta f \to 0$, $T \to \infty$) cause difficulty, for example, What happens in the limit to the product, $T\Delta f$?

A more precise definition of the power spectrum is obtained by defining P(f) as twice the Fourier transform of the autocorrelation function, $R(\tau)$, defined in the previous section. Thus we have

$$P(f) = 2 \int_{-\infty}^{\infty} R(\tau)\, e^{-j 2\pi f \tau}\, d\tau \tag{11}$$

$$R(\tau) = \lim_{T \to \infty} \frac{1}{2T} \int_{-T}^{T} x(t)\, x(t+\tau)\, d\tau. \tag{12}$$

The inverse Fourier transform relation gives

$$R(\tau) = \int_{0}^{\infty} P(f) \cos 2\pi f \tau \, df \tag{13}$$

$$R(\tau) = \frac{1}{2} \int_{-\infty}^{\infty} P(f)\, e^{-j 2\pi f \tau}\, df. \tag{14}$$

This definition of the power spectrum gives no intuitive feeling about the relation of P(f) to power. We must prove, then, that this definition has the properties stated above. Equations 9 and 10 are easily proved by setting $\tau = 0$ in Eqs. 12, 13, and 14. We find

$$R(0) = \lim_{T \to \infty} \frac{1}{2T} \int_{-T}^{T} x^2(t)\, dt \tag{15}$$

$$R(0) = \int_{0}^{\infty} P(f)\, df. \tag{16}$$

The right-hand side of Eq. 15 is identified as P_T, the total average power. Power is used in a loose sense of the word; P_T is the total average power dissipated in a 1-ohm resistor if x(t) is the voltage across its terminals; otherwise a constant multiplier is needed.

The proof that $P(f)\,\Delta f$ is the time-average power in the band Δf, $\Delta f \to 0$ and $T \to \infty$ is not as direct. Suppose that x(t) is applied to a filter having a power transfer function, G(f). It can be shown by using only Eqs. 11 and 12 that the output-power spectrum, $P_o(f)$, is given by (see Davenport and Root[1])

$$P_o(f) = G(f)\, P(f). \tag{17}$$

If G(f) is taken to be equal to unity for narrow bandwidths Δf, centered at +f and −f, and zero everywhere else, we find

$$\int_0^\infty P_o(f)\, df = P(f)\, \Delta f, \tag{18}$$

$\Delta f \to 0$. The left-hand side of Eq. 18 is simply the average power out of the filter (with the use of Eqs. 15 and 16), and hence $P(f)\,\Delta f$ must be the power in the bandwidth Δf.

1.3 GENERAL FORM OF ESTIMATES OF THE POWER SPECTRUM

The power spectrum of a random signal cannot be exactly measured by any means (even if the measurement apparatus has a perfect accuracy); the signal would have to be available for infinite time. Thus, when the term "measurement of the power spectrum" is used, what is really meant is that a statistical estimate, $P'(f)$, is measured.

The measured quantity, $P'(f)$, is a sample function of a random process; its value depends on the particular time segment of the random signal that is used for the measurement. It is an estimate of $P(f)$ in the sense that its statistical average, $\overline{P'(f)}$, is equal to a function, $P^*(f)$, which approximates $P(f)$. The statistical uncertainty of $P'(f)$ and the manner in which $P^*(f)$ approximates $P(f)$ appear to be invariant to the particular spectral-measurement technique, and will now be briefly discussed.

The function, $P^*(f)$, approximates $P(f)$ in the sense that it is a smoothed version of $P(f)$. It is approximately equal to the average value of $P(f)$ in a bandwidth Δf, centered at f,

$$P^*(f) \sim \frac{1}{\Delta f} \int_{f-\Delta f/2}^{f+\Delta f/2} P(f)\, df. \tag{19}$$

The statistical uncertainty, Δ_p, of $P'(f)$, will be given by an equation of the form

$$\Delta_p(f) \equiv \frac{\sqrt{\overline{[P'(f)-P^*(f)]^2}}}{P^*(f)} = \frac{a}{\sqrt{T\Delta f}}, \tag{20}$$

where T is the time interval during which the signal is used for the measurement, and a is a numerical factor of nearly unity, the factor being dependent on the details of the measurement.

Equations 19 and 20 are the basic uncertainty relations of spectral-measurement theory, and appear to represent the best performance that can be obtained with any measurement technique (see Grenander and Rosenblatt[3]). Note that as the frequency resolution, Δf, becomes small and thus makes $P^*(f)$ a better approximation of $P(f)$, the statistical uncertainty becomes higher [$P'(f)$ is a worse estimate of $P^*(f)$]. Optimum values of Δf, with the criterion of minimum mean-square error between $P'(f)$ and $P(f)$ are given by Grenander and Rosenblatt.[3a] In practice, Δf is usually chosen somewhat narrower than the spectral features one wishes to examine and T is chosen, if possible, to give the desired accuracy.

1.4 COMPARISON OF FILTER AND AUTOCORRELATION METHODS OF SPECTRAL ANALYSIS

Two general methods have been used in the past to measure the power spectrum. These are the filter method, illustrated in Fig. 2a and the autocorrelation method, illustrated in Fig. 2b. First, these two methods will be briefly discussed. Then, a filter-method system that is equivalent to a general autocorrelation-method system will be found.

This procedure serves two purposes: it helps to answer the question, "Which method is best?"; and it makes it possible to achieve an intuitive understanding of the filter-method system, which is not easily done for the autocorrelation-method system. Therefore, it is often helpful to think of the autocorrelation-method system in terms of the equivalent filter-method system.

The filter-method system of Fig. 2a is quite straightforward. The input signal is applied in parallel to a bank of N bandpass filters that have center frequencies spaced by δf. The power transfer function of the i^{th} bandpass filter ($i = 0$ to $N-1$) is $G_i(f)$ [impulse response, $h_i(t)$], which has passbands centered at $\pm i\delta f$. The N outputs of the filter bank are squared and averaged to give N numbers, $P'_F(i\delta f)$, $i = 0$ to $N-1$, which are estimates of the power spectrum, $P(f)$, at $f = i\delta f$.

The relation of the filter-method spectral estimate, $P'_F(i\delta f)$, to the input signal, $x(t)$, is given by

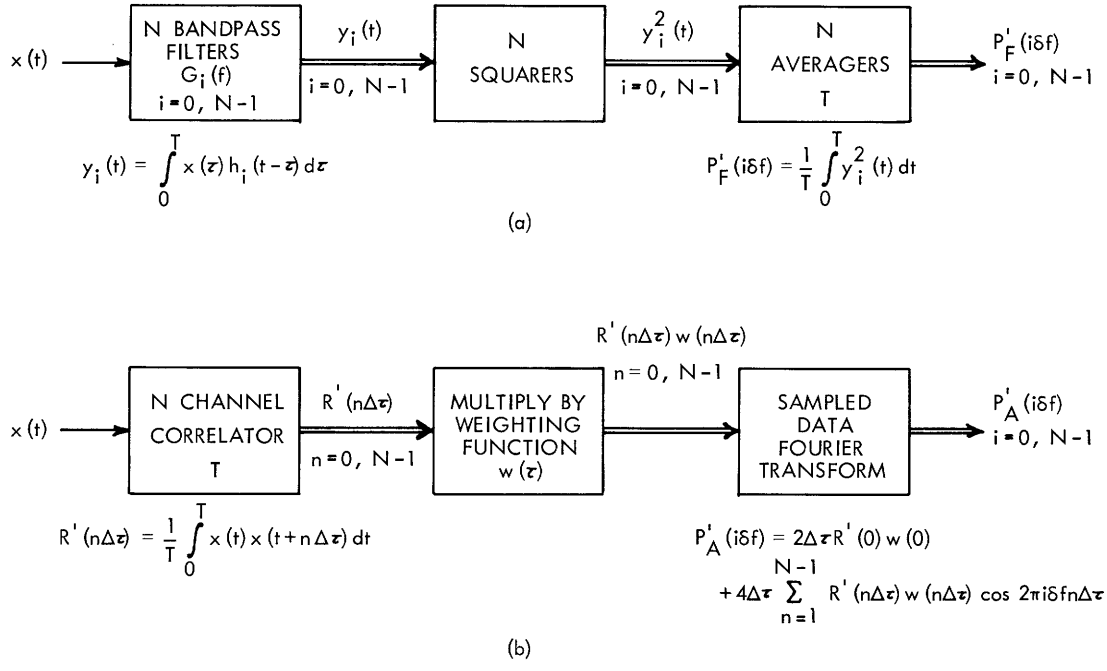

Fig. 2. Methods of spectral measurement.

$$P'_F(i\delta f) = \frac{1}{T}\int_0^T \left[\int_0^T x(t)\, h_i(\lambda - t)\, dt\right]^2 d\lambda \tag{21}$$

which is the time average of the square of the convolution integral expression for the filter output in terms of the input. It is assumed that x(t) is available for only a finite interval, T, and that the filter input is zero outside of this interval. The relation of $P'_F(i\delta f)$ to the true spectrum is of the form of Eqs. 19 and 20, where Δf is simply the filter bandwidth.

The autocorrelation method of spectral analysis is based upon the expression (called the Wiener-Khintchin theorem) giving the power spectrum as a Fourier transform of the autocorrelation function, $R(\tau)$. Indeed, this is the way we defined the power spectrum in section 1.2 (Eq. 11). The autocorrelation function can be expressed as a time average of the signal multiplied by a delayed replica of itself,

$$R(\tau) = \lim_{T\to\infty} \frac{1}{2T}\int_{-T}^{T} x(t)\, x(t+\tau)\, dt. \tag{22}$$

The operations indicated in Eqs. 11 and 22 cannot be performed in practice; an infinite segment of x(t) and an infinite amount of apparatus would be required. An estimate of $R(\tau)$ at a finite number of points, $\tau = n\Delta\tau$, can be determined by a correlator that computes

$$R'(n\Delta\tau) = \frac{1}{T}\int_0^T x(t)\, x(t+n\Delta\tau)\, dt. \tag{23}$$

A spectral estimate, $P'_A(i\delta f)$, can then be calculated as a modified Fourier transform of $R'(n\Delta\tau)$.

$$P'_A(i\delta f) = 2\Delta\tau\, R'(0)\, w(0) + 4\Delta\tau \sum_{n=1}^{N-1} R'(n\Delta\tau)\, w(n\Delta\tau) \cos(2\pi i\delta f\, n\Delta\tau). \tag{24}$$

The numbers, $w(n\Delta\tau)$, which appear in Eq. 24 are samples of a weighting function, $w(\tau)$, which must be chosen; the choice is discussed in Section II. The weighting function must be even and have $w(\tau) = 0$ for $\tau \geq N\Delta\tau$; its significance will soon become apparent. In order to use all of the information contained in $R'(n\Delta\tau)$, δf should be chosen equal to $1/[2(N-1)\Delta\tau]$. This follows from application of the Nyquist sampling theorem; $P'_A(i\delta f)$ is a Fourier transform of a function bandlimited to $(N-1)\Delta\tau$.

The relation of $P'_F(i\delta f)$ to the true power spectrum will again be of the form of Eqs. 19 and 20, where Δf, the frequency resolution, is approximately equal to $1/[(N-1)\Delta\tau]$. The calculation of the exact relation between $P'_F(i\delta f)$ and $P(f)$ will be the major topic of Section II. Our major concern now is to relate $P'_F(i\delta f)$ and $P'_A(i\delta f)$.

It is shown in Appendix A that $P'_A(i\delta f)$ will be equal to $P'_F(i\delta f)$ for any common input,

x(t), provided that the filter responses and the autocorrelation weighting function, $w(\tau)$, are related in a certain way. The only significant assumption that was required for this proof is that the duration of the data, T, be much longer than the filter time constants (or equivalently, $N\Delta\tau$). This requirement must be satisfied in practice in order to obtain a meaningful spectral estimate, and thus it is not an important restriction.

The required relation between the filter response and the autocorrelation weighting function can be most easily stated in terms of $G_i(f)$, the power transfer function of the i^{th} filter and W(f), the Fourier transform of the weighting function.

$$W(f) = 2 \int_0^\infty w(\tau) \cos 2\pi f\tau \, d\tau. \tag{25}$$

The relation is

$$G_i(f) = \sum_{k=-\infty}^{\infty} W(f - i\delta f - kf_s) + W(f + i\delta f + kf_s), \tag{26}$$

where $f_s = 1/\Delta\tau$. This result is illustrated in Fig. 3; $G_i(f)$ consists of narrow band-pass regions, each having the shape of W(f), centered at $\pm i\delta f$, $f_s \pm i\delta f$, $2f_s \pm i\delta f$, and so forth.

It is thus obvious that the autocorrelation spectral measurement system has many spurious responses. It can be seen that these spurious responses will have no effect if the input-power spectrum is restricted (by prefiltering) so that

$$\int_{-\infty}^{\infty} P(f') \, W(f - f') \, df' = 0 \qquad \text{for } |f| > f_s/2. \tag{27}$$

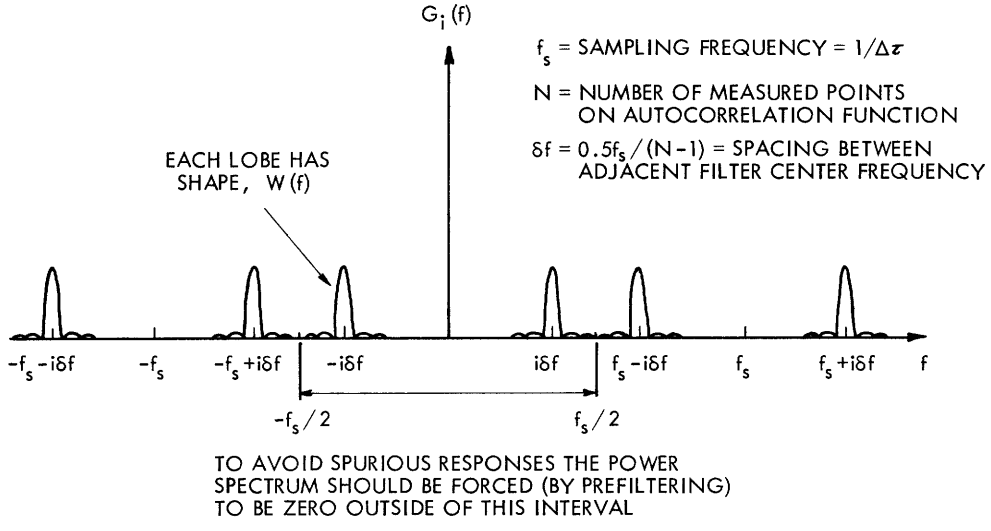

Fig. 3. Filter-array equivalent of the autocorrelation system.

This requirement, a necessary consequence of sampling of the autocorrelation function, is, of course, not required with the filter-method system, since filters without spurious response are easily constructed.

If the requirement of Eq. 27 is met, the terms in which $k \neq 0$ in Eq. 26 have no effect, and an equivalent set of filter power transfer functions is given by

$$G_i(f) = W(f-i\delta f) + W(f+i\delta f). \tag{28}$$

Furthermore, if we consider only positive frequencies not close to zero, we obtain

$$G_i(f) \sim W(f-i\delta f). \tag{29}$$

To summarize, we have shown that the estimation of N points on the autocorrelation function (Eq. 23) followed by a modified Fourier transform (Eq. 24) is equivalent to an N-filter array spectral measurement system if Eq. 26 is satisfied. Each method estimates the spectrum over a range of frequencies, $B = (N-1)\delta f = f_s/2$, with δf spacing between points. If the autocorrelation method is used, the spectrum must be zero outside of this range.

Note that the $G_i(f)$ that can be realized with practical filters is quite different from the equivalent $G_i(f)$ of an autocorrelation system (to the advantage of the filter system). The restriction on W(f) is that it be the Fourier transform of a function, $w(\tau)$, which must be zero for $\tau \geq N\Delta\tau$. This restriction makes it difficult to realize an equivalent $G_i(f)$ having half-power bandwidth, Δf, narrower than $2/(N\Delta\tau) \approx 2\delta f$ (high spurious lobes result). No such restriction between the bandwidth, Δf, and the spacing, δf, exists for the filter system.

In most filter-array spectrum analyzers, δf is equal to Δf; that is, adjacent filters overlap at the half-power points. This cannot be done with the autocorrelation method; δf will be from 0.4 to 0.8 times Δf, the value being dependent upon the spurious lobes that can be tolerated. This closer spacing gives a more accurate representation of the spectrum, but is wasteful in terms of the bandwidth analyzed, $B = (N-1)\delta f$, with a given resolution, Δf. For this reason, it appears that 2 autocorrelation points per equivalent filter is a fairer comparison.

1.5 CHOICE OF THE SPECTRAL-MEASUREMENT TECHNIQUE

We have compared the filter and autocorrelation methods of spectral analysis on a theoretical basis. The major result is that if we desire to estimate N points on the spectrum during one time interval, we may use either an N filter array as in Fig. 2a or a 2N point autocorrelation system as in Fig. 2b. The estimates of the power spectrum obtained by the two methods are equivalent; there is no theoretical advantage of one method over the other.

Both methods of spectral analysis can be performed with both analog and digital instrumentation as is indicated in Figs. 4 and 5. In addition, if digital instrumentation is chosen, a choice must be made between performing the calculations

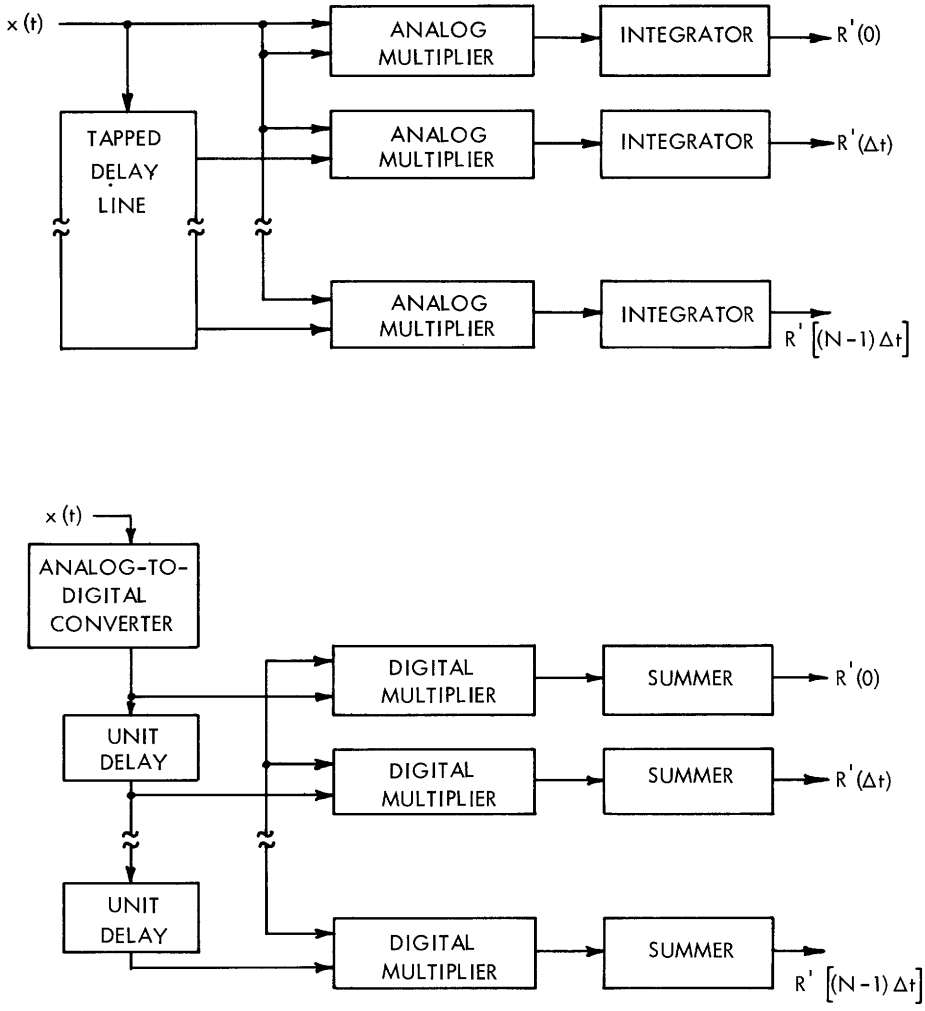

Fig. 4. Analog and digital autocorrelation methods of spectral measurement.

in a general-purpose digital computer or in a special-purpose digital spectrum analyzer or correlator.

The digital filter method[4b] shown in Fig. 5 deserves special mention because it is not too well known. The procedure indicated in the block diagram simulates a single-tuned circuit; the center frequency and Q are determined by α and β. The digital simulation of any analog filter network is discussed by Tou.[4] The digital filter method will be compared with the digital autocorrelation method below.

A way of classifying spectral measurement problems into ranges where various techniques are applicable is indicated in Fig. 6. The ordinate of the graph is N, the number of significant points that are determined on the spectrum, and the abcissa is the percentage error that can be tolerated in the measurement.

The error in a spectral measurement has two causes: (1) the unavoidable statistical fluctuation resulting from finite duration of data; and (2) the error caused by equipment inaccuracy and drift. The statistical fluctuation depends, through Eq. 20, on the

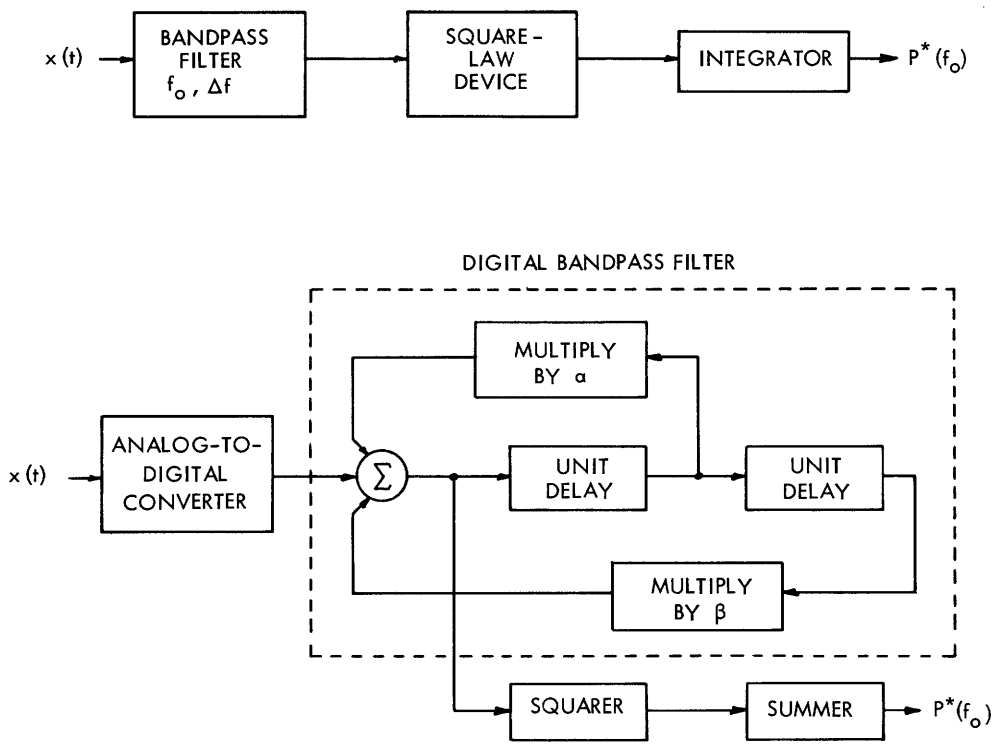

Fig. 5. Analog and digital filter methods of spectral measurement.

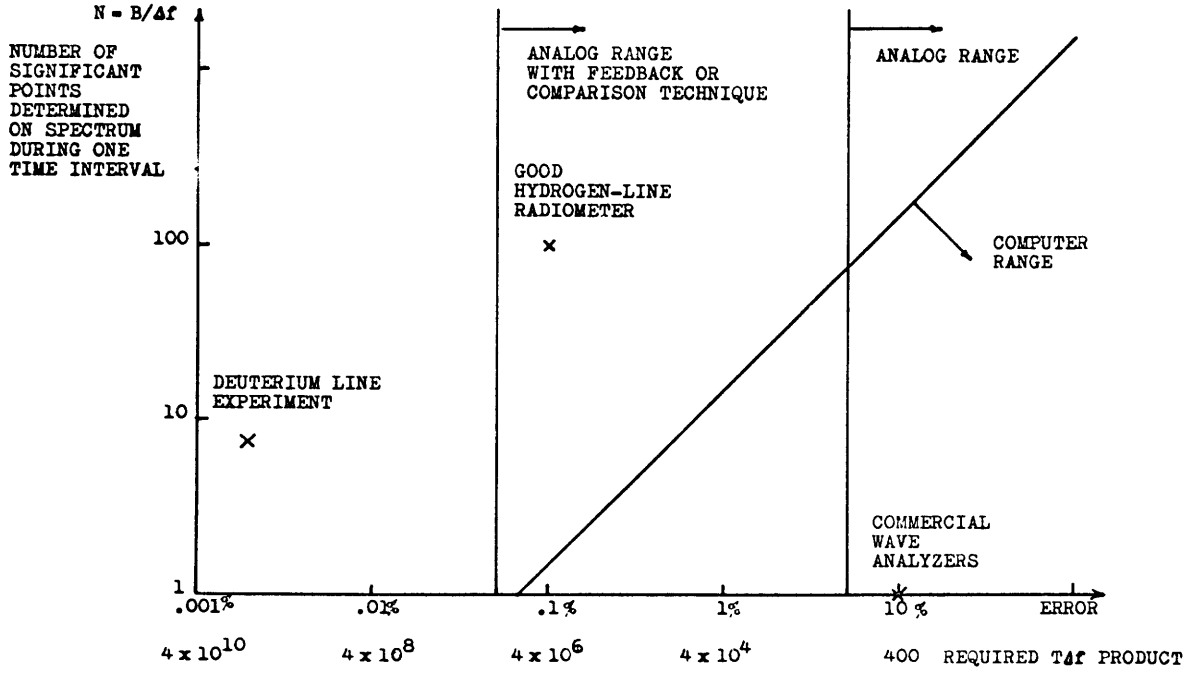

Fig. 6. Ranges of application of several spectral-measurement techniques.

frequency resolution-observation time product, $T\Delta f$. The value of $T\Delta f$ that is required for a given accuracy is plotted on the abscissa of Fig. 6.

The error caused by equipment inaccuracy and drift limits the range of application of analog techniques, as is indicated in Fig. 6. These ranges are by no means rigidly fixed; exceptions can be found. However, the line indicates the error level where the analog instrumentation becomes exceedingly difficult.

The range of application of digital-computer spectral analysis is limited by the amount of computer time that is required. The line that is drawn represents one hour of computer time on a high-speed digital computer performing 10^4 multiplications and 10^4 additions in 1 second. It is interesting that the required computer time is not highly dependent on whether the autocorrelation method or the filter method is programmed on the computer. This will now be shown.

Examination of Fig. 4 reveals that one multiplication and one addition are required per sample per point on the autocorrelation function. The sampling rate is 2B, and 2N autocorrelation points are required for N spectrum points; thus 4NB multiplications and additions per second of data are required. A similar analysis of the digital-filter method illustrated in Fig. 5 indicates that three multiplications and three additions per sample per point on the spectrum are required. This gives 6NB multiplications per second of data. The number of seconds of data that is required is given by solving Eq. 20 for T in terms of the statistical uncertainty, Δ_p, and the resolution, Δf. This gives $T = 4/\left(\Delta_p^2 \Delta f\right)$ in which the numerical factor a has been assumed to be equal to 2. We then find $16N^2/\Delta_p^2$ and $24N^2/\Delta_p^2$ to be the total number of multiplications and additions required with the autocorrelation method and filter method, respectively. Because of the square dependence on N and Δ_p, the computer time increases very rapidly to the left of the 1-hour line in Fig. 6.

Some other considerations concerning the choice of a spectral-analysis technique are the following.

1. If analog instrumentation is used, the filter method is the one that can be more easily instrumented, and, of course, it does not require the Fourier transform. The bandpass filter, squarer, and averager can be realized with less cost and complexity than the delay, multiplier, and averager required for the autocorrelation system. Analog correlation may be applicable to direct computation of autocorrelation functions and crosscorrelation functions, but not to spectral analysis.

2. Analog instrumentation is not suited for spectral analysis at very low frequencies (say, below 1 cps), although magnetic tape speed-up techniques can sometimes be used to advantage.

3. Digital instrumentation cannot be used if very large bandwidths are involved. At the present time, it is very difficult to digitally process signals having greater than 10-mc bandwidth.

4. If digital instrumentation, or a computer, is used for the spectral analysis, there seems to be little difference between the autocorrelation and the filter methods if the

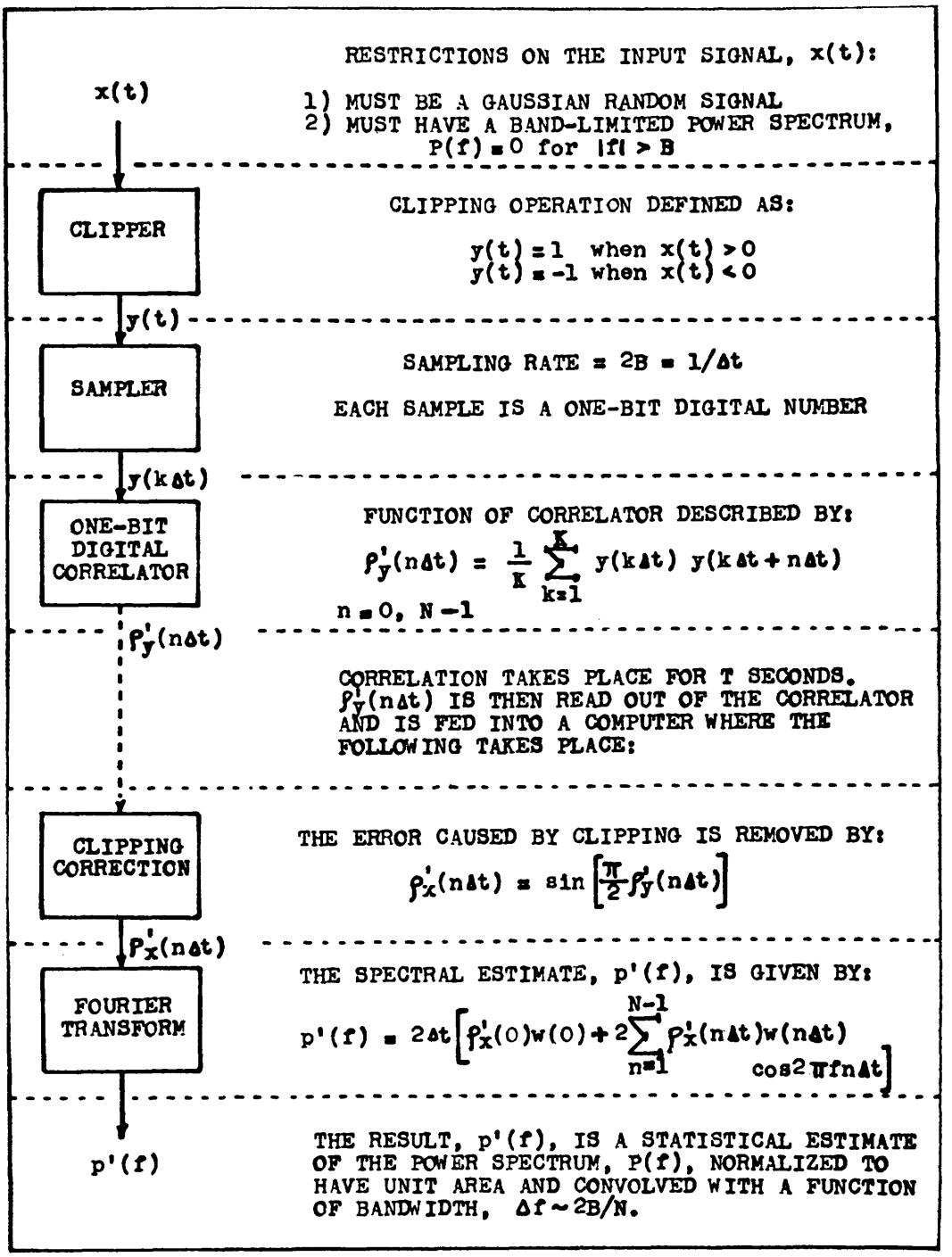

Fig. 7. The 1-bit autocorrelation method of spectral analysis.

same degree of quantization (the number of bits per sample) can be used. This is evident from the computation of the required number of multiplications and additions. If the autocorrelation method is used, however, only 1 bit per sample is necessary, and the multiplications and additions can be performed very easily. This method will now be discussed.

1.6 THE ONE-BIT AUTOCORRELATION METHOD OF SPECTRAL ANALYSIS

The one-bit autocorrelation method of spectral analysis as used here is presented with explanatory notes in Fig. 7. Most of the rest of this report will be concerned with the analysis of this system, its application to radio astronomy, and the experimental results obtained with this system.

The key "clipping correction" equation given in Fig. 7 was derived by Van Vleck,[5] in 1943. At that time, before the era of digital data processing, the present use of this relation was not foreseen; it was then simply a means of finding the correlation function at the output of a clipper when the input was Gaussian noise. Its use for the measurement of correlation functions has been noted by Faran and Hills,[6] Kaiser and Angell,[7] and Greene.[8] The principal contributions of the present report are: the investigation of the mean and statistical uncertainty (Eq. 20) of a spectral estimate formed as indicated in Fig. 7, and the application of this technique to the measurement of spectral lines in radio astronomy.

It should be understood that the spectral-measurement technique as outlined in Fig. 7

Table I. Comparison of two one-bit methods of autocorrelation-function measurement.

	A1B Method (Fig. 7)	E1B Method (Appendix B)
Restrictions on signal, x(t)	Must have Gaussian statistics	Must be bounded by ±A
Differences in procedure	1) Clipping level, 0 volt 2) SIN correction of one-bit autocorrelation function	1) Clipping level is randomly varied from -A to +A 2) No correction
Mean of result	Normalized autocorrelation function	Unnormalized autocorrelation function
RMS deviation of result compared with rms deviation of many-bit autocorrelation	Increased by less than $\pi/2$	A preliminary analysis indicates that increase depends on $A^2/\overline{x^2}$

applies only to time functions with Gaussian statistics (as defined by Eq. 8). Furthermore, only a normalized autocorrelation function and a normalized (to have unit area) power spectrum are determined. The normalization can be removed by the measurement of an additional scale factor (such as $\int_0^\infty P(f)\, df$). These restrictions do not hamper the use of the system for the measurement of spectral lines in radio astronomy.

Recently, some remarkable work, which removes both of the above-mentioned restrictions, has been done in Europe by Veltmann and Kwackernaak,[9] and by Jespers, Chu, and Fettweis.[10] These authors prove a theorem that allows a 1-bit correlator to measure the (unnormalized) autocorrelation function of any bounded time function. The proof of the theorem and the measurement procedure are summarized in Appendix B. A comparison of this procedure with that illustrated in Fig. 7 is outlined in Table I.

It is suggested (not too seriously) that the above-mentioned method of measurement of autocorrelation functions be referred to as the E1B (European 1-bit) method, and the procedure in Fig. 7 as the A1B (American 1-bit) method. Any hybrid of the two procedures could be called the MA1B (mid-Atlantic 1-bit or modified American 1-bit) method.

II. THE AUTOCORRELATION FUNCTION METHOD OF MEASURING POWER SPECTRA

2.1 INTRODUCTION

The theory of measuring the power spectrum through the use of the autocorrelation function will now be presented. We shall start with the defining equations of the power spectrum, P(f), of a time function, x(t):

$$P(f) = 2 \int_{-\infty}^{\infty} R(\tau)\, e^{-j 2\pi f \tau}\, d\tau \tag{31}$$

$$R(\tau) = \lim_{T \to \infty} \frac{1}{2T} \int_{-T}^{T} x(t)\, x(t+\tau)\, dt \tag{32}$$

If these equations are examined with the thought of measuring P(f) by directly performing the indicated operations, we reach the following conclusions.

1. In practice, the time function is available for only a finite time interval, and thus the limits on τ and t cannot be infinite as in Eqs. 31 and 32. Both the time function and the autocorrelation function must be truncated.

2. If the operation of Eq. 32 is performed by a finite number of multipliers and integrators, then τ cannot assume a continuous range of values. The autocorrelation function, $R(\tau)$, must be sampled; that is, it will be measured only for $\tau = n\Delta\tau$, where n is an integer between 0 and N-1.

3. If digital processing is used, two more modifications must be made. The time function will be sampled periodically and will give samples $x(k\Delta t)$, where k is an integer between 1 and (K+N), the total number of samples. Each of these samples must be quantized. If its amplitude falls in a certain interval (say, from $x_m - \Delta/2$ to $x_m + \Delta/2$) a discrete value (x_m) is assigned to it. It will be shown in Section III that the quantization can be done extremely coarsely; just two intervals, $x(k\Delta t) < 0$ and $x(k\Delta t) > 0$, can be used with little effect on the spectral measurement.

These considerations lead us to define the following estimates of the power spectrum and autocorrelation function,

$$P''(f) \equiv 2\Delta\tau \sum_{n=-\infty}^{\infty} R''(n\Delta\tau)\, w(n\Delta\tau)\, e^{-j 2\pi f n \Delta\tau} \tag{33}$$

$$R''(n\Delta\tau) \equiv \frac{1}{K} \sum_{k=1}^{K} x(k\Delta t)\, x(k\Delta t + |n|\Delta\tau) \tag{34}$$

The function, $w(n\Delta\tau)$, is an even function of n, chosen by the observer, which is zero for $|n| \geq N$, and has $w(0) = 1$. It is included in the definition as a convenient method of handling the truncation of the autocorrelation function measurement; $R''(n\Delta\tau)$ need

not be known for $|n| \geq N$. The choice of $w(n\Delta\tau)$ will be discussed in section 2.2b.

The estimates given by Eqs. 33 and 34 contain all of the modifications (sampling and truncation of the time function and autocorrelation function) discussed above except for quantization of samples which will be discussed in Section III. We shall call these estimates the many-bit estimates (denoted by a double prime) as contrasted with the one-bit estimates (denoted by a single prime) in Section III.

The main objective now will be to relate the many-bit estimates, $P''(f)$ and $R''(n\Delta\tau)$, to the true values, $P(f)$ and $R(n\Delta\tau)$. Many of the results will be applicable to the discussion of the one-bit estimates; other results were found for the sake of comparison with the one-bit results.

It is assumed that $x(t)$ is a random signal having Gaussian statistics. The estimates $P''(f)$ and $R''(n\Delta\tau)$ are therefore random variables, since they are based on time averages (over a finite interval) of functions of $x(t)$. The particular values of $P''(f)$ and $R(n\Delta\tau)$ depend on the particular finite-time segment of $x(t)$ on which they are based.

The mean and variance of $P''(f)$ and $R''(f)$, for our purposes, describe their properties as estimates of $P(f)$ and $R(n\Delta\tau)$. The mean, $\overline{R''(n\Delta\tau)}$, of $R''(n\Delta\tau)$, is easily found to be

$$\overline{R''(n\Delta\tau)} = \frac{1}{K} \sum_{k=1}^{K} \overline{x(k\Delta t)\, x(k\Delta t + |n|\Delta\tau)} \tag{35}$$

$$\overline{R''(n\Delta\tau)} = R(n\Delta\tau). \tag{36}$$

Here we have made use of the fact that the statistical average of $x(k\Delta t)\, x(k\Delta t + |n|\Delta\tau)$ is simply $R(n\Delta\tau)$. $R''(n\Delta\tau)$ is called an unbiased estimate of $R(n\Delta\tau)$.

The mean of $P''(f)$ is also easily found by taking the statistical average of both sides of Eq. 33 and using Eq. 36. Defining $P^*(f)$ as the mean of $P''(f)$, we find

$$P^*(f) \equiv \overline{P''(f)} = 2\Delta\tau \sum_{n=-\infty}^{\infty} R(n\Delta\tau)\, w(n\Delta\tau)\, e^{-j2\pi f n\Delta\tau}. \tag{37}$$

If it were not for the sampling and truncation of $R(\tau)$, $P^*(f)$ would simply be equal to $P(f)$, and hence $P''(f)$ would be an unbiased estimate of $P(f)$. The relationship of $P^*(f)$ to $P(f)$ is discussed below. The variances of $P''(f)$ and $R''(n\Delta\tau)$ will also be found.

Much of the material presented here is contained in a different form in a book by Blackman and Tukey.[11] For the sake of completeness this material has been included here. An extensive bibliography of past work in this field is listed in this book.

2.2 MEAN OF THE SPECTRAL ESTIMATE

a. Relation of $P^*(f)$ to $P(f)$

It has been shown that the mean, $P^*(f)$, of the many-bit spectral estimate is given (Eq. 37) as the Fourier transform of the truncated and sampled autocorrelation function.

In Section III we shall find that the mean of the one-bit spectral estimate is equal to $P^*(f)$ divided by a normalization factor. It is thus quite important that the relationship between $P^*(f)$, the quantity that we estimate, and $P(f)$, the true power spectrum, be well understood.

This relationship is found by substituting the following Fourier transform relations for $R(n\Delta\tau)$ and $w(n\Delta\tau)$ in Eq. 37.

$$R(n\Delta\tau) = \frac{1}{2}\int_{-\infty}^{\infty} P(\alpha)\, e^{j2\pi\alpha n\Delta\tau}\, d\alpha \tag{38}$$

$$w(n\Delta\tau) = \int_{-\infty}^{\infty} W(\beta)\, e^{j2\pi\beta n\Delta\tau}\, d\beta \tag{39}$$

The result is

$$P^*(f) = \sum_{i=-\infty}^{\infty} \int_{-\infty}^{\infty} P(\alpha)\, W(f-\alpha-if_s)\, d\alpha, \tag{40}$$

where $f_s = 1/\Delta\tau$, and we have made use of the relation

$$\Delta\tau \sum_{n=-\infty}^{\infty} e^{j2\pi n\Delta\tau(\alpha+\beta-f)} = \sum_{i=-\infty}^{\infty} \delta(\alpha+\beta-f+if_s).$$

Equation 40 not only specifies $P^*(f)$ in terms of $P(f)$, but it should also be considered as the general definition of the * operator which will be used in this report. This operation is described in Fig. 8. Two modifications of $P(f)$ are involved; the first is a consequence of truncation of the autocorrelation function and the second is a consequence of sampling of the autocorrelation function:

1. The spectrum is convolved with $W(f)$, a narrow-spike function of bandwidth, $\Delta f \approx f_s/N$. This convolution should be considered as a smoothing or scanning operation. Features in the spectrum narrower than Δf are smoothed out.

2. The smoothed spectrum is repeated periodically about integer multiples of f_s. If the convolution of $P(f)$ and $W(f)$ is zero for $|f| > f_s/2$, then Eq. 40 simplifies to

$$P^*(f) = \int_{-\infty}^{\infty} P(\alpha)\, W(\alpha-f)\, d\alpha \qquad |f| < f_s/2. \tag{41}$$

In practice f_s will be chosen to be twice the frequency at which the smoothed spectrum is 20 db below its midband value. In this case, little error (<1 per cent in the midband region) occurs because of sampling, and $P^*(f)$ can be considered as a smoothed version of $P(f)$. If $P(f)$ does not change much in a band of width Δf, then

$$P^*(f) \approx P(f). \tag{42}$$

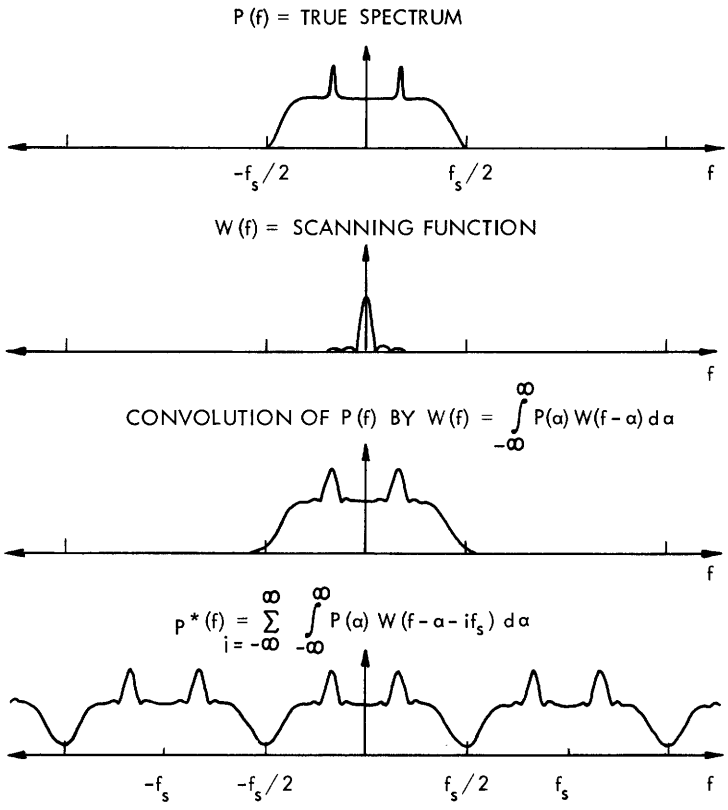

Fig. 8. Effect of sampling and truncation of the autocorrelation function. The quantity $P^*(f)$ is the mean of a spectral measurement performed with an autocorrelation system.

The relationship between $P^*(f)$ and $P(f)$ should be quite familiar to those versed in the theory of antenna arrays (or multiple-slit diffraction theory). The function $\sum_{i=-\infty}^{\infty} W(f-if_s)$ is analogous to the antenna field pattern of a line array of N point sources with amplitudes weighted by $w(n\Delta\tau)$.

b. The Weighting Function, $w(n\Delta\tau)$

The shape of the spectral scanning function, $W(f)$, is determined by the choice of its Fourier transform, the autocorrelation weighting function, $w(n\Delta\tau)$. The weighting function can be arbitrarily chosen except for the following restrictions:

$$w(0) = 1 = \int_{-\infty}^{\infty} W(f)\, df \tag{43}$$

$$w(n\Delta\tau) = w(-n\Delta\tau) \tag{44}$$

$$w(n\Delta\tau) = 0 \qquad \text{for } |n| \geq N. \tag{45}$$

The choice of $w(n\Delta\tau)$ is usually a compromise between obtaining a $W(f)$ with a narrow

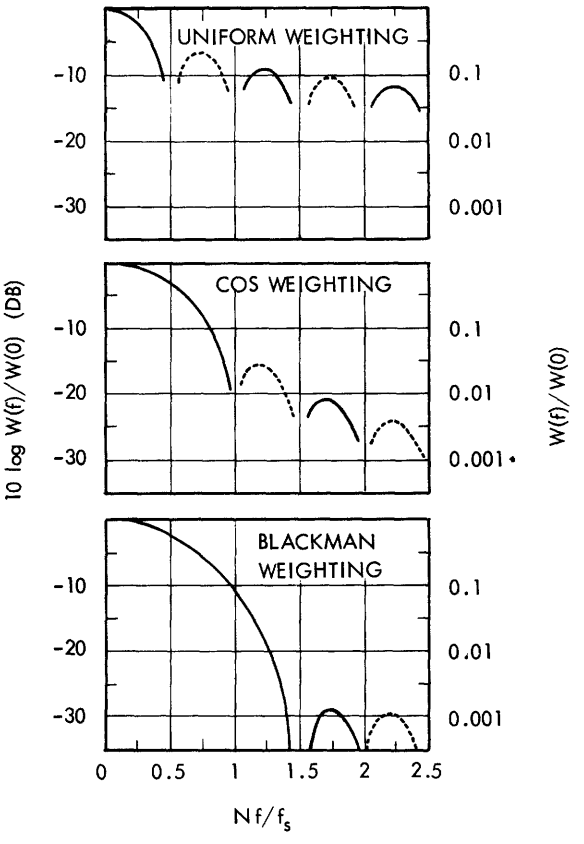

Fig. 9. Three scanning functions that result from the uniform and cosine weighting functions (after Blackman and Tukey[11]). The broken lines indicate that W(f) is negative. See also Table II.

main lobe and high spurious lobes, or a W(f) with a broadened main lobe and low spurious lobes.

This problem is a common one in antenna theory and optics. The "optimum" $w(n\Delta\tau)$ obviously depends on some exact specification of the performance of W(f). This criterion will usually depend on the particular measurement that is being made. Some weighting functions that appear to be optimum in some sense are: the uniform weighting function (to be discussed below) which gives a narrow main lobe; the binomial weighting function (Kraus[12]) which gives no spurious lobes; and the Tchebycheff weighting function (see Dolph[13]) which gives equal spurious lobes.

It appears that little can be gained by making a very careful choice of $w(n\Delta\tau)$. Blackman and Tukey[11] describe five weighting functions; three of these should be adequate for most applications and are given in Table II and Fig. 9. The cos weighting function appears to be a good compromise for most spectral-line observations in radio astronomy; the uniform weighting function gives sharper resolution, whereas the Blackman weighting function gives low (-29 db) spurious lobes.

Table II. Properties of three weighting functions.

Name	Weighting Function $w(n\Delta\tau)$	Scanning Function $W(f)$	RMS Deviation Factor σ	Half Power Bandwidth Δf	Strongest Spurious Response
Uniform	$w(n\Delta\tau) = 1 \quad \lvert n\rvert < N$ $w(n\Delta\tau) = 0 \quad \lvert n\rvert \geq N$	$W(f) = W_o(f) =$ $2N\Delta\tau \frac{\sin 2\pi Nf/f_s}{2\pi Nf/f_s}$	1.099	$\frac{0.604\, f_s}{N}$	-7 db
Cos or Hamming	$w(n\Delta\tau) = 0.5 + 0.5\cos\frac{\pi n}{N}$ $\lvert n\rvert < N$ $w(n\Delta\tau) = 0 \quad \lvert n\rvert \geq N$	$W(f) = 0.5\, W_o(f)$ $+ 0.25\, W_o(f+\frac{f_s}{2N})$ $+ 0.25\, W_o(f-\frac{f_s}{2N})$	0.866	$\frac{f_s}{N}$	-16 db
Blackman	$w(n\Delta\tau) = 0.42 + 0.5\cos\frac{\pi n}{N}$ $+ 0.08\cos\frac{2\pi n}{N} \quad \lvert n\rvert < N$ $w(n\Delta\tau) = 0 \quad \lvert n\rvert \geq N$	$W(f) = 0.42\, W_o(f)$ $+ 0.25\, W_o(f+f_s/2N)$ $+ 0.25\, W_o(f-f_s/2N)$ $+ 0.04\, W_o(f+f_s/N)$ $+ 0.04\, W_o(f-f_s/N)$	0.686	$\frac{1.13\, f_s}{N}$	-29 db

c. Some Useful Properties of $P^*(f)$

Some useful relations between $P^*(f)$ and $R(n\Delta\tau)$ can be obtained by using conventional Fourier techniques. These relations are all derived from Eq. 37:

$$P^*(f) = 2\Delta\tau \sum_{n=-\infty}^{\infty} R(n\Delta\tau)\, w(n\Delta\tau)\, e^{-j\,2\pi f\, n\Delta\tau}.$$

This equation, with $P^*(f)$ and $R(n\Delta\tau)$ replaced by different quantities, will often occur, and hence, the results of this section will also apply to the following quantities which replace $P^*(f)$ and $R(n\Delta\tau)$:

$P''(f)$ and $R''(n\Delta\tau)$	The many-bit estimates of $P^*(f)$ and $R(n\Delta\tau)$
$p''(f)$ and $\rho''(n\Delta\tau)$	Normalized many-bit estimates that will be discussed below
$p^*(f)$ and $\rho(n\Delta\tau)$	Normalized quantities analogous to $P^*(f)$ and $R(n\Delta\tau)$
$p'(f)$ and $\rho'(n\Delta\tau)$	Normalized one-bit estimates that will be defined in Section III.

If Eq. 37 is multiplied by $e^{j\,2\pi f\, k\Delta\tau}$ and the result is integrated from zero to $f_s/2$, we find

$$R(n\Delta\tau)\, w(n\Delta\tau) = \int_0^{f_s/2} P^*(f) \cos 2\pi f\, n\Delta\tau\, d\tau. \tag{46}$$

This is analogous to the inverse transform relationship (Eq. 14) between $R(\tau)$ and $P(f)$. Setting $n = 0$ in Eq. 46 and $\tau = 0$ in Eq. 14 gives

$$R(0) = \int_0^{f_s/2} P^*(f)\, df \tag{47}$$

and

$$R(0) = \int_0^{\infty} P(f)\, df, \tag{48}$$

where $R(0)$ is the total time average power.

The Parseval theorem for $P^*(f)$ can be derived by substituting Eq. 37 for one $P^*(f)$ in the quantity $\int_0^{f_s/2} P^*(f) \cdot P^*(f)\, df$. The result is easily recognized if Eq. 46 is used. The result is

$$\int_0^{f_s/2} [P^*(f)]^2\, df = 2\Delta\tau \sum_{n=-\infty}^{\infty} R^2(n\Delta\tau)\, w^2(n\Delta\tau) \tag{49}$$

which is sometimes useful.

2.3 COVARIANCES OF MANY-BIT ESTIMATES OF THE AUTOCORRELATION FUNCTION AND POWER SPECTRUM

We shall examine the covariances $\sigma^2_{Pm}(f_1,f_2)$ and $\sigma^2_{Rm}(n,m)$ of estimates $P''(f)$ and $R''(n\Delta\tau)$ (defined in Eqs. 33 and 34), of the power spectrum and autocorrelation function,

respectively. These estimates are based on many-bit (or unquantized) samples of the time function as opposed to estimates based on one-bit samples that are the major topic of this report. The calculations of the covariances in the many-bit case are included for the sake of comparison. The following discussion applies to both many-bit and one-bit cases.

a. Definitions: Relation of the Spectral Covariance to the Autocorrelation Covariance

The covariance of the power spectrum estimate is defined as

$$\sigma^2_{Pm}(f_1,f_2) \equiv \overline{[P''(f_1)-P^*(f_1)][P''(f_2)-P^*(f_2)]} \tag{50}$$

$$\sigma^2_{Pm}(f_1,f_2) = \overline{P''(f_1)\,P''(f_2)} - P^*(f_1)\,P^*(f_2). \tag{51}$$

A special case arises when $f_1 = f_2 = f$ and the covariance becomes the variance, $\sigma^2_{Pm}(f)$. The positive square root of the variance is the rms deviation, $\sigma_{Pm}(f)$. The variance and rms deviation specify the way in which $P''(f)$ is likely to vary from its mean, $P^*(f)$. The covariance also specifies how the statistical error at one frequency, f_1, is correlated with the statistical error at another frequency, f_2.

The definition of the autocorrelation covariance is quite similar.

$$\sigma^2_{Rm}(n,m) \equiv \overline{[R''(n\Delta\tau)-R(n\Delta\tau)][R''(n\Delta\tau)-R(n\Delta\tau)]} \tag{52}$$

$$\sigma^2_{Rm}(n,m) = \overline{R''(n\Delta\tau)\,R''(n\Delta\tau)} - R(n\Delta\tau)\,R(n\Delta\tau) \tag{53}$$

and the meaning of the autocorrelation variance and rms deviation follow accordingly.

The spectral covariance or variance can be expressed in terms of the autocorrelation covariance by substitution of Eqs. 33 and 37 in Eq. 51. This gives

$$\sigma^2_{Pm}(f_1,f_2) = 4\Delta\tau^2 \sum_{n=-\infty}^{\infty} \sum_{n=-\infty}^{\infty} \sigma^2_{Rm}(n,m)\; w(n\Delta\tau)\; w(m\Delta\tau)\; e^{-j\,2\pi\,\Delta\tau(nf_1+mf_2)}. \tag{54}$$

Our first step will be to calculate the autocorrelation covariance. This is not only needed for the calculation of the spectral covariance, but is also of interest on its own accord.

Note that the autocorrelation covariance is required to calculate the spectral variance or covariance; the autocorrelation variance is not sufficient. The integrated (over frequency) spectral variance can be expressed in terms of the autocorrelation variance summed over the time index, n. This relation is found by integrating both sides of Eq. 54 (with $f_2 = f_1$) from 0 to $f_s/2$. The result is

$$\int_0^{f_s/2} \sigma^2_{Pm}(f_1)\, df_1 = 2\Delta\tau \sum_{n=-\infty}^{\infty} \sigma^2_{Rm}(n)\, w^2(n\Delta\tau). \tag{55}$$

b. Results of the Autocorrelation Covariance Calculation

The covariance, $\sigma^2_{Rm}(n,m)$, of the many-bit autocorrelation function estimate is calculated in Appendix C; the results will be discussed here.

The covariance, expressed in terms of the autocorrelation function, is found to be

$$\sigma^2_{Rm}(n,m) = \frac{1}{K} \sum_{i=-K}^{K} [R(i\Delta t + |n|\Delta\tau - |m|\Delta\tau)\, R(i\Delta t) + R(i\Delta t + |n|\Delta\tau)\, R(i\Delta t - |m|\Delta\tau)]. \tag{56}$$

A plot of a typical autocorrelation function and its rms deviation, $\sigma_{Rm}(n)$, is given in Fig. 10.

It is informative to investigate the autocorrelation variance (n=m) in two limiting cases:

Case 1

Suppose that Δt is large enough so that

$$R(i\Delta t) = 0 \qquad \text{for } i \neq 0. \tag{57}$$

Equation 56 then reduces to

$$\sigma^2_{Rm}(n) = \frac{R^2(0) + R^2(n\Delta\tau)}{K}. \tag{58}$$

The condition of Eq. 57 implies that successive products, $x(k\Delta t)\, x(k\Delta t + |n\Delta\tau|)$, which go into the estimate of the autocorrelation function, are linearly independent. There are K such products and the form of Eq. 58 is a familiar one in statistical estimation problems.

In order to minimize the variance, K should be made as large as possible. If the duration, T, of the data is fixed, then the only recourse is to reduce $\Delta t = T/K$. As Δt is reduced, a point will be reached where Eq. 57 is not satisfied. The minimum value of Δt which satisfies Eq. 57 is equal to 1/2B if x(t) has a rectangular power spectrum extending from -B to B, and if $\Delta\tau$ is set equal to 1/2B. The variance at this value of Δt is

$$\sigma^2_{Rm}(n) = \frac{R^2(0) + R^2(n\Delta\tau)}{2BT}, \tag{59}$$

where $R(n\Delta\tau) = 0$, $n \neq 0$ for the rectangular spectrum with $\Delta\tau = 1/2B$.

The next example will illustrate the point that the variance cannot be reduced further by reduction of Δt beyond the point required by Eq. 57.

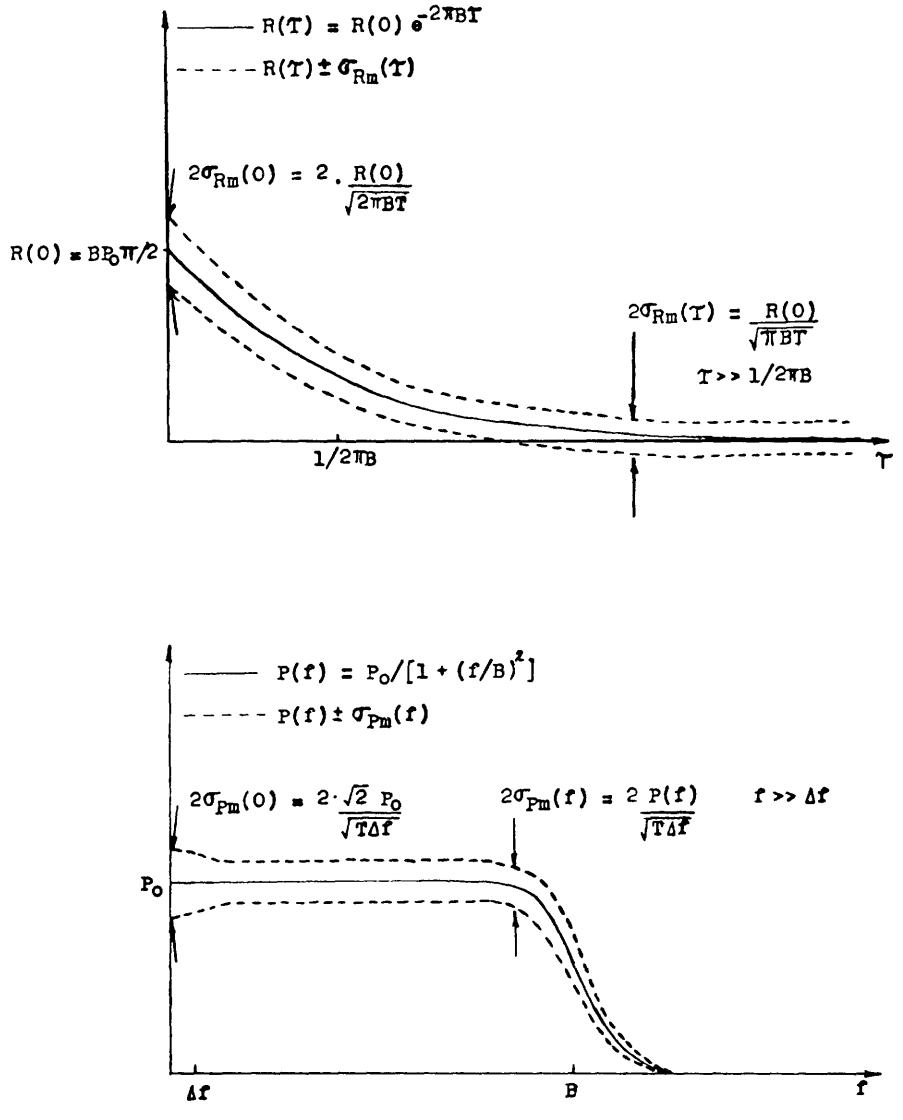

Fig. 10. An autocorrelation function and its transform, the power spectrum. The form of the rms deviation is indicated. Note that $\sigma_{Pm}(f)$ is proportional to P(f) (except near f = 0), whereas $\sigma_{Rm}(\tau)$ is nearly constant.

Case 2

Suppose that $\Delta t \to 0$ and $K \to \infty$ in such a manner that $K\Delta t = T$ is constant. The case of continuous data (analog correlation) is approached and Eq. 56 (with n = m) becomes

$$\sigma^2_{Rm}(n) = \frac{1}{T}\int_{-T}^{T} [R^2(t)+R(t+n\Delta\tau)\,R(t-n\Delta\tau)]\,dt. \qquad (60)$$

If again we take the case of a rectangular spectrum between -B and B, Eq. 60 gives

$$\sigma^2_{Rm}(n) = \frac{R^2(0) + R^2(0)\ (\sin 4\pi B\, n\Delta\tau)/(4\pi B\, n\Delta\tau)}{2BT}. \tag{61}$$

This result, with $\Delta\tau = 1/2B$, agrees exactly with Eq. 59. Thus, reducing the time-function sampling interval Δt from 1/2B to 0 has had no effect on $\sigma^2_{Rm}(n)$ for the case of a rectangular spectrum.

Examinations of Eqs. C.8 and C.11 in Appendix C give more general results. These equations show that both the autocorrelation variance and the spectral variance do not change for values of Δt less than 1/2B if $P(f) = 0$ for $f \geq B$.

c. Results of the Spectral Covariance Calculation

The spectral covariance, $\sigma^2_{Pm}(f_1,f_2)$, is calculated in Appendix C with the following result.

$$\sigma^2_{Pm}(f_1,f_2) = \frac{1}{T}\int_{-\infty}^{\infty} P^2(f)\ W(f+f_1)\ [W(f+f_2) + W(f-f_2)]\ df. \tag{62}$$

It has been assumed that: (a) the signal has Gaussian statistics; (b) both P(f) and W(f) are smooth over frequency bands of width 1/T; (c) the spectrum smoothed by [or convolved with] W(f) is zero for frequencies greater than B; (d) both the time-function sampling interval, Δt, and the autocorrelation-function sampling interval, $\Delta\tau$, have been chosen equal to 1/2B; and (e) Eq. 62 is valid only for $|f_1|$ and $|f_2|$ less than B.

The manner in which the spectral estimate covaries is observed in Eq. 62. If f_1 and f_2 are such that $W(f+f_1)$ and $W(f\pm f_2)$ do not overlap, then $\sigma^2_{Pm}(f_1,f_2) = 0$. In other words, the statistical errors at two frequencies separated by more than Δf, the bandwidth of W(f), are uncorrelated. This result might have been expected from the analogy with the filter-array spectrum analyzer discussed in Section I.

The spectral variance ($f_1 = f_2$) can be put in a simpler form if some further approximations are made. It can be seen that at $f_1 = f_2 = 0$ the variance becomes

$$\sigma^2_{Pm}(0) = \frac{2}{T}\int_{-\infty}^{\infty} P^2(f)\ W^2(f)\ df, \tag{63}$$

while, for $f_1 = f_2 \gg \Delta f$, we obtain

$$\sigma^2_{Pm}(f_1) = \frac{1}{T}\int_{-\infty}^{\infty} P^2(f)\ W^2(f+f_1)\ df. \tag{64}$$

In the following discussion we shall assume that f_1 is positive and not close to zero so that Eq. 64 applies.

If the spectrum is smooth over bands of width Δf, then P(f) can be taken out from under the integral sign in Eq. 64 to give

$$\sigma^2_{Pm}(f_1) = \frac{P^2(f_1)}{T} \int_{-\infty}^{\infty} W^2(f')\, df', \tag{65}$$

where a change of variable, $f' = f + f_1$, has been made. The integral depends only on the weighting function $w(\tau)$ and has dimensions of a reciprocal bandwidth. It is, therefore, convenient to define a dimensionless parameter, a, with the property that

$$\frac{a}{\Delta f} \equiv \int_{-\infty}^{\infty} W^2(f')\, df' = \int_{-\infty}^{\infty} w^2(\tau)\, d\tau, \tag{66}$$

where Δf is the half-power bandwidth of W(f). The equality in Eq. 66 follows from Parseval's theorem for Fourier transforms. It should be remembered that W(f) must have unit area as specified by Eq. 43.

The numerical factor, a, will be of the order of unity and is specified for various weighting functions in Table II. If W(f) is a rectangular function of width Δf and height $1/\Delta f$, then $a = 1$. The rms deviation of the spectral measurement can now be put in the familiar form,

$$\sigma_{Pm}(f) = \frac{a}{\sqrt{T\Delta f}}\, P(f). \tag{67}$$

The appearances of a typical spectrum and its rms deviation are sketched in Fig. 10.

2.4 NORMALIZED, MANY-BIT ESTIMATES OF THE SPECTRUM AND AUTOCORRELATION FUNCTION

[Reminder concerning notation: A ρ denotes a normalized autocorrelation function; a lower-case p denotes a normalized power spectrum; a double prime or subscript m denotes a quantity determined from many-bit samples; a single prime or subscript 1 denotes a quantity obtained from one-bit samples.]

The one-bit method of spectral analysis produces a spectral estimate, $p'(f)$, and an autocorrelation function estimate, $\rho'(n\Delta\tau)$, which are (unavoidably) normalized so that

$$\rho'(0) = 1 \tag{68}$$

and

$$\int_0^{f_s/2} p'(f)\, df = 1. \tag{69}$$

In order to compare the many-bit results here with the one-bit results in Section III, the many-bit estimates must be similarly normalized. A computer-simulated, experimental comparison of normalized many-bit estimates with one-bit estimates is given in Section VI, and the results in Section II will be used there.

It is important to note that $\rho'(0)$ has no statistical fluctuation; it is constrained to equal unity. (This is more stringent than having $\overline{\rho'(0)} = 1$.) The variance, $\sigma^2_{\rho 1}(0)$, must

be zero. A quantity derived from many-bit samples that has the same property is

$$\rho''(n\Delta\tau) = \frac{R''(n\Delta\tau)}{R''(0)}, \tag{70}$$

where $R''(n\Delta\tau)$ is defined in Eq. 34. Note that $R''(n\Delta\tau)$ has been divided by $R''(0)$, a random variable, and not by $R(0)$, which is constant (but unknown). If $\rho''(n\Delta\tau)$ had been defined as $R''(n\Delta\tau)/R(0)$, only trivial modifications of previous results would be required. However, this definition does not give a $\rho''(n\Delta\tau)$ that is analogous to $\rho'(n\Delta\tau)$.

The normalized many-bit power-spectrum estimate, $p''(f)$, is similarly defined as $P''(f)/R''(0)$. The definition of $P''(f)$ (Eq. 33) may be used to give

$$p''(f) = 2\Delta\tau \sum_{n=-\infty}^{\infty} \rho''(n\Delta\tau)\, w(n\Delta\tau)\, e^{-j2\pi f n\Delta\tau}. \tag{71}$$

This definition will give (see section 2.2c)

$$\int_0^{f_s/2} p''(f)\, df = 1 \tag{72}$$

analogously with Eq. 69.

Our main purpose now is to find the mean and variance of $\rho''(n\Delta\tau)$ and $p''(f)$. The calculation of the mean or variance of the quotient of two dependent random variables is a difficult problem. A drastic simplification results, however, if the denominator random variable $R''(0)$ has a random fluctuation that is small compared with its mean. This simplification will now be used.

a. Mean and Variance of the Normalized Autocorrelation Estimate

The mean and variance of $\rho''(n\Delta\tau) = R''(n\Delta\tau)/R''(0)$ can be found by expanding $R''(n\Delta\tau)$ and $R''(0)$ as

$$R''(n\Delta\tau) = R(n\Delta\tau) + R(0)\,\epsilon(n), \tag{73}$$

where $\epsilon(n)$ is a small $[\epsilon(n) \ll 1]$ random variable. It can be seen by solving Eq. 73 for $\epsilon(n)$ that

$$\overline{\epsilon(n)} = 0 \tag{74}$$

$$\overline{\epsilon(n)\,\epsilon(m)} = \frac{\sigma^2_{Rm}(n,m)}{R^2(0)}. \tag{75}$$

The requirement $\epsilon(n) \ll 1$ is met by ensuring that the observation time, T, is long enough so that $\sigma_{Rm}(n)$ is much less than $R(0)$. This must be true in practice if the estimate of $R''(n\Delta\tau)$ is to be at all accurate.

The normalized autocorrelation function estimate, $\rho''(n\Delta\tau)$, can then be written

$$\rho''(n\Delta\tau) = \frac{R(n\Delta\tau) + R(0)\,\epsilon(n)}{R(0) + R(0)\,\epsilon(0)}. \tag{76}$$

Since $\epsilon(n) \ll 1$ (including $n = 0$), Eq. 76 can be expanded, and terms of higher order than first in $\epsilon(n)$ or $\epsilon(0)$ be dropped to give

$$\rho''(n\Delta\tau) = \rho(n\Delta\tau) - \rho(n\Delta\tau)\,\epsilon(0) + \epsilon(n). \tag{77}$$

The mean can now be found:

$$\overline{\rho''(n\Delta\tau)} = \rho(n\Delta\tau), \tag{78}$$

and the covariance, $\sigma^2_{\rho m}(n,m)$, can be expressed as

$$\sigma^2_{\rho m}(n,m) \equiv \overline{[\rho''(n\Delta\tau)-\rho(n\Delta\tau)][\rho''(m\Delta\tau)-\rho(m\Delta\tau)]} \tag{79}$$

$$= \overline{\epsilon(n)\,\epsilon(m)} + \overline{\epsilon^2(0)}\,\rho(n\Delta\tau)\,\rho(m\Delta\tau) - \overline{\epsilon(n)\,\epsilon(0)}\,\rho(m\Delta\tau) - \overline{\epsilon(m)\,\epsilon(0)}\,\rho(n\Delta\tau) \tag{80}$$

The terms $\overline{\epsilon(n)\,\epsilon(m)}$ (in which n or m may be zero) in Eq. 80 are expressed in terms of $\sigma^2_{Rm}(n,m)$ by Eq. 75. This quantity is given by Eq. 56 and substitution in Eq. 75 gives

$$\overline{\epsilon(n)\,\epsilon(m)} = \frac{1}{K}\sum_{i=-K}^{K}[\rho(i\Delta t+|n|\Delta\tau-|m|\Delta\tau)\,\rho(i\Delta\tau)+\rho(i\Delta t+|n|\Delta\tau)\,\rho(i\Delta t-|m|\Delta\tau)]. \tag{81}$$

Equations 80 and 81 specify the covariance of the normalized, many-bit estimate of the autocorrelation function. A feeling for this result can be obtained by substitution in Eq. 80 of an approximate form of Eq. 81. This approximate form is valid for Δt large enough so that successive samples are independent (as discussed in connection with Eq. 58) and is

$$\overline{\epsilon(n)\,\epsilon(m)} = \frac{\rho(|n|\Delta\tau-|m|\Delta\tau) + \rho(n\Delta\tau)\,\rho(m\Delta\tau)}{K}.$$

Substitution of Eq. 81 in Eq. 80 gives a simple result for the variance (n=m).

$$\sigma^2_{\rho m}(n) = \frac{1 - \rho^2(n\Delta\tau)}{K} \tag{82}$$

This result should be compared with Eq. 58; this gives $\sigma^2_{Rm}(n)$ with the same approximations. The major result has been the reduction of the variance near $n = 0$, as would be expected.

b. Mean and Variance of the Normalized Spectral Estimate

The mean of the spectral estimate is found by taking the mean of both sides of Eq. 71 and using Eq. 78. This mean will be denoted $p^*(f)$, and is given by

$$p^*(f) = \overline{p''(f)} = 2\Delta\tau \sum_{n=-\infty}^{\infty} \frac{R(n\Delta\tau)}{R(0)} w(n\Delta\tau)\, e^{-j2\pi f n\Delta\tau} \tag{83}$$

$$= \frac{P^*(f)}{R(0)} \tag{84}$$

$$= \frac{P^*(f)}{\int_0^{f_s/2} P^*(f)\, df} = \frac{P^*(f)}{\int_0^{\infty} P(f)\, df}. \tag{85}$$

Here, Eq. 37 has been used to give Eq. 84 and Eqs. 47 and 48 have been used to give Eq. 85. $P^*(f)$ is the smoothed spectrum discussed in section 2.2. The mean of $p''(f)$ thus is the smoothed spectrum normalized to have unit area in the range $0\text{-}f_s/2$.

The spectral variance or covariance can be calculated in a straightforward manner through the use of Eq. 54 which relates the spectral variance or covariance to the autocorrelation covariance. The autocorrelation covariance for the normalized estimate is given by Eqs. 80 and 81. Combination of these equations gives a very long expression for the spectral variance. This will not be presented in this report, in view of its complexity and minor importance. A heuristic argument that gives an approximate, but simple, expression for the spectral variance will be given below.

Suppose that we consider the normalized spectrum to be of uniform height, $1/b$, over a bandwidth, b. The effect of constraining the spectral estimate to have unit area is then equivalent to requiring that the average height of the spectrum be $1/b$, its true value. This is analogous to correcting a set of measured points so that their average value is equal to the true value. In this case (see Kenney and Keeping,[14] Sec. 8.7) the variance is reduced by $1 - 1/N$, where N is the number of independent points. In section 2.2 it was shown that points on the spectrum spaced Δf apart are independent; thus $N = b/\Delta f$. The rms deviation, $\sigma_{pm}(f_1)$, of the normalized spectral estimate then becomes

$$\sigma_{pm}(f_1) = \frac{a}{\sqrt{T\Delta f}} \cdot p(f) \cdot \sqrt{1 - \Delta f/b}. \tag{86}$$

Here, Eq. 67 has been used for the rms deviation before normalization. This result approximates the result of a formal derivation by using Eqs. 54, 80, and 81.

III. THE ONE-BIT METHOD OF COMPUTING AUTOCORRELATION FUNCTIONS

3.1 INTRODUCTION

The theory of estimating the power spectrum through the use of a finite number of samples, K, of the input signal x(t) was presented in Section II. This theory would be sufficient if analog techniques or very finely quantized digital techniques were used to compute an estimate of the autocorrelation function. The analog techniques are not usable for high-sensitivity spectral-line analysis in radio astronomy, because of the lack of accuracy. (As stated in section 1.5, if accuracy requirements permit the use of analog instrumentation, then the conventional bandpass-filter method of spectral analysis is preferable.)

Many-bit digital techniques are unwieldy for most radio-astronomy applications, because of the large number of operations that must be performed. In section 1.5 it was shown that $16N^2/\Delta p^2$ is the total number of multiplications required for the estimation of N points on the spectrum with an accuracy of 100 Δp per cent. For the deuterium-line experiment, $\Delta p = 3 \times 10^{-5}$ and N = 8 which results in 10^{12} multiplications. A typical high-speed digital computer performs 10^4 many-bit multiplications per second, and thus approximately four years of computer time would be required. If one-bit multiplications could be used, this computer time could be reduced by a factor of 10. Of greater significance is the fact that a special-purpose one-bit digital-correlation computer can be built for approximately 1/10 the cost of a similar many-bit machine. The cost of a one-bit digital correlator is roughly $1000 per point on the autocorrelation function (or, according to the discussion in section 1.4, $2000 per point on the spectrum). A one-bit digital correlator, capable of measuring 21 points on the autocorrelation function was built for the deuterium-line experiment; the experimental results will be discussed in this report.

The term, "many-bit autocorrelation," needs further explanation. By this, we mean that the quantization levels are so small that the quantization error can be disregarded. This is usually the case in digital computers in which the usual word lengths of 20 bits, or more, allow the quantization error to be 10^{-6} or less of the maximum value of the signal.

A general relationship between quantization error and the error in a spectrum measurement does not seem to be known. At first thought, one might think that to measure the power spectrum with an accuracy of X per cent, a quantization error of less than X per cent is required. This is not true because the spectral estimate is based on an average computed from many samples, and the quantization error tends to average out. Kaiser and Angell[7] have measured autocorrelation functions with 8, 3, and 1 bits per sample with surprisingly little difference in the results.

The main spectral analysis procedure discussed in this report is one in which quantization is performed with one bit per sample, and a correction is applied to the resulting

autocorrelation function estimate; the procedure is illustrated in Fig. 7. This method is based on a theorem of Van Vleck. The theorem is stated as follows:

Suppose that x(t) is a sample function of a Gaussian random process with zero mean, and y(t) is the function formed by infinite clipping of x(t). That is,

$$\begin{aligned} y(t) &= 1 \qquad \text{when } x(t) > 0 \\ y(t) &= -1 \qquad \text{when } x(t) < 0. \end{aligned} \tag{87}$$

Then the normalized autocorrelation functions of x(t) and y(t) are related by

$$\rho_x(\tau) = \sin\left[\frac{\pi}{2}\rho_y(\tau)\right]. \tag{88}$$

For completeness, a derivation of this equation will be given in section 3.2; some of the steps in the derivation will also be useful for other work.

Equation 88 is valid for the true normalized autocorrelation functions, $\rho_x(\tau)$ and $\rho_y(\tau)$, which cannot be measured from a finite number of samples of x(t) or y(t). An estimate of $\rho_y(\tau)$ can be defined as $\rho'_y(\tau)$, with

$$\rho'_y(\tau) \equiv \frac{1}{K}\sum_{k=1}^{K} y(k\Delta t)\, y(k\Delta t+\tau). \tag{89}$$

Equation 89 describes the function performed by a one-bit digital correlator. An estimate of $\rho_x(\tau)$ is defined as

$$\rho'_x(\tau) \equiv \sin\left[\frac{\pi}{2}\rho'_y(\tau)\right]. \tag{90}$$

The problem now is to find the mean and variance of $\rho'_x(\tau)$. This is not easily computed, because of the complicated manner in which $\rho'_x(\tau)$ is related to x(t) through Eqs. 87, 89, and 90. It has only been possible to calculate the mean and variance in the case in which successive products, $y(k\Delta t)\, y(k\Delta t+\tau)$, in the summation of Eq. 89 are statistically independent. In practice, this will be approximately the case. If Δt is chosen so small that successive products are dependent, then some of the data processing is redundant. The case of independent successive products is analogous to the special case examined in Section II concerning many-bit samples (see Eqs. 55 and 56).

An estimate of the normalized power spectrum will be defined as a weighted Fourier transform of samples of $\rho'_x(\tau)$ in a manner similar to that used in Eq. 33. This estimate will be discussed here.

It should be remembered that Eq. 88 is true only for certain classes of functions. The Gaussian random process is the example of interest. The relation is also true for a single sine wave, and McFadden[15] has shown that it is approximately true for a weak sine wave in Gaussian noise.

3.2 THE VAN VLECK RELATION

The derivation of Eq. 88 is based on the definition of the autocorrelation function as a statistical average,

$$\rho_y(\tau) \equiv \frac{\overline{y(t)\, y(t+\tau)}}{\overline{y^2(t)}}. \tag{91}$$

Due to the fact that y(t) is defined as +1 or -1, the term $\overline{y^2(t)}$ is equal to unity, and the term $\overline{y(t)\, y(t+\tau)}$ may be expressed as follows:

$$\overline{y(t)\, y(t+\tau)} = (1)\,(P_{++}+P_{--}) + (-1)\,(P_{+-}+P_{-+}), \tag{92}$$

where P_{++} is the joint probability that y(t) = +1 and y(t+τ) = +1, and the other P's are similarly defined. These probabilities can be written in terms of the joint Gaussian probability density of x(t) by making use of the definition of y(t). For example, P_{++} is equal to the joint probability that x(t) > 0 and x(t+τ) > 0,

$$P_{++} = \int_0^\infty \int_0^\infty p[x(t), x(t+\tau)]\, dx(t)\, dx(t+\tau). \tag{93}$$

The term $p[x(t), x(t+\tau)]$ is the joint Gaussian probability density function, and is given by Eq. 8.

Equations entirely similar to Eq. 93 exist for P_{--}, P_{+-} and P_{-+}, and are identical except for the obvious changes in the limits of integration. Because of the evenness and symmetry of $p[x(t), x(t+\tau)]$, it can be seen that

$$P_{--} = P_{++} \tag{94}$$

$$P_{+-} = P_{-+}. \tag{95}$$

Additional inspection of $p[x(t), x(t+\tau)]$ reveals that P_{+-} or P_{-+} can be obtained from P_{++} by reversing the sign of $\rho_x(\tau)$ after Eq. 93 has been integrated.

Equation 8 is substituted in Eq. 93, and the remaining task is the integration of this equation. Fortunately, this can be done and a simple result is obtained. The integration is performed by a transformation to cylindrical coordinates, that is, x(t) = r cos θ and x(t+τ) = r sin θ, with θ going from 0 to π/2, and r going from 0 to infinity. The integral is thus transformed to

$$P_{++} = \frac{1}{2\pi\, \sigma^2\left(1-\rho_x^2\right)} \int_0^{\pi/2} \int_0^\infty \exp\left[\frac{r^2(1-\rho_x \sin 2\theta)}{2\sigma^2\left(1-\rho_x^2\right)}\right] r\, dr\, d\theta. \tag{96}$$

The integral in r is of the form $e^u\, du$, and the resulting integral in θ has been tabulated by Dwight[16] (p. 93, Integral #436.00). The result is

$$P_{++} = 1/4 + (1/2\pi)\ \tan^{-1} \frac{\rho_x}{\left(1-\rho_x^2\right)^{1/2}}$$

$$= 1/4 + (1/2\pi)\ \sin^{-1} \rho_x \tag{97}$$

and, according to the previous discussion, the other probabilities are given by

$$P_{--} = P_{++} = 1/4 + (1/2\pi)\ \sin^{-1} \rho_x \tag{98}$$

$$P_{+-} = P_{-+} = 1/4 - (1/2\pi)\ \sin^{-1} \rho_x. \tag{99}$$

Substitution of these terms in Eq. 92 gives

$$\rho_y(\tau) = (2/\pi)\ \sin^{-1} \rho_x(\tau) \tag{100}$$

which can be solved for $\rho_x(\tau)$ to give Eq. 88.

3.3 MEAN AND VARIANCE OF THE ONE-BIT AUTOCORRELATION FUNCTION ESTIMATE

The mean and variance of the one-bit autocorrelation function estimate, $\rho'_x(\tau)$, will now be calculated. The equations defining $\rho'_x(\tau)$ are

$$\rho'_x(\tau) \equiv \sin\left[\frac{\pi}{2}\rho'_y(\tau)\right] \tag{101}$$

$$\rho'_y(\tau) \equiv \frac{1}{K} \sum_{k=1}^{K} y(k\Delta t)\ y(k\Delta t+\tau). \tag{102}$$

It will be necessary to assume that the terms $y(k\Delta t)\ y(k\Delta t+\tau)$ in the summation of Eq. 94 are independent of each other as discussed above. An approach in which characteristic functions are utilized (see Davenport and Root,[1] pp. 50-55) will be used.

The mean of $\rho'_y(\tau)$ can be shown to be $\rho_y(\tau)$; however, the mean of $\rho'_x(\tau)$ is not so easily found. (Since the sine is a nonlinear operation, one cannot say, in general, "$\overline{\sin x} = \sin \overline{x}$".) The mean and mean square of ρ'_x can be expressed in terms of $p(\rho'_y)$, the probability density function of ρ'_y:

$$\overline{\rho'_x} = \int_{-\infty}^{\infty} \sin\ (\pi\rho'_y/2)\ p(\rho'_y)\ d\rho'_y \tag{103}$$

$$\overline{\rho'^2_x} = \int_{-\infty}^{\infty} \sin^2\ (\pi\rho'_y/2)\ p(\rho'_y)\ d\rho'_y. \tag{104}$$

The probability density function $p(\rho'_y)$ is the Fourier transform of $M_y(v)$, the

characteristic function of ρ'_y.

$$p(\rho'_y) = \frac{1}{2\pi} \int_{-\infty}^{\infty} M_y(v)\, e^{-jv\rho'_y}\, dv. \tag{105}$$

Through application of Fourier-transform properties (or directly by substitution of Eq. 105 in Eqs. 103 and 104), the mean and mean square of ρ'_x can be expressed in terms of $M_y(v)$;

$$\overline{\rho'_x} = (1/2j)\,[M_y(\pi/2) - M_y(-\pi/2)] \tag{106}$$

$$\overline{\rho'^2_x} = 0.5\, M_y(0) - 0.25\, M_y(\pi) - 0.25\, M_y(-\pi). \tag{107}$$

Since the characteristic function of a sum of statistically independent random variables is the product of the characteristic functions of the individual terms (see Davenport and Root,[1] p. 54), $M_y(v)$ can be expressed as

$$M_y(v) = \prod_{k=1}^{K} M_k(v), \tag{108}$$

where $M_k(v)$ is the characteristic function of a term, $(1/K) \cdot y(k\Delta t) \cdot y(k\Delta t+\tau)$, in the summation of Eq. 92.

Each of the terms $(1/K)\, y(k\Delta t)\, y(k\Delta t+\tau)$ can assume either of two values, plus or minus $1/K$, with probabilities $2P_{++}$ and $2P_{+-}$, respectively. The probability density function of $(1/K)\, y(k\Delta t)\, y(k\Delta t+\tau)$ then consists of an impulse of area $2P_{++}$ at $1/K$, and an impulse of area $2P_{+-}$ at $-1/K$. The probabilities, $2P_{++}$ and $2P_{+-}$, are given by Eqs. 98 and 99. A Fourier transformation gives the characteristic function, M_k,

$$M_k = 2P_{++}\, e^{jv/K} + 2P_{+-}\, e^{-jv/K}. \tag{109}$$

The mean and mean square of ρ'_x are now given as follows by combining Eqs. 109, 108, 107, 106, 99, and 98.

$$\overline{\rho'_x} = \frac{1}{2j}\left[\left(\cos\frac{\pi}{2K} + j\frac{2}{\pi}\sin^{-1}\rho_x \sin\frac{\pi}{2K}\right)^K - \left(\cos\frac{\pi}{2K} - j\frac{2}{\pi}\sin^{-1}\rho_x \sin\frac{\pi}{2K}\right)^K \right] \tag{110}$$

$$\overline{\rho'^2_x} = \frac{1}{2} - \frac{1}{4}\left[\left(\cos\frac{\pi}{K} + j\frac{2}{\pi}\sin^{-1}\rho_x \sin\frac{\pi}{K}\right)^K + \left(\cos\frac{\pi}{K} - j\frac{2}{\pi}\sin^{-1}\rho_x \sin\frac{\pi}{K}\right)^K \right] \tag{111}$$

Thus expressions giving the mean and mean square of $\rho'_x(\tau)$ have been found in terms of $\rho_x(\tau)$, the true normalized autocorrelation function, and K, the number of statistically independent one-bit products used in the estimate.

Fortunately, the case of interest is for K very large compared with π; in this case Eqs. 110 and 111 are greatly simplified. Terms of higher order than π/K are dropped in the final result. The approximations, in order of their application, are (a and b are constants of the order of π):

1) $\cos a/k \sim 1 - \frac{a^2}{2K^2}$

2) $\sin a/k \sim a/k$

3) $\left(1 + \frac{a}{K} + \frac{b}{K^2}\right)^K \sim e^a\left(1 - \frac{a^2}{2K} + \frac{b}{K}\right)$

The validity of approximation 3) can be demonstrated by taking the logarithm of both sides of the equation and then expanding the logarithm.

Through the use of these approximations the following results are obtained for the mean and variance $\sigma^2_{\rho 1} = \overline{\rho'^2_x} - \overline{\rho'_x}^2$:

$$\overline{\rho'_x} = \rho_x\left[1 + \frac{\pi^2}{8K}\left(\rho_y^2 - 1\right)\right] \tag{112}$$

$$\sigma^2_{\rho 1} = \frac{\pi^2}{4K}\left(1-\rho_x^2\right)\left(1-\rho_y^2\right). \tag{113}$$

Equation 112 reveals that the mean of the estimate is biased by an amount $\rho_x\pi^2\left(1-\rho_y^2\right)/8K$ from the desired value, ρ_x. This bias will be approximately $\sqrt{K}$ times smaller than the rms deviation $\sigma_{\rho 1}$, and hence can be neglected in most cases.

The variance, given by Eq. 113, should be compared with the variance $\sigma^2_{\rho m}$, given by Eq. 82 for an estimate of the normalized autocorrelation function computed from unquantized or many-bit samples. This variance relation also contains the assumption of independent successive products and is repeated here.

$$\sigma^2_{\rho m} = \frac{1 - \rho_x^2}{K} \tag{114}$$

Our conclusion is that the rms deviation of an autocorrelation-function estimate based on K statistically independent products is increased by $(\pi/2)\left[1-\rho_y^2(\tau)\right]^{1/2} \leq \pi/2$ when the samples are quantized to one-bit. In the unquantized case we were able to show that decreasing the time between samples so that successive products become dependent did not decrease the rms deviation. We have not shown that this is true in the one-bit case. It may be possible to reduce the rms deviation by increasing the sampling rate. But this is doubtful, and seems hardly worth the factor of $\pi/2$ which might be gained.

A comparison of one-bit and many-bit autocorrelation function estimates performed as a simulation experiment on a digital computer is given in section 6.2.

3.4 MEAN AND VARIANCE OF THE ONE-BIT POWER SPECTRUM ESTIMATE

An estimate of the power spectrum, p'(f), can be determined from the one-bit autocorrelation-function estimate $\rho'_x(\tau)$ in a manner similar to that used in Eq. 33. This relation is

$$p'(f) = 2\Delta\tau \sum_{n=-\infty}^{\infty} \rho_x'(n\Delta\tau)\, w(n\Delta\tau)\, e^{-j2\pi fn\Delta\tau}. \tag{115}$$

It is assumed that $\rho_x'(n\Delta\tau) = \rho_x'(-n\Delta\tau)$ defines $\rho_x'(n\Delta\tau)$ for negative n, and that the weighting function $w(n\Delta\tau)$ is zero for $|n| \geq N$. Thus $p'(f)$ requires that $\rho_x'(\tau)$ be computed for N equally spaced values of τ going from $\tau = 0$ to $\tau = (N-1)\,\Delta\tau$. The estimate $p'(f)$ is a normalized spectral estimate; that is, Eq. 47 may be used to show that

$$\int_0^{f_s/2} p'(f)\, df = \rho'(0) = 1, \tag{116}$$

where $f_s = 1/\Delta\tau$.

It has been shown that the mean of $\rho_x'(n\Delta\tau)$ is equal to the true normalized autocorrelation function plus a small bias term. This bias term will be neglected, since it is approximately $\sqrt{K}$ times smaller than the rms deviation of $\rho_x'(n\Delta\tau)$. Thus, by taking the mean of both sides of Eq. 115, we find

$$\overline{p'(f)} = 2\Delta\tau \sum_{n=-\infty}^{\infty} \rho(n\Delta\tau)\, w(n\Delta\tau)\, e^{-j2\pi fn\Delta\tau}. \tag{117}$$

The right-hand side of Eq. 117 can be recognized as $p^*(f)$, the smoothed and normalized power spectrum defined by Eq. 83:

$$\overline{p'(f)} = p^*(f). \tag{118}$$

The properties of $p^*(f)$ are fully discussed in sections 2.2 and 2.4b; they will not be discussed further in this section.

A calculation of the variance of $p'(f)$ is quite difficult and was not performed. The spectral variance calculation requires that the covariance of the autocorrelation function estimate be known (see section 2.3a). In section 3.3 the autocorrelation variance was computed through the characteristic-function method. An attempt to extend this method to computation of the autocorrelation covariance leads to difficulty because integrals similar to that for P_{++} (Eq. 96) must be carried out over the trivariate or quadvariate Gaussian probability density functions. The trivariate integral arises if statistically independent products are assumed, and the quadvariate integral arises if this assumption is not made. In neither case was a closed-form evaluation of the integrals found.

It is possible, of course, to evaluate these integrals numerically on a computer for a specific autocorrelation function or power spectrum. Some expansions of the quadvariate normal integral by McFadden[17] may be helpful in this regard. Instead of doing this, we decided to simulate one-bit spectral analysis on a computer and hence determine "experimentally" the spectral variance. This work is presented in section 6.2. An experimental value of the spectral variance as computed from data taken in the deuterium-line experiment is given in section 6.5.

A value for the spectral variance integrated over frequency can be obtained from a mere knowledge of the autocorrelation variance. The following relation is easily derived from the Parseval relation (Eq. 49).

$$\int_0^{f_s/2} \sigma_{p1}^2(f)\, df = 2\Delta\tau \sum_{n=-\infty}^{\infty} \sigma_{\rho 1}^2(n)\, w^2(n\Delta\tau), \tag{119}$$

where $\sigma_{p1}^2(f)$ and $\sigma_{\rho 1}^2(n)$ are the spectral and autocorrelation variances, respectively. The results of the previous section show that, in the case of statistically independent products, $\sigma_{\rho 1}$ is increased by less than $\pi/2$ because of the one-bit quantization. Thus we can say that the integrated spectral variance is increased by less than $\pi^2/4$ on account of one-bit quantization. If it were known that the frequency distribution of the one-bit spectral variance is the same as that of the many-bit spectral variance (this is approximately the case), then it could be said that the spectral variance is increased by less than $\pi/2$ because of one-bit quantization.

It appears safe to postulate that $\sigma_{p1}(f)$ will have the same dependence on the observation time T and resolution Δf as in the many-bit case. Thus we shall express $\sigma_{p1}(f)$ in the form of the many-bit spectral rms deviation $\sigma_{pm}(f)$, given by Eq. 86, multiplied by a numerical factor, β.

$$\sigma_{p1}(f) = \frac{\alpha\beta}{\sqrt{T\Delta f}} \cdot p(f) \cdot \sqrt{1 - \Delta f/b}. \tag{120}$$

Here, α is a dimensionless parameter discussed in section 2.3c, p(f) is the true normalized power spectrum, and b is the total bandwidth of the spectrum being analyzed.

The numerical factor, β, depends somewhat on the particular p(f) that is being analyzed. The experimental results of sections 6.2 and 6.5 indicate that β is equal to 1.39 in the constant bandpass region of a spectrum similar to that shown in Fig. 22. Most spectra analyzed in radio astronomy will have the same gross appearance as the spectrum shown in Fig. 22. This is true because the input spectrum is nearly constant, and thus the gross shape of the measured spectrum is determined primarily by the receiver-bandpass function. At the edges of the receiver bandpass, β increases (see Fig. 22 and Eq. 162), and measurements at frequencies beyond the half-power points have markedly increased statistical uncertainty.

IV. THE RADIO ASTRONOMY SYSTEM

4.1 SYSTEM INPUT-OUTPUT EQUATION

A technique for the measurement of the power spectrum P(f) of a time function x(t) has been presented; the procedure is illustrated in Fig. 7. A spectral estimate, p'(f), is produced. The mean and variance of this estimate are discussed in section 3.4 and reference was made there to sections 2.2 and 2.4b; these results will be briefly summarized here.

It has been assumed that x(t) is a signal in the video-frequency portion of the spectrum; P(f) is zero for f above an upper cutoff frequency, B_{20}. Thus the spectra that we wish to measure in radio astronomy must be restricted (by filtering) to a bandwidth B_{20}, and then must be shifted (by heterodyning) down to the frequency range $0\text{-}B_{20}$. For practical reasons, the heterodyning and filtering will usually be performed in a few steps with the utilization of intermediate frequencies.

The spectrum that we wish to measure in radio astronomy is $T_a(f)$, the power spectrum, expressed in degrees Kelvin, which is available at the antenna terminals. A receiver noise term, $T_r(f)$, must unavoidably be added to $T_a(f)$. According to this statement and that in the preceding paragraph, the function of the radio-frequency portion of the receiver (that is, everything between the antenna and the clipper input) is described by the following equation:

$$P(f) = [T_a(f+f_o) + T_r(f+f_o)]\, G(f+f_o) \qquad f > 0. \tag{121}$$

($P(f) = P(-f)$ defines $P(f)$ for $f < 0$.)

In Eq. 121, f is a frequency in the video-frequency range, f_o is a frequency that is $B_{20}/2$ below the center frequency of the observed frequency range, and $G(f+f_o)$ is the power transfer function of the receiver. $G(f+f_o)$ should be zero outside of the band extending from f_o to $f_o + B_{20}$. The frequency f_o is determined by local oscillator frequencies. These may be chosen so that f_o lies above f; in this case $f_o - f$ should replace $f + f_o$ wherever it occurs.

Equation 121 describes the modifications of the antenna temperature spectrum, $T_a(f)$, by the radio-frequency portion of the receiver. These modifications can be removed, since $T_r(f+f_o)$ and $G(f+f_o)$ can be measured; this topic will be discussed in section 4.2. The modifications resulting from other operations indicated in Fig. 7 are as follows:

1. The clipping of the time function removes the amplitude scale from the measured spectrum; only the shape of the spectrum is determined. All of the measured spectra are necessarily normalized to have unit area. A scale factor can be determined by some other means if it is needed. The measured spectra are thus independent of receiver gain to a high degree.

2. The fact that the autocorrelation function is determined only at discrete points spaced $\Delta\tau$ apart limits the bandwidth that may be analyzed to $1/2\Delta\tau = f_s/2 = B_{20}$. The power spectrum must be forced (by filtering) to be zero outside of this band, or spurious

results will occur. The sampling frequency f_s must be at least twice the bandwidth analyzed.

3. The truncation of the autocorrelation function to N points ($(N-1)\Delta\tau$ is the maximum lag time) limits the frequency resolution Δf of the spectral measurement to approximately $1/(N\Delta\tau) = f_s/N = 2B_{20}/N$. The parameter N is the number of correlation channels provided in the digital correlator. The number of significant points determined on the spectrum, $B_{20}/\Delta f$, thus is equal to $N/2$.

4. The power spectrum of a random time function cannot be exactly measured by any means, since an infinite duration of data is required; this topic was discussed in section 1.3. The quantity that we measure, $p'(f)$, is a statistical estimate of the power spectrum. Its properties are described, for our purposes, by its mean or expected value, $\overline{p'(f)}$, and its variance, $\sigma^2_{p1}(f)$.

The modifications stated above are contained in the equations given below which, together with Eq. 121, relate the measured quantity, $p'(f)$, to the antenna power spectrum, $T_a(f)$:

$$\overline{p'(f)} = \frac{P^*(f)}{\int_0^{f_s/2} P^*(f)\, df} \tag{122}$$

$$P^*(f) = \sum_{i=-\infty}^{\infty} \int_{-\infty}^{\infty} P(a)\, W(f-a-if_s)\, da. \tag{123}$$

Equation 122 expresses the normalization of the spectral estimate; $\overline{p'(f)}$ (and also $p'(f)$) has unit area between 0 and $f_s/2$.

Equation 123 expresses the effects of sampling and truncation of the autocorrelation function. The quantity $P^*(f)$ is related to the true power spectrum $P(f)$ by Eq. 123. This equation is discussed in section 2.2a, and is described in Fig. 8. If sampling is performed at a fast enough rate, all terms in the summation of Eq. 123 are zero, except for the i=0 term, and $P^*(f)$ becomes simply the convolution (or smoothing) of $P(f)$ by $W(f)$. The function $W(f)$ is determined by the choice of the weighting function, $w(\tau)$; this topic is discussed in section 2.2b. In general, $W(f)$ is a narrow, spike-type function of bandwidth $\Delta f = f_s/N$. Thus features in the spectrum narrower then Δf are smoothed out. If $P(f)$ does not change appreciably over bands of width Δf, then $P^*(f) \sim P(f)$, for $0 < f < f_s/2$.

Equation 123 should also be considered as the definition of the star operator which will be used here. A starred quantity is related to the unstarred quantity in the same manner as $P^*(f)$ and $P(f)$ are related. For example,

$$[T(f+f_o)\, G(f+f_o)]^* = \sum_{i=-\infty}^{\infty} \int_{-\infty}^{\infty} T(a+f_o)\, G(a+f_o)\, W(f-a-if_s)\, da. \tag{124}$$

Through the use of the star operator, it is possible to combine Eqs. 121-123 into one compact equation relating the measured quantity, $p'(f)$, to the true power spectrum referred to the receiver input, $T(f) = T_a(f) + T_r(f)$:

$$\overline{p'(f)} = \frac{[T(f+f_o)\, G(f+f_o)]^*}{\int_0^{f_s/2} [T(f+f_o)\, G(f+f_o)]^*\, df} . \tag{125}$$

4.2 SPECIFICATION OF ANTENNA TEMPERATURE

The noise-power spectrum available at the antenna terminals, $T_a(f+f_o)$, can be estimated if some auxiliary calibration measurements are made in addition to the measurement of $p'(f)$. These auxiliary measurements are of the receiver bandpass $G(f+f_o)$; the average (over frequency) noise temperature referred to the receiver input T_{av}; and the receiver noise power spectrum $T_r(f+f_o)$.

a. Correction of the Effect of Receiver Bandpass

The receiver bandpass can be accurately measured by observing the system output, $p'_o(f)$, when the input, $T(f+f_o)$, is white noise (uniform spectrum over the frequency range $G(f+f_o)$ is nonzero). In this case, Eq. 125 gives the system output

$$\overline{p'_o(f)} = \frac{G^*(f+f_o)}{\int_0^{f_s/2} G^*(f+f_o)\, df} . \tag{126}$$

Before discussing the manner in which $p'_o(f)$ is applied, the problem of obtaining a white $T(f+f_o) = T_a(f+f_o) + T_r(f+f_o)$ will be discussed. This problem is simplified if $T_r(f+f_o)$ is white, as is often the case when the receiver front-end is broadband compared with B_{20}. If this is the case, a white $T(f+f_o)$ can be produced by any of three methods:

1. Pointing the antenna at a region where no spectral line is expected.
2. Connecting a white-noise generator (such as a match load at 300° K) to the receiver input in place of the antenna.
3. By detuning the first local oscillator, if the receiver is broadband between the input and the first converter.

Each of these methods has special problems that must be considered. It should be pointed out that the receiver bandpass need not be determined too accurately once the large receiver noise term is subtracted off (see section 4.2c).

If the receiver noise is not white, a $T(f+f_o)$ that is nearly white can still be obtained by application of a white T_a that is much greater than $T_r(f+f_o)$. This may be accomplished with method 2 or with method 1 if a large enough T_a can be obtained from a

strong radio source. Attenuation should be inserted into the receiver so that the clippers are operating at approximately the normal signal level.

The measurement of $p'_o(f)$ is applied by dividing $p'(f)$ by $p'_o(f)$ to give

$$\left[\overline{\frac{p'(f)}{p'_o(f)}}\right] = \frac{[T(f+f_o)\, G(f+f_o)]^*}{T_{av} \cdot G^*(f+f_o)}, \tag{127}$$

where T_{av} is a measured quantity that will be discussed below and is given by

$$T_{av} = \frac{\int_0^{f_s/2} [T(f+f_o)\, G(f+f_o)]^*\, df}{\int_0^{f_s/2} G^*(f+f_o)\, df}. \tag{128}$$

An approximation has been used in Eq. 127, in that $\overline{p'(f)/p'_o(f)}$ has been assumed equal to $\overline{p'(f)}/\overline{p'_o(f)}$. This is quite valid, since the random part of $p'_o(f)$ is small compared with its mean.

The quantity $[T(f+f_o)\, G(f+f_o)]^*/G^*(f+f_o)$ has an important interpretation, and it is therefore convenient to assign a special dagger symbol for this operation on $T(f+f_o)$. Thus $T^\dagger(f+f_o)$ is defined as

$$T^\dagger(f+f_o) \equiv \frac{[T(f+f_o)\, G(f+f_o)]^*}{G^*(f+f_o)} \tag{129}$$

with identical relations between $T^\dagger(f+f_o)$ and $T_a(f+f_o)$ and between $T_r^\dagger(f+f_o)$ and $T_r(f+f_o)$. The mathematical relationship between $T^\dagger(f+f_o)$ and $T(f+f_o)$ is quite complicated; however, the relationship greatly simplifies when a restriction is applied to the shape of $G(f+f_o)$. The restriction is that $G(f+f_o)$ must be smooth over frequency bands of width Δf for values of f in the passband region (say, between 1-db points). Stated another way,

$$G^*(f+f_o) \sim G(f+f_o) \tag{130}$$

for f in the passband region. This condition is easily met in practice.

Under this condition, $T^\dagger(f+f_o)$ becomes simply the convolution or smoothing of $T(f+f_o)$ by $W(f)$; that is,

$$T^\dagger(f+f_o) = \int_{-\infty}^{\infty} T(\alpha+f_o)\, W(f-\alpha)\, d\alpha \tag{131}$$

for values of f in the bandpass region. (The requirement that $G(f+f_o)$ be bandlimited to half the sampling frequency has also been used in Eq. 131.) Thus a dagger superscript

on $T(f+f_o)$, $T_a(f+f_o)$ or $T_r(f+f_o)$ should be considered as a smoothing operation on these spectra. If f is outside the 1-db receiver bandwidth, or if the condition of Eq. 130 is not true, then the dagger operator must be interpreted by Eq. 129. Note that one cannot say "$[G(f+f_o)\, T(f+f_o)]^* = G^*(f+f_o)\, T^*(f+f_o)$."

Through the use of the dagger operator, then, Eq. 127 becomes

$$\overline{\left[\frac{p'(f)}{p'_o(f)}\right]} = \frac{T^\dagger(f+f_o)}{T_{av}} \tag{132}$$

$$= \frac{T_a^\dagger(f+f_o) + T_r^\dagger(f+f_o)}{T_{av}} \,. \tag{133}$$

The smoothed antenna temperature $T_a^\dagger(f+f_o)$ is thus expressed in terms of measurable quantities by Eq. 133.

b. Measurement of T_{av}

The quantity T_{av} defined by Eq. 128 can be expressed in a more usable form through the use of a property of the star operator given by Eqs. 47 and 48. These equations show that the integral of a starred variable between limits 0 and $f_s/2$ is equal to the integral of the unstarred variable between limits of 0 and ∞. Thus T_{av} becomes

$$T_{av} = \frac{\int_0^\infty T(f+f_o)\, G(f+f_o)\, df}{\int_0^\infty G(f+f_o)} \,, \tag{134}$$

and is recognized to be the average input noise temperature weighted by the receiver bandpass. It is the temperature that is determined if the receiver is used for continuum (broadband) measurements.

T_{av} is proportional to the power in the signal at the clipper input and is easily determined by conventional means. Note that T_{av} includes both the antenna temperature and the receiver-noise temperature, $T_{av} = T_{a\,av} + T_{r\,av}$. All temperature measurements performed with the one-bit autocorrelation system are normalized to T_{av}, as expressed in Eq. 133.

c. Measurement of $T_r^\dagger(f+f_o)$

The spectral-measurement system determines the sum, $T^\dagger(f+f_o)$, of the smoothed antenna-temperature spectrum, $T_a^\dagger(f+f_o)$, and the smoothed receiver noise-temperature spectrum, $T_r^\dagger(f+f_o)$. Thus, we wish to determine $T_r^\dagger(f+f_o)$ and subtract this from $T^\dagger(f+f_o)$. The measurement of $T_r^\dagger(f+f_o)$ is accomplished by applying a signal with a known, white, comparison spectrum, T_c, to the antenna terminals. The system output, $p'_c(f)$, divided by $p'_o(f)$, then gives

$$\left[\overline{\frac{p_c'(f)}{p_o'(f)}}\right] = \frac{T_c + T_r^\dagger(f+f_o)}{T_{c\,av}}\,, \tag{135}$$

where $T_{c\,av} = T_c + T_{r\,av}$ is the measured average input temperature with the comparison source connected. Equation 135 thus determines $T_r^\dagger(f+f_o)$ in terms of measured quantities.

It should be noted that if T_r is white, the measurements of $p_c'(f)$ and $p_o'(f)$ are identical and $p_c'(f) = p_o'(f)$. In this case, T_r is completely determined by the measurement of $T_{c\,av}$.

d. Summary

The smoothed antenna-temperature spectrum, $T_a^\dagger(f+f_o)$, is specified by the measurement of two frequency-averaged antenna temperatures, T_{av} and $T_{c\,av}$, and three normalized power spectra, $p'(f)$, $p_c'(f)$, and $p_o'(f)$. Both T_{av} and $p'(f)$ are signal measurements; they are performed with the antenna connected to the receiver input and pointed in the desired direction. The three other quantities are auxiliary measurements used to specify the receiver noise-temperature spectrum $T_r(f+f_o)$ and the receiver response $G(f+f_o)$. They are determined with a known comparison spectrum applied to the receiver input at some time before or after the signal measurements are performed. Equations 133 and 135 can be combined to specify $T_a^\dagger(f+f_o)$ in terms of these five measured quantities:

$$T_a^\dagger(f+f_o) = T_{av}\left[\overline{\frac{p'(f)}{p_o'(f)}}\right] - T_{c\,av}\left[\overline{\frac{p_c'(f)}{p_o'(f)}}\right] + T_c. \tag{136}$$

Here, T_c is the temperature of a known, white, comparison spectrum, and f_o is known from the local-oscillator frequencies.

If the receiver noise-temperature spectrum is equal to a constant value, T_r, over the frequency band under observation, B_{20}, then $p_c'(f) = p_o'(f)$, and Eq. 136 reduces to

$$T_a^\dagger(f+f_o) = T_{av}\left[\overline{\frac{p'(f)}{p_o'(f)}}\right] - (T_{c\,av} - T_c), \tag{137}$$

where $T_{c\,av} - T_c = T_r$.

4.3 THE SWITCHED MODE OF OPERATION

a. Motivation and Description

We have seen that the measurement of the antenna temperature depends on auxiliary measurements performed before or after the actual observation. The problem of error resulting from changes in the receiver characteristics [$T_r(f+f_o)$ and $G(f+f_o)$] between the time the observation is made and the time the auxiliary measurements are made then

arises. These changes may be made small (of the order of a few tenths of a per cent in a 10-minute interval) by careful circuitry, but are important in view of the high accuracy needed in spectral measurements in radio astronomy. The high accuracy is required because the spectrum that we wish to measure, $T_a(f+f_o)$, is superimposed on a receiver-noise spectrum, $T_r(f+f_o)$, which may be many times $T_a(f+f_o)$. The problem is aggravated by the fact that the time duration, T, that is required for a spectral measurement increases as higher accuracy is desired (Eq. 20).

An approach to this problem is to periodically switch between the actual signal measurement and the calibration measurement. The switching is accomplished with a mechanical, ferrite or diode switch which alternately connects the receiver input to the antenna terminals, or to a noise source generating a uniform comparison spectrum, T_c. Switching rates between 10 cps and 400 cps are usual. While the switch is at the antenna position, the signal measurements $p'(f)$ and T_{av} are being performed (that is, a segment of integration time is accumulated); with the switch at the noise source position, the comparison measurements $p'_c(f)$ and $T_{c\,av}$ are performed. At the output end of the receiver, a second switch (usually of the diode type) is used either to separately totalize signal and comparison variables or, more commonly, to totalize the difference between signal and comparison variables. The switching technique has been extensively used in radio astronomy; the Dicke radiometer is based on this principle.

The switching technique, as it is used with the digital autocorrelation system, is diagrammed in Figs. 11 and 12. The digital correlator is gated in phase with the front-end switch to add the products $y(k\Delta t)\, y(k\Delta t + n\Delta\tau)$, which occur when the switch is at the antenna position, and subtract the products that occur when the switch is at the noise-source position. The quantity that is determined by the digital correlator is $\delta\rho'_y(n\Delta\tau) = \rho'_y(n\Delta\tau) - \rho'_{yc}(n\Delta\tau)$, the difference between the estimates of the one-bit autocorrelation functions of the antenna signal (plus receiver noise) and the noise-source signal (plus receiver noise). When $\delta\rho'_y(n\Delta\tau)$ is properly corrected and Fourier transformed, the difference spectrum $\delta p'(f) = p'(f) - p'_c(f)$ is determined.

The correction of $\delta\rho'_y(n\Delta\tau)$ to give the difference of the unclipped autocorrelation function estimates, $\delta\rho'_x(n\Delta\tau) = \rho'_x(n\Delta\tau) - \rho'_{xc}(n\Delta\tau)$, is not straightforward. Application of the usual correction, Eq. 101, gives

$$\delta\rho'_x(n\Delta\tau) = \sin\left[\pi\rho'_y(n\Delta\tau)/2\right] - \sin\left[\pi\rho'_{yc}(n\Delta\tau)/2\right]. \tag{138}$$

This relation is not usable as it stands because $\rho'_y(n\Delta\tau)$ and $\rho'_{yc}(n\Delta\tau)$ are not separately determined in the digital correlator; only their difference, $\delta\rho'_y(n\Delta\tau)$, is available. This is due to an economic consideration in the design of the digital correlator. But $\rho'_{yc}(n\Delta\tau)$ can be determined at some time, before or after the actual observation time, and the correction equation can be put in the usable form

$$\delta\rho'_x(n\Delta\tau) = 2\sin\frac{\pi\delta\rho'_y(n\Delta\tau)}{4}\cdot\cos\frac{\pi[2\rho'_{yc}(n\Delta\tau) + \delta\rho'_y(n\Delta\tau)]}{4}. \tag{139}$$

Small errors in the measurement of $\rho'_{yc}(n\Delta\tau)$ are not important, since $\rho'_{yc}(n\Delta\tau)$ is used

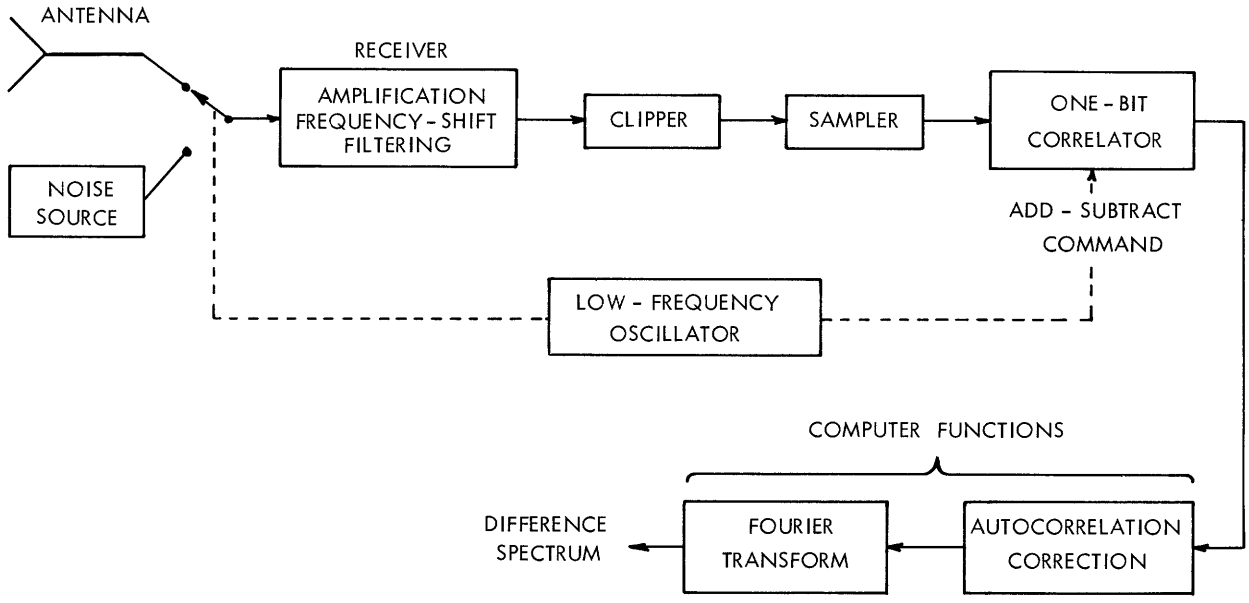

Fig. 11. The switched one-bit autocorrelation radiometer system. The detailed receiver and correlator block diagrams are given in Figs. 13 and 17.

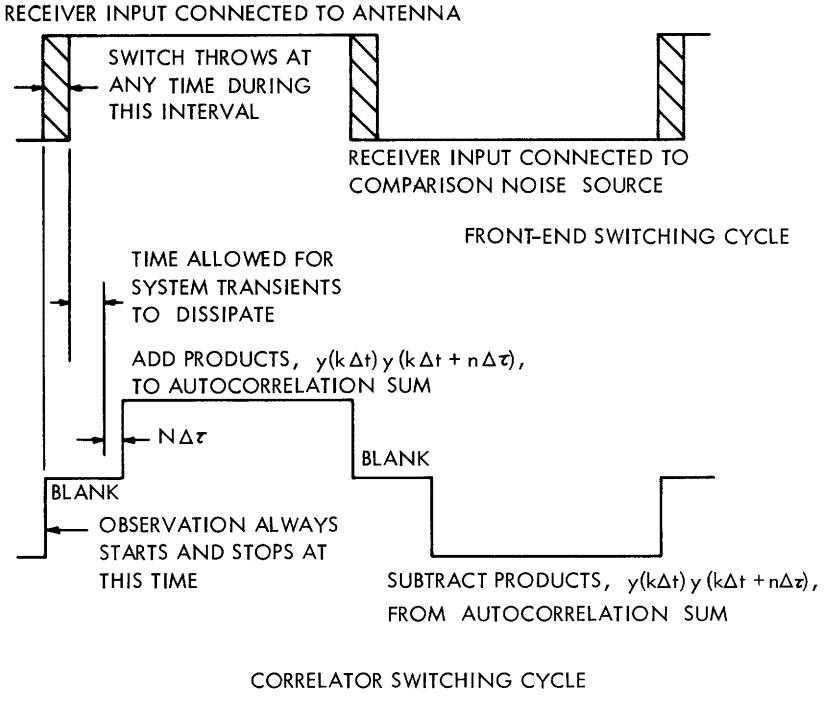

Fig. 12. Illustrating the timing of the front-end switch and correlator operations in a switched autocorrelation radiometer. The timing of operations is best controlled by precise counts of the correlator sampling pulses. For example, in the deuterium-line correlator the blanking interval is 256 counts long, and the add and subtract intervals are each 768 counts long. This gives 2048 counts for a complete cycle, and thus the switching rate is 37.4 cps for the 75-kc sampling rate.

here only to modify a difference of autocorrelation functions.

It should be noted that the analysis of the switched system is being treated on a static basis. We are neglecting the fact that the system "remembers" the signal from the previous switch position. If the system time constants (the longest is of the order of $1/\Delta f$) are short compared with the switching period, the static approximation is good. If, however, a blanking interval is inserted after each switch throw (see Fig. 12), the static approximation is almost exact. During the blanking interval, the correlator samples, delays, and multiplies as usual; however, the products $y(k\Delta t)\, y(k\Delta t + n\Delta\tau)$ that occur are not added into the sum that forms the autocorrelation-function estimate. The blanking interval simplifies the analysis, eliminates possible error arising from the switching transient, and removes the problem of fluctuations in a switch dwell time or "jitter" in a mechanical switch.

b. Antenna-Temperature Equation

The antenna temperature can be expressed in terms of the difference quantities $\delta p'(f)$ and δT_{av} by substitution of $p'(f) = p'_c(f) + \delta p'(f)$ and $T_{av} = T_{c\,av} + \delta T_{av}$ in Eq. 136. The result is

$$T_a^{\dagger}(f+f_o) = (T_{c\,av} + \delta T_{av}) \left[\overline{\frac{\delta p'(f)}{p'_o(f)}}\right] + \delta T_{av} \left[\overline{\frac{p'_c(f)}{p'_o(f)}}\right] + T_c. \tag{140}$$

The quantities $T_{c\,av}$, $p'_o(f)$, and $p'_c(f)$ must still be measured at some time before or after the signal measurements. But they have only a weak effect upon the spectral measurement, since they only modify the difference quantities $\delta p'(f)$ and δT_{av}.

If the receiver-noise spectrum is white, $p'_c = p'_o$, and Eq. 140 can be put in the convenient form

$$\frac{T_a^{\dagger}(f+f_o) - T_{a\,av}}{T_{av}} = \left[\overline{\frac{\delta p'(f)}{p'_o(f)}}\right], \tag{141}$$

in which the relations $T_{av} = T_{c\,av} + \delta T_{av}$ and $T_{a\,av} = T_c + \delta T_{av}$ have been used. This same result arises, even if T_r is not white, if the radiometer is balanced so that $\delta T_{av} = 0$ and $T_c = T_{a\,av}$.

The antenna temperature equation can be put in many other forms that may have special value or interpretation for specific experiments. A form that was used in the deuterium-line and Zeeman experiments is

$$\frac{T^{\dagger}(f+f_o) - T_{av}}{T_{av}} = \left[\overline{\frac{\delta p'(f)}{p'_o(f)}}\right], \tag{142}$$

which is easily derived from Eq. 140 under the assumption of a white receiver-noise spectrum.

4.4 SYSTEM SENSITIVITY

The sensitivity of a radiometer is specified by the rms deviation, $\Delta T(f+f_o)$, of the antenna-temperature measurement from its mean value, $T_a^{\dagger}(f+f_o)$. The minimum detectable antenna temperature depends on the desired confidence limits; a value of a few times $\Delta T(f+f_o)$ is usually adopted.

The rms deviation, $\sigma_{p1}(f)$, of a normalized spectral estimate, $p'(f)$, obtained by the one-bit autocorrelation method is given by Eq. 120 as

$$\frac{\sigma_{p1}(f)}{p(f)} = \frac{\alpha\beta}{\sqrt{\tau\Delta f}} \cdot \sqrt{1-\Delta f/b}, \tag{143}$$

where

τ is the duration of the signal observation;

Δf is the frequency resolution (it is the half-power bandwidth of $W(f)$);

α is a dimensionless parameter of the order of unity; it depends on the exact shape of $W(f)$, and is given in section 2.2c.

β is the increase in rms deviation caused by the clipping or one-bit operation; it is discussed in sections 3.4, 6.2, and 6.5. It has the value 1.39 in the midband region (say, between 1-db points) of the receiver bandpass, and increases according to Eq. 160 on the edges of the receiver bandpass.

b is the total noise bandwidth of the measured spectrum; it is approximately equal to the half-power receiver bandwidth.

The specification of the antenna temperature depends, through Eq. 156, on three normalized spectral measurements, $p'(f)$, $p'_c(f)$, and $p'_o(f)$, and two frequency-averaged antenna temperature measurements, T_{av} and $T_{c\,av}$. The rms deviation of the antenna temperature can be expressed in terms of the rms deviations of each of these measurements. This is accomplished by expanding each of these quantities in Eq. 136 as its mean plus a small random part. The random part is then squared, a statistical average is taken, and higher order terms are dropped. The result of these operations is that $\Delta T(f+f_o)$ is equal to the square root of the sum of the squares of the following terms:

$$T_{av}\frac{(\sigma_{p1})_s}{p_o}, \quad T_{c\,av}\frac{(\sigma_{p1})_c}{p_o}, \quad \frac{p_1}{p_o}\Delta T_{av}$$

$$\frac{p_c}{p_o}\Delta T_{c\,av}, \quad \text{and} \quad (T_a - T_c)\frac{(\sigma_{p1})_o}{p_o}$$

in which $(\sigma_{p1})_s$, $(\sigma_{p1})_c$, and $(\sigma_{p1})_o$ refer to the rms deviations of $p'(f)$, $p'_c(f)$, and $p'_o(f)$, respectively.

We now make two assumptions: (a) the radiometer is near balance, so that $T_{av} \sim T_{c\,av}$; and (b) the amplitude of the observed spectral line is small compared with

white receiver noise, so that $p(f) \sim p_c(f) \sim p_o(f)$. The expression for the rms deviation then becomes

$$\frac{\Delta T^2}{T_{av}^2} = \frac{(\sigma_{p1})_s^2}{p^2} + \frac{(\sigma_{p1})_c^2}{p^2} + \frac{\Delta T_{av}^2}{T_{av}^2} + \frac{\Delta T_{c\,av}^2}{T_{c\,av}^2} + \frac{(T_a^\dagger - T_c)^2}{T_{av}^2} \frac{(\sigma_{p1})_o^2}{p^2}. \tag{144}$$

The first two terms of Eq. 144 are the largest, and represent the variances of the measurements of the normalized signal and comparison spectra, $p'(f)$ and $p'_c(f)$, respectively. These variances are given by Eq. 143 with the observation time τ equal to τ_s in the signal case, and to τ_c in the comparison case. The third and fourth terms represent the variance of the measurements of T_{av} and $T_{c\,av}$. Their exact values depend on the manner in which T_{av} and $T_{c\,av}$ are measured. Since they are approximately $b/\Delta f$ times smaller than the first two terms, they are given with sufficient accuracy by

$$\frac{\Delta T_{av}^2}{T_{av}^2} = \frac{a^2\beta^2}{\tau_s b} \tag{145}$$

and

$$\frac{\Delta T_{c\,av}^2}{T_{c\,av}^2} = \frac{a^2\beta^2}{\tau_c b}. \tag{146}$$

The final term in Eq. 144 is very small if the radiometer is near balance, or equivalently if $(T_a^\dagger - T_c)/T_{av} \ll 1$. If $(T_a^\dagger - T_c)/T_{av}$ is equal to ϵ, then the observation time for the measurement of $p'_o(f)$ can be as short as $10\epsilon^2\tau_s$ before the final term becomes 0.1 of the first term. This final term will be neglected in further equations.

Accordingly, then, the rms deviation can be expressed as

$$\frac{\Delta T}{T_{av}} = a\beta\sqrt{\frac{1}{\tau_s \Delta f} + \frac{1}{\tau_c \Delta f}}, \tag{147}$$

where τ_s and τ_c are the signal and comparison observation times. If τ is the total observation time (not including time spent in blanking), $\tau_s = 0.5\tau$ and $\tau_c = 0.5\tau$, so that Eq. 147 becomes

$$\frac{\Delta T}{T_{av}} = \frac{2a\beta}{\sqrt{\tau \Delta f}}. \tag{148}$$

V. SYSTEM COMPONENTS

A brief discussion of the design parameters and design approaches of the major components of a switched one-bit autocorrelation radiometer (see Fig. 11) will be presented here. The deuterium-line detection system will be used as an example. The discussion is presented in sections concerning the radio-frequency part of the system, the clipping and sampling operation, and the one-bit digital correlator.

5.1 RADIO-FREQUENCY PART OF THE SYSTEM

This section is concerned with the part of the system that lies between the antenna terminals and the input to the clipper. The material in Section IV is drawn upon heavily in this section. The block diagram of the radio-frequency portion of the deuterium-line detection system is shown in Fig. 13.

a. Front-End Switch and Noise Source

Two highly important components in any switched radiometer are the switch and the comparison noise source. The quantity that is directly measured by the radiometer is the difference between the comparison noise-source spectrum, T_c, transferred through the switch, and the antenna temperature spectrum, T_a, transferred through the other arm of the switch. The comparison spectrum and switch-transfer characteristics must either be measured or assumed to be linear functions of frequency. The first of these alternatives can be achieved by using a celestial radio source of known spectrum as a "primary" standard to measure T_c, which then becomes a "secondary" standard.

The frequency variations of the switch and noise source have little effect if they can be assumed to be linear with frequency and if the linear component of the true spectrum is known or is not needed. The linear-with-frequency assumption is justified when the analyzed bandwidth, B_1, is narrow compared with the frequency scale of changes in the characteristics of the switch and noise source. The linear component of the true spectrum is known when the analyzed bandwidth is somewhat greater than the bandwidth of the spectral line so that the background spectrum at frequencies above and below the spectral line can be established.

In the deuterium-line experiment B_1 = 30 kc at a center frequency of 327 mc. The switch and noise source are by no means high-Q devices, and thus their characteristics change appreciably only over a scale of tens of megacycles. The measured spectra had slopes of approximately 0.05 per cent/30 kc which were removed in a computer so that the final result had zero slope. This slope correction did not disturb the results of the experiment because the spectrum should have nearly zero slope whether or not the deuterium line is present.

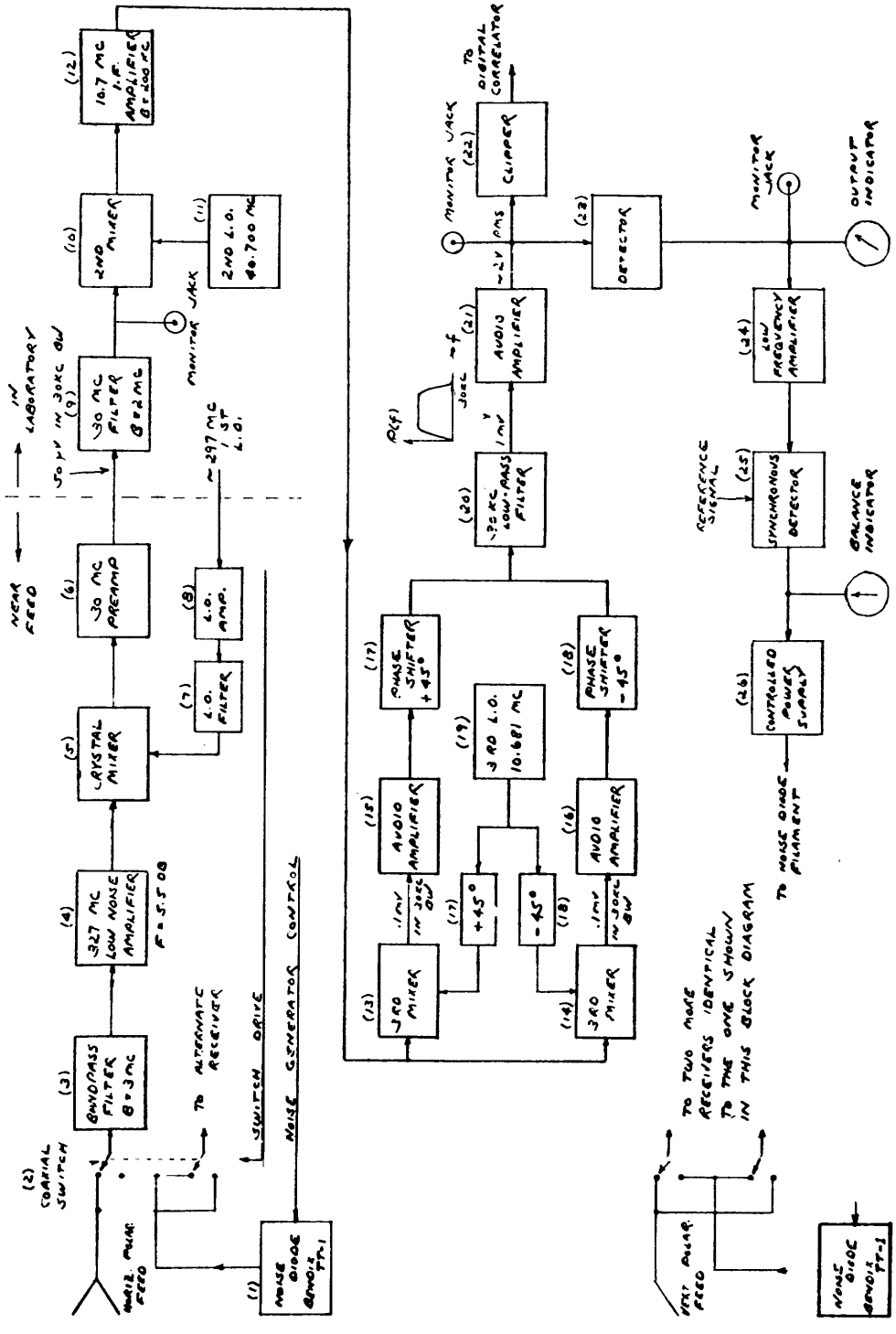

Fig. 13. Radio-frequency part of the deuterium-line system.

b. Balance Requirements

The antenna-temperature equation (120) contains a term, $\delta T_{av}\,\overline{p'_c(f)/p'_o(f)}$, which represents the effect of unbalance ($\delta T_{av} \neq 0$) in the radiometer. This term should be kept small in order to avoid errors arising from time variations in the receiver-noise spectrum, $T_r(f+f_o)$. The magnitude of this term is placed in evidence by application of Eq. 115 and expansion of $T_r^\dagger(f+f_o)$ as $T_{r\,av} + \delta T_r^\dagger(f+f_o)$, and $T_c^\dagger(f+f_o)$ as $(T_c)_{av} + \delta T_c^\dagger(f+f_o)$. The terms $\delta T_r^\dagger(f+f_o)$ and $\delta T_c^\dagger(f+f_o)$ thus represent the frequency variations of the receiver-noise spectrum about their frequency-averaged values. The result is

$$\delta T_{av}\overline{\left[\frac{p'_c(f)}{p'_o(f)}\right]} = \frac{\delta T_{av}}{T_{c\,av}}\left[T_{c\,av} + \delta T_r^\dagger(f+f_o) + \delta T_c^\dagger(f+f_o)\right] \tag{149}$$

which is small if the radiometer is near balance; and is nearly constant if the receiver-noise spectrum and the comparison spectrum are nearly constant with frequency.

In the deuterium-line experiment a servo loop was used to hold $\delta T_{av}/T_{c\,av}$ to less than 0.3 per cent, and $\delta T_r^\dagger(f+f_o)$ and $\delta T_c^\dagger(f+f_o)$ were each estimated to be less than 1° (they are small because of the narrow bandwidth B_1). The term given by Eq. 149 is equal to a constant (<6°) and a frequency-varying component that is less than 0.006°. The constant term has negligible effect and the small frequency-varying term will be linear to first order, and will be removed by the previously mentioned linear correction. Therefore, in the deuterium-line experiment, the unbalance term $\delta T_{av}\,\overline{p'_c(f)/p'_o(f)}$ could be neglected. In other applications it may be necessary to determine $p'_c(f)$ and δT_{av} ($p'_o(f)$ is needed anyway) and include the unbalance term in the antenna-temperature equation.

There are two more reasons for operating the radiometer near balance. The first is due to the fact that the clippers have different characteristics when operated at different signal levels (see section 5.2 and Fig. 14). If the signal and comparison power levels differ appreciably, a resulting error may occur in the difference spectrum $\delta p'(f)$. This error should be negligible with proper clipper design, and if $\delta T_{av}/T_{av}$ is kept below a few per cent. A final reason for operating the radiometer near the balanced condition is that T_{av} must be measured by conventional Dicke radiometer techniques. It is well known that the error owing to gain fluctuations in this measurement will be small if the radiometer is near balance.

c. Shape of the Receiver Bandpass, $G(f+f_o)$

The function of the radio-frequency part of the system is described by the equation

$$P(f) = G(f+f_o)\,T(f+f_o) \qquad f > 0, \tag{150}$$

where $P(f)$ is the power spectrum at the input of the clipper, $G(f+f_o)$ is the power transfer function of the receiver, $T(f+f_o)$ is the power spectrum referred to the receiver input, and f_o is determined by local-oscillator frequencies ($P(f) = P(-f)$ defines $P(f)$ for $f<0$).

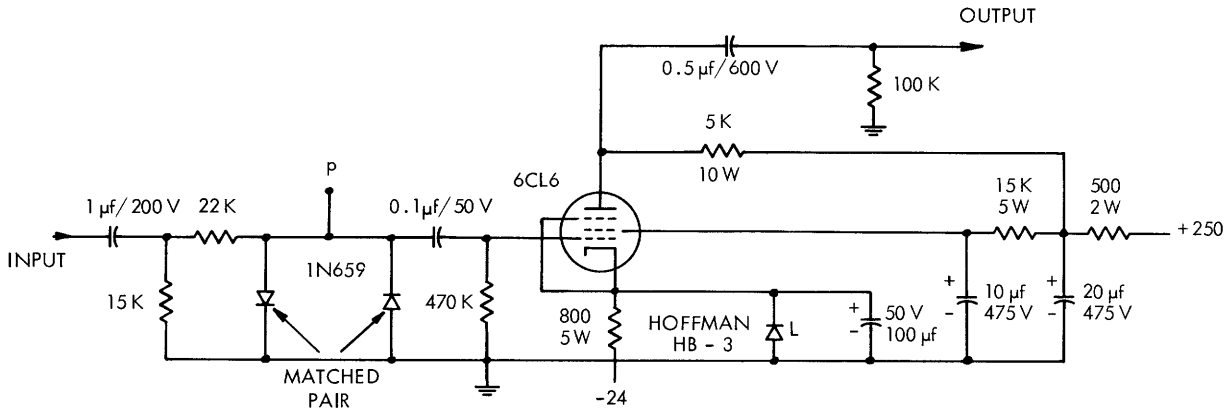

TYPICAL CLIPPER STAGE

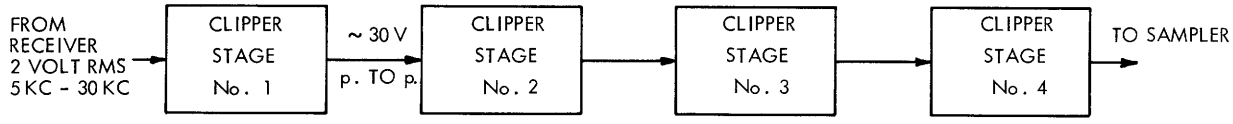

Fig. 14. Clipping circuitry for the deuterium-line receiver. The IN659 silicon diodes conduct heavily when their forward-bias voltage exceeds 0.5 volt; thus the voltage at point P is approximately a 1-volt peak-to-peak square wave. The gain of the amplifier stage is approximately 30.

The requirements concerning the shape of $G(f+f_o)$ will be presented here; in section 5.1c the frequency-conversion problem will be discussed.

A major requirement of $G(f+f_o)$ is that it be very small for f greater than half the sampling frequency, f_s. This is necessary in order to avoid spurious responses caused by sampling (see Figs. 3 and 8). For the deuterium-line receiver, $G(f+f_o)$ was designed to be 20 db down at half the sampling frequency.

A second requirement for $G(f+f_o)$ is that it have a fairly uniform passband. This is necessary because the statistical uncertainty (rms deviation divided by the mean) of the spectral measurement increases at frequencies when $G(f+f_o)$ decreases (see Fig. 22 and Eq. 162). Experimental results presented in section 6.2 indicate that the statistical uncertainty will increase less than 10 per cent in regions where $G(f+f_o)$ is within 1 db (26 per cent) of its maximum value. A criterion of a passband flat within ±0.5 db was chosen for the deuterium-line receiver.

A third requirement for $G(f+f_o)$ is that it become very small for f near zero frequency. This requirement arises because of several practical considerations such as difficulty in constructing DC coupled amplifiers and clippers, difficulty in obtaining image rejection in the final frequency converter for frequencies near zero, and errors resulting from DC offset in the clipping operation. If a spectrum containing low-frequency components is fed into AC coupled clipper stages, the spectral measurement

at higher frequencies may be upset. Thus, these low-frequency components should be removed by highpass filtering previous to the clipping operation. The spectrum that is within 1 or $2\Delta f$ of zero frequency should be disregarded, as it may contain an error caused by DC offset in the clippers (although the switching technique removes most of this error).

Assuming that the 20-db bandwidth B_{20} is set equal to half the sampling frequency and that the 1-db bandwidth B_1 is the region where a good spectral measurement is obtained, the ratio $r = B_1/B_{20}$ becomes an important parameter describing $G(f+f_o)$. The frequency resolution Δf is proportional to the sampling frequency ($\Delta f \sim f_s/N \sim 2B_{20}/N$); and thus the ratio of the usable bandwidth analyzed, B_1, to the frequency resolution, Δf, is proportional to r ($B_1/\Delta f \sim rN/2$). For efficient use of N, the number of correlator channels, r, should be as close to unity as possible with practical filter designs. A value $r = 0.67$ was used in the deuterium-line receiver; other parameters were $f_s = 75$ kc, $B_{20} = 37.5$ kc, $B_1 = 25$ kc, $N = 21$, and $\Delta f = 3.75$ kc.

d. Frequency Conversion and Filtering

There are a few approaches to the frequency-conversion problem. If a crystal filter with the desired bandwidth is available, it may be used in the IF amplifier (usually 10.7 mc or 30 mc center frequency) to give the desired response. A second mixer then shifts the spectrum down to $0\text{-}B_{20}$ cps. This technique was not used in the deuterium-line experiment because it was feared that the ripples in the crystal-filter bandpass might cause a false deuterium-line result. Of course, a correction is made for the receiver response (by division by $p'_o(f)$, see section 4.2a) but some error may result in this correction. This is another reason why it is desirable to have a uniform passband.

In the deuterium-line receiver, a phase-shift technique used in single-sideband receivers[18] was applied to give a $G(f+f_o)$ with a sharp cutoff and a uniform passband. By conventional means, a wideband portion of the input spectrum is converted to a center frequency of 10,700 kc. This signal is then heterodyned with a 10,681-kc local oscillator and passed through a lowpass filter having $B_{20} = 37.5$ kc. The output of the lowpass filter contains the desired spectrum (which was between 10,681 kc and 10,718.5 kc) but also contains the image spectrum (which was between 10,643.5 kc and 10,681 kc). A method utilizing 90° phase-shift networks (see Fig. 13) is utilized to cancel this image.

The advantage of the phase-shift method is that the bandpass is primarily determined by a stable lowpass filter that is more easily realized (requiring lower Q elements, less affected by variations in the elements, little or no adjustments necessary) than a bandpass filter. The disadvantage is that it is difficult to obtain constant phase shift over a wide range of frequencies; a phase-shift error results in incomplete cancellation of the image. In the deuterium-line receiver, phase-shift networks giving 25-db image rejection for frequencies between 3.75 kc and 37.5 kc were designed according to information

given by Luck.[19] The band of frequencies below 3.75 kc was eliminated by a highpass filter. The final result was a usable, uniform passband between 5 kc and 30 kc.

A third method of performing the filtering and frequency conversion is to utilize L-C bandpass filters with multiple-stage frequency conversion to reduce Q problems and image-rejection problems. (It is difficult to realize bandpass filters having good skirt selectivity unless the center frequency to bandwidth ratio is not too large, say, less than 15. Furthermore, if this ratio is large, the shape of the response is very critical to small changes in the L and C values.) For example, suppose it is desired to select a 30-kc band out of a 2-mc wide IF bandpass centered at 30 mc. A reasonable conversion process would be to place a second IF bandpass, 200 kc wide, centered at 2000 kc and a third IF bandpass, 30 kc wide, centered at 200 kc. A fourth mixer would then shift this band down between 0 and 30 kc. The obvious disadvantage of this method is the complexity.

5.2 CLIPPERS AND SAMPLERS

It is quite easy to describe the ideal clipper and ideal sampler. The clipper output $y(t)$ equals 1 when the input $x(t)$ is greater than 0, and $y(t) = 1$ when $x(t) < 0$. The sampler output $y(k\Delta t)$ is the instantaneous value of $y(t)$ at $t = k\Delta t$. (The clipper output is not actually 1 or −1, but is either of two voltage levels that are interpreted to mean 1 and −1 by the sampler and digital correlator.)

Real clippers and samplers can come close to this ideal behavior. They are very difficult to describe and analyze, and, most important, it is difficult to calculate the error in the spectral measurement that is caused by nonideal sampling and clipping. The areas in which this nonideal behavior exists and the approaches used in the deuterium-line receiver are as follows:

1. Real clippers are more accurately characterized by an output $y(t)$, which is equal to +1 when $x(t)$ is greater than a small voltage ϵ_+, and $y(t) = -1$ when $x(t)$ is smaller than ϵ_-. When $x(t)$ is between ϵ_- and ϵ_+, the output may be +1 or −1 or some value in between. Furthermore, ϵ_- and ϵ_+ may depend on the past history of $x(t)$ and may themselves be functions of time (caused by noise fluctuations, 60-cps hum, or slow drifts caused by temperature changes).

Fortunately, the effect of nonzero clipping levels can be reduced to any degree simply by increasing the amplitude of the signal before clipping. The clippers used in the deuterium-line receiver (see Fig. 14) had values ϵ_+ and ϵ_- of less than 20 mv. A signal level 40 db above this (2 volts rms) was used with satisfactory results.

2. The ideal clipper response is independent of the frequency of the input signal. The real clipper is affected at high frequencies by stray capacities, and at low frequencies by coupling capacitors (if successive stages are AC coupled). In the deuterium-line receiver, the time constants were arranged so that each stage had half-power points of 50 cps and 2 mc, while the spectrum under analysis extended from 5 kc to 30 kc.

3. In the deuterium-line experiment, sampling was accomplished by the arrangement

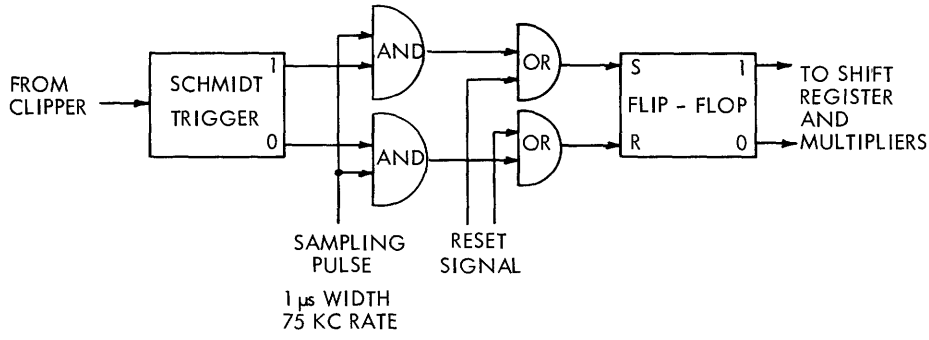

Fig. 15. Sampling configuration for the deuterium-line receiver.

shown in Fig. 15. The flip-flop is set $[y(k\Delta t)=1]$ or reset $[y(k\Delta t)=-1]$ according as the input signal was 1 or -1 during the duration t_s of the sampling pulse. If the signal is making a transition during t_s, the flip-flop will be set, reset or will stay in its previous state according to the result of a weighted average of the signal during t_s. The flip-flop is randomly set or reset between samples so that the error is random if the flip-flop refers to its previous state. This precaution was taken (it is not known if it is necessary) in order to prevent a false high correlation between successive samples; this would lead to false features in the spectrum (again, the switching technique would cancel most of these errors anyway).

The duration t_s of the sampling pulse was 1 μsec which is 1/30 of the period of the highest frequency component of the signal. This gave satisfactory performance. In the case of many-bit or unquantized samples, it is possible to show that if the sampling pulse has the shape p(t), the effect is to multiply the spectrum by the square of the magnitude of the Fourier transform of p(t). Thus, if $1/t_s$ is much larger than the highest component in the power spectrum, little change occurs.

The experimental results of Section VI indicate satisfactory performance of the clippers and samplers used in the deuterium-line receiver. Of particular importance toward evaluating the samplers and clippers was the comparison of a spectrum measured by the system (not using switched operation) with that measured by another means (see section 6.3). The agreement was within 1.5 per cent and the error is most likely due to the error of the "other" measurement method.

The results of another test, which is useful for evaluating the clipping circuitry in the deuterium-line receiver, are presented in Fig. 16. A spectrum is measured (not using switched operation), and then the signal level is changed by large amounts. If the clipper were ideal, no change would occur in the measured spectrum. The results indicate that gain changes of approximately 100 per cent cause a few per cent change in the measured spectrum. The spectral error probably decreases more than linearly with the gain change; in other words, a 1 per cent gain change would cause less than a few hundredths of a per cent change in the measured spectrum. Of course, in actual operation the switching technique cancels most of this error.

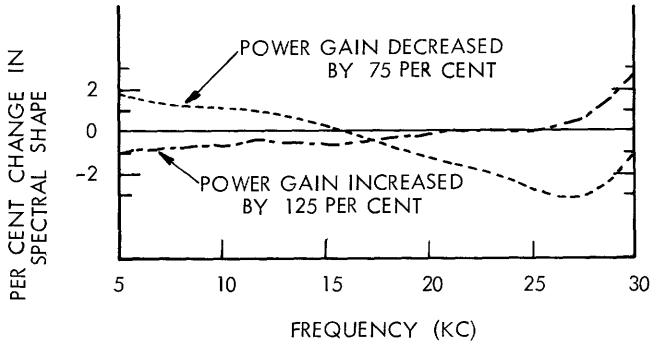

Fig. 16. Effect of large gain changes upon a spectral measurement performed with the one-bit autocorrelation system; this effect is the result of nonideal clipper operation. The measurements were repeated with the gain varied by different means and identical results were obtained. In actual operation these large gain changes would not occur and the switched mode of operation greatly reduces the effect of the small gain changes that do occur.

5.3 DIGITAL CORRELATOR

The basic block diagram of a one-bit digital correlator is presented in Fig. 17. The function of each block should be understood from its title, the logical equations on the diagram, and the definition of symbols given at the right of the diagram. Although the individual blocks can be realized in many ways, only two major variations of the block diagram come to mind. These are

1. The set of N counters, each having a capacity of M bits (usually $M > 20$), may be replaced by an $N \cdot M$ bit memory (ferrite core, delay line or other) and a high-speed serial adder. The sums ν_n of the F_n pulses would be stored in memory and would be periodically brought out to be increased by the new F_n pulse. The $N \cdot M$ bit memory will be cheaper and have less components than the $N \cdot M$ flip-flops required by the counters; however, speed will be a problem. A combination of counters and memory may be optimum. If a computer is available, it may provide the memory and the adder. A straight counter system was used in the deuterium-line correlator.

2. The sum of K simultaneously computed autocorrelation functions can be calculated by providing K sets of all elements in the block diagram except the counters, for which only one set capable of counting K times faster is needed. The outputs of K one-bit multipliers are OR'ed (with proper timing) into a common counter. Since the cost of counters is an appreciable part of the total cost, the cost of the correlator is not proportional to K. One cost study has indicated that the cost increases by 1.25 for $K = 2$, and by 1.75 for $K = 4$. This technique is useful if one wishes to gain factors of 2 or 4 in effective observation time by observing simultaneously the orthogonal component of polarization and/or using an additional receiver switched 180° out of phase with the first. Both of these steps were taken in the deuterium-line attempt so that $K = 4$ for the deuterium-line correlator.

The correlator, as it is shown in the block diagram, is connected for the switched

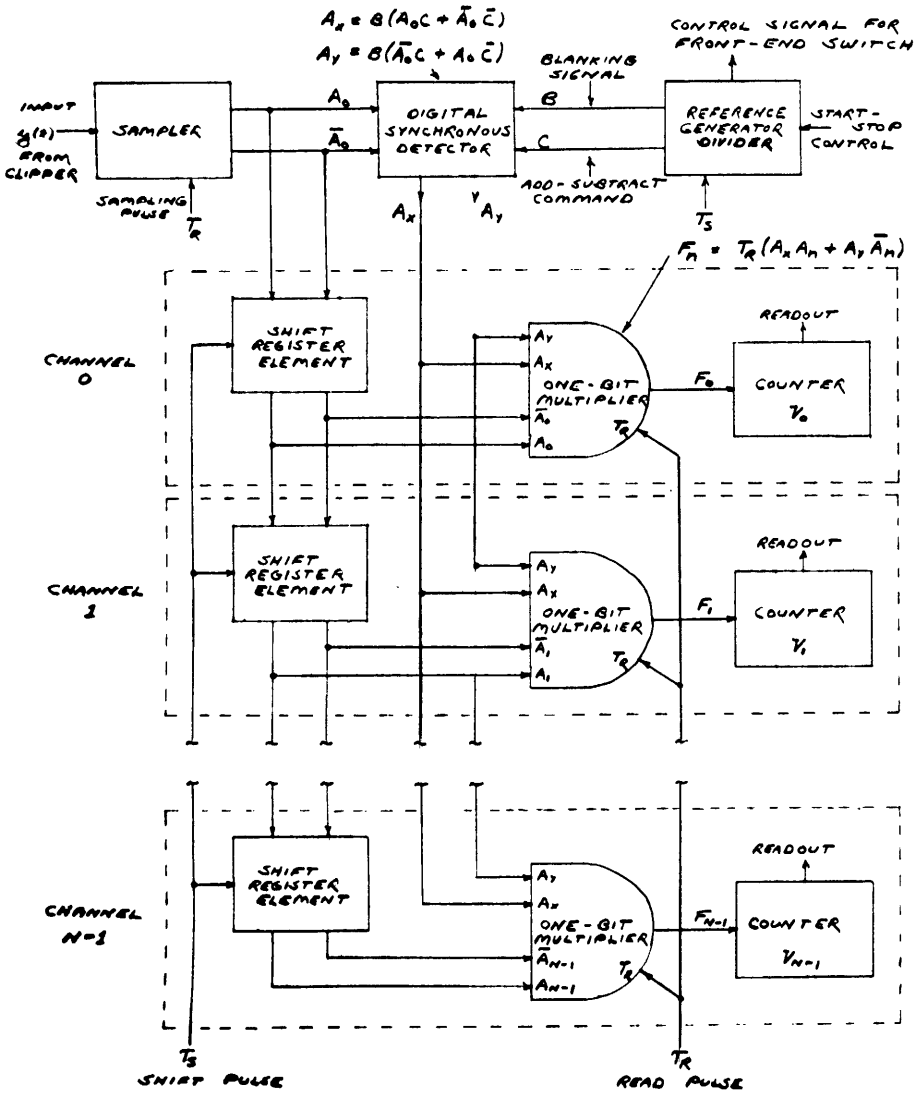

A_n represents the input sample which occurred n units back in time. $A_n = 1$ if this sample was 1 and $A_n = 0$ if this sample was -1. A_n is stored in the n'th shift-register element. A_o is the value of the current sample.

$\bar{A}_n$ is the complement of A_n.

B equals 0 when blanking is applied or the correlator is stopped. B = 1 otherwise.

C equals 1 when the front-end switch is in the antenna position. C = 0 when the front-end switch is in the comparison position.

A_x, A_y are the variables which multiply each A_n (see definition of F_n). When B = 1 and C = 1, $A_x = A_o$ and $A_y = \bar{A}_o$; when B = 1 and C = 0, $A_x = \bar{A}_o$ and $A_y = A_o$; and when B = 0, $A_x = 0$ and $A_y = 0$. In Boolean equations:

$$A_x = B(A_oC + \bar{A}_o\bar{C})$$

$$A_y = B(\bar{A}_oC + A_o\bar{C})$$

T_R is a timing pulse. $T_R = 1$ when it is time to interrogate the one-bit multipliers $T_R = 0$, otherwise. T_R occurs periodically at a rate, f_s. It is also used to sample the signal.

T_S is another timing pulse. $T_R = 1$ when it is time to shift the shift register; $T_S = 0$, otherwise. T_S is shifted by 1/2 clock period from T_R. All changes in B and C should occur during the time T_S occurs.

F_n is the output pulse of the n'th one-bit multiplier. If B = 0, then $F_n = 0$ (no pulse occurs); if B = 1 and C = 1, then $F_n = 1$ if A_n and A_o are alike; and if B = 1 and C = 0, then $F_n = 1$ if A_n and A_o are not alike. If the pulse occurs ($F_n = 1$), it occurs at the same time as T_R. Expressed in a Boolean equation:

$$F_n = T_R(A_xA_n + A_y\bar{A}_n)$$

v_n is the contents of the n'th counter which counts the number of F_n pulses.

Fig. 17. Basic block diagram of a one-bit digital correlator.

mode of operation. The difference autocorrelation function $\delta\rho'_y(n\Delta\tau)$ is computed, and after proper correction (Eq. 121) and Fourier transformation (Eq. 116), the difference, $\delta p'(f)$, between the signal spectrum $p'(f)$ and comparison spectrum $p'_c(f)$ is computed. These spectra (and also $p'_o(f)$) may be individually measured by locking the control signal C at 1, and locking the front-end switch in the antenna position or comparison position. The correlator is stopped (that is, counting stops, the counters may be read out and cleared) by locking the blanking control signal B at zero.

An interesting test of the correlator is provided by locking the front-end switch in one position, or the other, and operating the correlator in switched mode so that products are added (C=1) during half the switching cycle, and subtracted (C=0) during the other half-cycle. The resulting autocorrelation function and power spectrum should be zero within a few rms deviations. A more sensitive and easily interpreted test is provided by feeding a periodic square wave (derived from the reference-generator divider) into the sampler input and locking C at 1. The resulting autocorrelation function should be an exactly known triangular function. A single error in millions of operations can be detected in this way. A constant can also be fed into the sampler input; the resulting autocorrelation function should be exactly constant. Controls for inserting these test signals, along with controls for B, C, and the front-end switch, should be provided on the correlator front panel.

The contents of the N counters ν_n, n = 0 to N-1, must be either visually or electronically read out, recorded, and prepared for entry into a computer. In the deuterium-line experiment the counter contents were visually indicated, written down, and then manually punched on cards. Automatic readout and recording on a medium suitable for computer entry is obviously desirable. The counters' contents are not directly equal to values of points on the autocorrelation function, as this would require more costly add-subtract types of counters. The autocorrelation function is given in terms of the counters' contents by

$$\delta\rho'_y(n\Delta\tau) = \frac{2\nu_n - 2\nu_o}{\nu_o} \qquad n = 0,\ N-1 \tag{151}$$

for the switched mode of operation, and

$$\rho'_y(n\Delta\tau) = \frac{2\nu_n - \nu_o}{\nu_o} \qquad n = 0,\ N-1 \tag{152}$$

for the unswitched (C=1) mode of operation.

There are four major parameters that specify the capability of a one-bit digital correlator. The first and most obvious is N, the number of channels or points on the autocorrelation function. This determines the ratio of the analyzed bandwidth B_1 to the frequency resolution Δf. The value of this ratio depends on the choice of the weighting function $w(\tau)$ and the shape of the receiver bandpass $G(f+f_o)$. In the practical case, $B_1/\Delta f$ will be between N/1.5 and N/3. The second parameter K, the number of signals

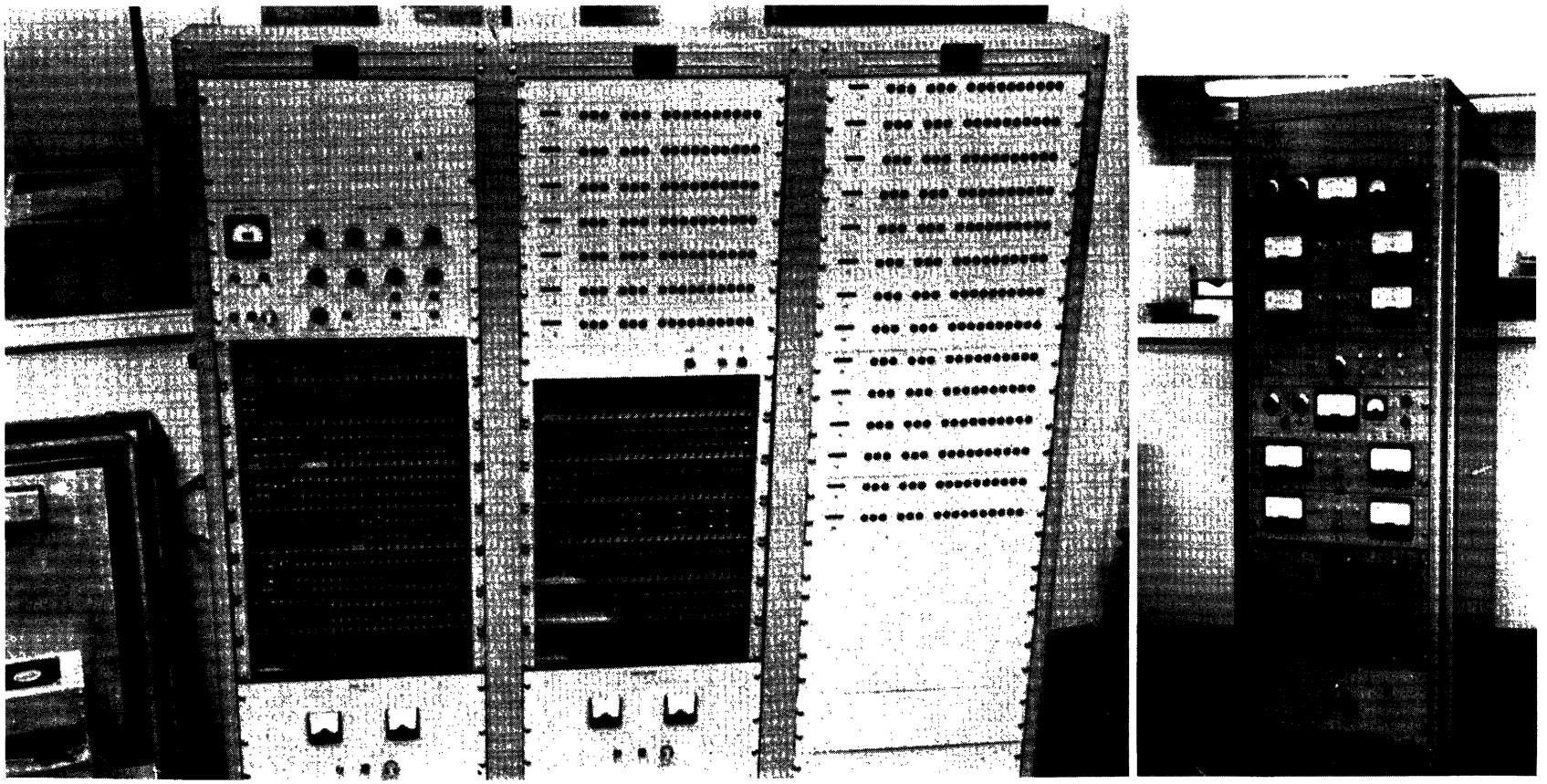

Fig. 18. The one-bit digital correlator used for the deuterium-line and Zeeman experiments is shown at the left, and the receiver console is shown at the right. The left and lower middle bays of the correlator cabinet contain printed circuit cards that comprise four 21-bit shift registers and 84 one-bit multipliers. The right and upper middle bays contain 21 sets of 16-bit binary counters with neon-bulb read-out plus 6-digit electromechanical counters. The receiver console contains, from top to bottom, the clippers, a noise-generator control unit, 2 receivers, local oscillators, a second noise-generator control unit, 2 more receivers, and power supplies. The receiver front-ends are in a box mounted on the radio telescope.

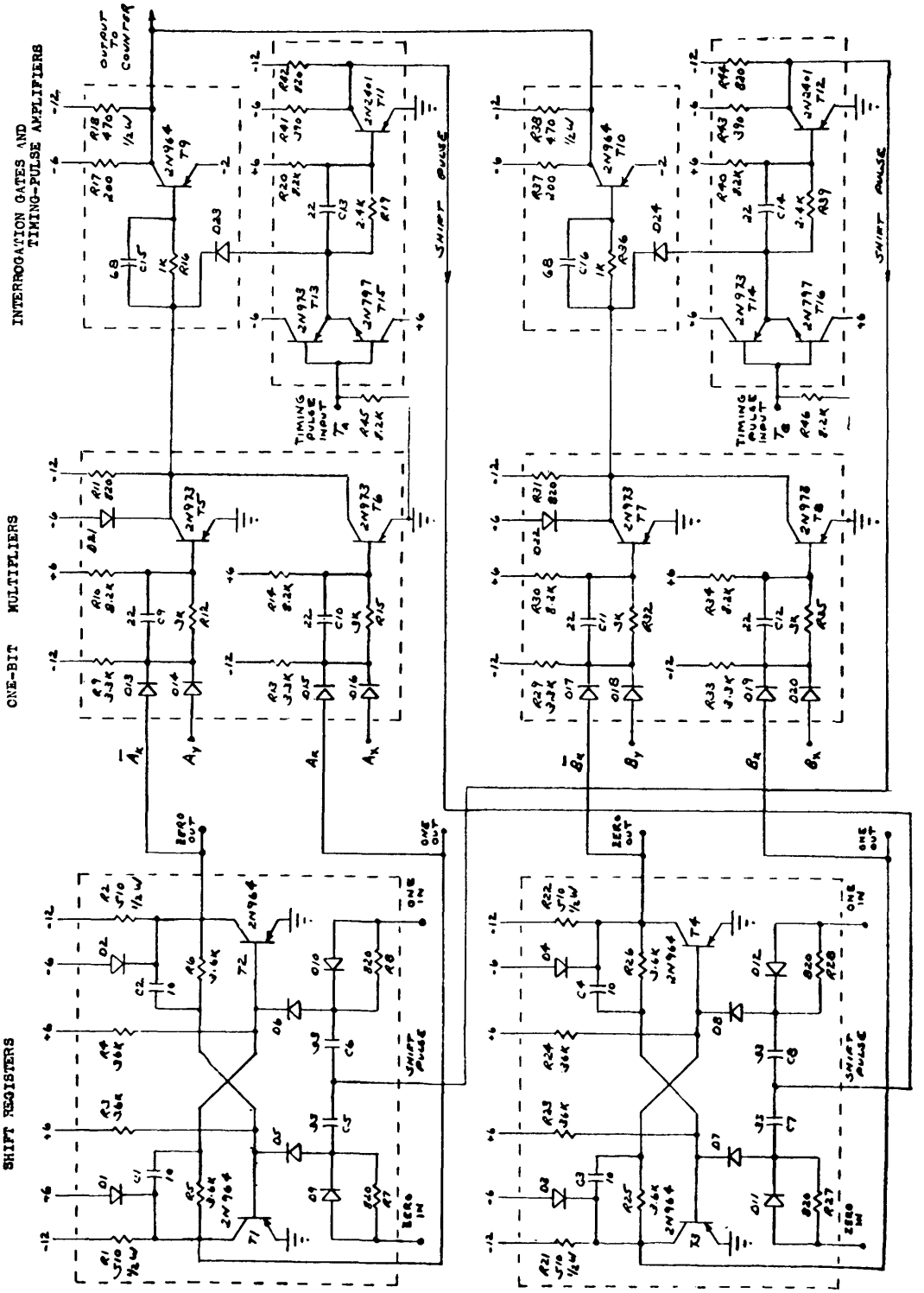

Fig. 19. Circuit diagram of a high-speed correlator channel.

autocorrelated at one time, has already been discussed.

A third major parameter is the maximum sampling frequency, $(f_s)_{max}$, which is limited by the repetition rate of the digital logic elements. The value $(f_s)_{max}$ determines the maximum bandwidth that can be analyzed, $(B_1)_{max} \sim 0.4(f_s)_{max}$. For present transistor logic circuits, the cost of the correlator will increase by approximately a factor of 2 if $(f_s)_{max}$ is increased from 500 kc to 10 mc. Above 10 mc, the price will rapidly increase, although future developments may change this picture.

The final parameter is M, the bit capacity of the counters. This determines the maximum time, T_{max}, which may elapse before the counter is full and readout must occur. The maximum number of counts that a counter may receive is one for each sample; thus T_{max} is specified by $f_s T_{max} = 2^M - 1$.

All M bits in the counters need not be read out, as some bits at the input end will be insignificant and L bits at the slow end will always be zero if $f_s T < 2^{M-L}$. The number of insignificant bits is also a function of $f_s T$. The rms deviation of ν_n $(n \neq 0)$ is approximately $\sqrt{f_s T}$ for either the switched or unswitched mode of operation. (This follows from application of Eq. 114 which gives the rms deviation of an autocorrelation function estimate.) Thus, a round-off error that is much less than $\sqrt{f_s T}$ can be neglected. If $f_s T = 2^{M_o}$, then it is safe to discard the $M_o/2 - 3$ most insignificant bits. Since $f_s T$ will rarely be less than $10^6 \sim 2^{20}$ in radio astronomy applications, the 7 bits at the high-speed end of the counter need not be read out.

The digital correlator that was used for the deuterium-line and Zeeman experiments is pictured in Fig. 18. This machine has 21 channels, can simultaneously autocorrelate 4 signals, has a maximum sampling rate of 300 kc, and contains counters with a capacity of 36 bits. The slowest 20 bits of each counter are provided inexpensively by a 6-digit electromechanical counter with visual readout; the remaining 16 bits are transistorized counters with neon-bulb indicators. With the exception of the counters, the machine was built by Control Equipment Corporation at a cost of $14,000. The counters were designed by the author and constructed by an outside vendor for an additional $5,000. The machine uses 2100 transistors and has operated for its first 4500 hours without failure, except for some minor difficulties with the electromechanical counters.

A schematic diagram of shift-register and one-bit multiplier circuitry designed for a high-speed correlator channel is given in Fig. 19. This circuitry was developed by Control Equipment Corporation for the National Radio Astronomy Observatory. The design parameters of this machine are: N = 100 channels, K = 2 receivers, $(f_s)_{max}$ = 10 mc, and a counter capacity M of 30 bits. Electronic readout (to a computer or paper tape punch) is provided on the slowest 24 bits of the counter. An expected cost of this machine is from $400 to $700 per channel.

VI. SYSTEM TESTS

6.1 SUMMARY OF TESTS

A series of experiments, designed to test various aspects of the digital autocorrelation spectral-analysis system, are described here. The objectives of these tests are also discussed.

Computer Simulation of the Signal and the Signal-Processing System

Samples of a time function having Gaussian statistics and known power spectrum are generated in a computer. This time series is analyzed in the computer through the use of both many-bit and one-bit autocorrelation processing. One-hundred such time series (1050 samples each) were analyzed in order to give statistical information concerning the mean and variance of both one-bit and many-bit estimates of the autocorrelation function and power spectrum. The main objective was to find the variance of the one-bit power spectrum estimate; this is difficult to calculate theoretically and is needed to specify the sensitivity of the radio-astronomy system for which the one-bit autocorrelation-function method is used.

Measurement of a Known Noise-Power Spectrum

A noise-power spectrum that is "known" within 1 per cent is produced by passing white noise through a filter whose power transfer function is measured by conventional sinusoidal techniques. This signal is in the video-frequency range and is analyzed by using the same clippers, one-bit correlator, and computer program that were used in the deuterium-line attempt. This was the first measurement performed with the system and served mainly as an equipment check.

Measurements of Artificial Deuterium Lines

A small signal having a spectrum similar to the deuterium line (except that it is a "bump" instead of the deuterium-absorption "dip") was produced and injected into the deuterium-line receiver input (at 327 mc). A second large, broadband noise signal, simulating the radio source Casseopeia was also injected into the receiver input. A means of calibrating the artificial deuterium-line signal in relation to the noise was provided. Artificial lines of various magnitudes were detected, the weakest being 37 db (0.02 per cent) below the noise level.

Analysis of the rms Deviation of the Deuterium-Line Data

A major advantage that is expected of the digital autocorrelation system is that the theoretical sensitivity (which increases as the square root of the observation time) is achieved when observations are carried out for long periods of time. This is often not

the case with analog equipment, because of nonstationariness or drift in the apparatus. The realization of this advantage is demonstrated by an analysis of the rms deviation of 68 days of deuterium-line data.

Before discussing these tests, it should be mentioned that the digital correlator itself can be checked by the application of a few simple test signals. Two such test signals are a constant, which gives a constant autocorrelation function, and a square wave (derived from the correlator clock circuitry) which gives a triangular autocorrelation function. These tests were built into the digital correlator that was used for the deuterium experiment and were periodically performed. The only errors that were ever found were missed counts in electromechanical counters used in this machine. The tests are very sensitive; with a 10-second run at 300-kc sampling rate, a single error in 3×10^6 operations can be detected.

6.2 COMPUTER SIMULATION OF THE SIGNAL AND THE SIGNAL-PROCESSING SYSTEM

The procedure and objective discussed in this section have already been summarized. Computer-generated estimates of the mean and variance of both one-bit and many-bit estimates of the autocorrelation function and power spectrum will be discussed. (The reader should not be confused by the fact that we are considering statistical estimates of the mean and variance of another statistical estimate.) Many terms must be defined and this will be our first task. After this has been done, a large portion of the experimental procedure and results can be understood by referring to Figs. 20-22. A discussion of the procedure and results will be given below.

a. Definitions and Terminology

The notation of this section is the same as that used in Sections II and III, with one minor exception. The time intervals Δt and $\Delta\tau$ will be assumed to be equal, and $k\Delta t$ and $n\Delta\tau$ will be replaced simply by k and n. As usual, ρ refers to normalized autocorrelation functions; p refers to normalized power spectra; a single prime, or a subscript 1 refers to one-bit samples; a double prime, or a subscript m refers to many-bit samples; and a sigma with appropriate subscripts refers to rms deviation of the variable indicated by the subscript.

An example is $\sigma_{p1}(f)$ which is the rms deviation of the spectral estimate computed from one-bit samples. A statistical estimate of $\sigma_{p1}(f)$ is $\sigma'_p(f)$. In a similar manner, the meaning of $\sigma_{pm}(f)$ and $\sigma''_p(f)$, $\sigma_{\rho 1}(n)$ and $\sigma'_\rho(n)$, and $\sigma_{\rho m}(n)$ and $\sigma''_\rho(n)$ should be clear. The many-bit rms deviations, $\sigma_{\rho m}(n)$ and $\sigma_{pm}(f)$, were discussed in Section II, and the one-bit rms deviations, $\sigma_{\rho 1}(n)$ and $\sigma_{\rho 1}(f)$, were computed in Section III. The statistical estimates of these quantities will be defined below.

The quantity x(k) denotes a sample of a time function having Gaussian statistics. These samples will be generated in the computer by a method described below. As in

earlier work, y(k) is the one-bit sample corresponding to x(k); y(k) = 1 when x(k) > 0, and y(k) = −1 when x(k) < 0. The time between samples, $\Delta t = \Delta\tau$, will always be assumed to be equal to 1/75 kc so that the time and frequency scale of our computer-generated results will be the same in the deuterium-line results.

Following the procedure already used, we define the one-bit and many-bit autocorrelation function estimates as:

$$\rho_i'(n) = \sin\left[\frac{\pi}{2}\cdot\frac{1}{K}\sum_{k=1}^{K} y(k)\, y(k+|n|)\right] \tag{153}$$

and

$$\rho_i''(n) = \frac{\sum_{k=1}^{K} x(k)\, x(k+|n|)}{\sum_{k=1}^{K} x^2(k)}. \tag{154}$$

The subscript i, with i going from 1 to 100, is used to denote each of 100 independent, but statistically alike, estimates of $\rho(n)$. Each $\rho_i'(n)$ is determined from a different group of K+n randomly generated samples; however, each group is generated under the same conditions. The sample size K is fixed at 1050. The values of $\rho_i'(n)$ and $\rho_i''(n)$ are calculated for n = 0 to 20 which is analogous to the deuterium-line processing.

The one-bit and many-bit estimates of the power spectrum, $p_i'(f)$ and $p_i''(f)$, respectively, are computed from $\rho_i'(n)$ and $\rho_i''(n)$ in the same manner as previously (Eq. 33). For example,

$$p_i'(f) = 2\Delta\tau \sum_{n=-20}^{20} \rho_i'(n)\, w(n\Delta\tau)\, e^{-j\,2\pi f n\Delta\tau}. \tag{155}$$

Here, the cos weighting function is used analogously with the deuterium-line data processing. According to the theory presented in Sections II and III, the mean or expected value of $p_i'(f)$ and $p_i''(f)$ is the smoothed spectrum, $p^*(f)$, which is discussed in sections 2.4b and 2.2.

$$\overline{p'(f)} = \overline{p''(f)} = p^*(f). \tag{156}$$

The arithmetic averages of $\rho_i'(n)$, $\rho_i''(n)$, $p_i'(f)$, and $p_i''(f)$ are denoted $\rho_{av}'(n)$, $\rho_{av}''(n)$, $p_{av}'(f)$, and $p_{av}''(f)$, respectively, for which, for example,

$$p_{av}'(f) = \frac{1}{100}\sum_{i=1}^{100} p_i'(f). \tag{157}$$

Similarly, estimates of the rms deviations of $\rho_i'(n)$, $\rho_i''(n)$, $p_i'(f)$, and $p_i''(f)$ are denoted

$\sigma'_\rho(n)$, $\sigma''_\rho(n)$, $\sigma'_p(f)$, and $\sigma''_p(f)$, respectively, for which, for example,

$$\sigma'_p(f) = \sqrt{\frac{1}{100}\sum_{i=1}^{100}\left[p'_i(f)-p^*(f)\right]^2}. \tag{158}$$

It can be shown (see Burington and May,[20] p. 149) that if I functions are used to estimate the rms deviation of a function (as in Eq. 158 where I = 100), then the rms error of the estimate is $100/\sqrt{2I}$ per cent. For example,

$$\frac{\sqrt{\overline{\left[\sigma'_p(f)-\sigma_{p1}(f)\right]^2}}}{\sigma_{p1}(f)} = \frac{1}{\sqrt{2I}}. \tag{159}$$

Since I = 100 in our case, the true rms deviations, $\sigma_{p1}(f)$, $\sigma_{pm}(f)$, $\sigma_{\rho 1}(n)$, and $\sigma_{\rho m}(n)$, are estimated by $\sigma'_p(f)$, $\sigma''_p(f)$, $\sigma'_\rho(n)$, and $\sigma''_\rho(n)$, respectively, with an rms error of approximately 7 per cent.

b. Computer Method

A block diagram of the computer program used to generate the one-bit and many-bit estimates of the autocorrelation function and power spectrum is shown in Fig. 20. This program was run 100 times with a different (but statistically alike) sequence of random numbers each time. The results which will be presented are the arithmetic averages and rms deviation estimates defined in the previous section.

A complete listing of the computer program is given in Appendix D and should be referred to for details. The main steps in the program should be fairly obvious from Fig. 20 and the previous definitions. The generation of the Gaussian time series x(k), with known spectrum, will be briefly discussed here. The generation of this time series occurs in three steps.

Step 1

Random numbers with uniform probability density are generated by taking the last 4 digits of a nonconvergent, iterative, arithmetic operation (see program, statements 67 to 73).

Step 2

A sum of 5 uniform random numbers is used to form a new random number which has an approximate Gaussian probability density function (see Davenport and Root,[1] pp. 81-84, "The Central Limit Theorem"). The probability density function of this sum consists of the uniform density function convolved with itself 5 times; this will closely approximate a Gaussian distribution.

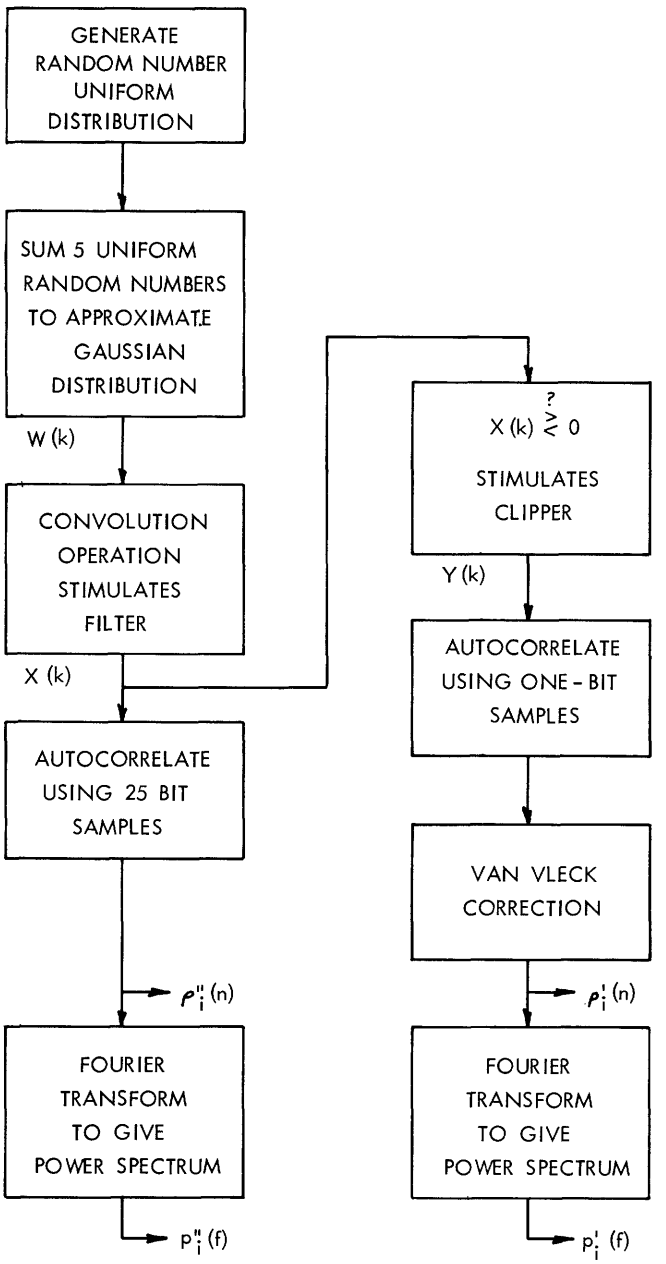

Fig. 20. Block diagram of the computer program used to simulate the signal and the signal-processing system.

Step 3

The Gaussianly distributed random numbers are statistically independent, and thus they have the character of samples of Gaussian noise with uniform spectrum (white noise). These samples must then be passed through a sampled-data filter to give the desired spectrum. This is accomplished by convolving the white-noise samples with a filter impulse response. The output samples x(k) are then Gaussian with a spectrum equal to the square of the magnitude of the Fourier transform of the impulse response.

c. Results and Conclusions

All of the results of the computer-simulation experiment are given in Tables III and IV; the more important results are also plotted in Figs. 21 and 22.

The arithmetic averages $\rho''_{av}(n)$, $\rho'_{av}(n)$, $p''_{av}(f)$, and $p'_{av}(f)$ should be within a few

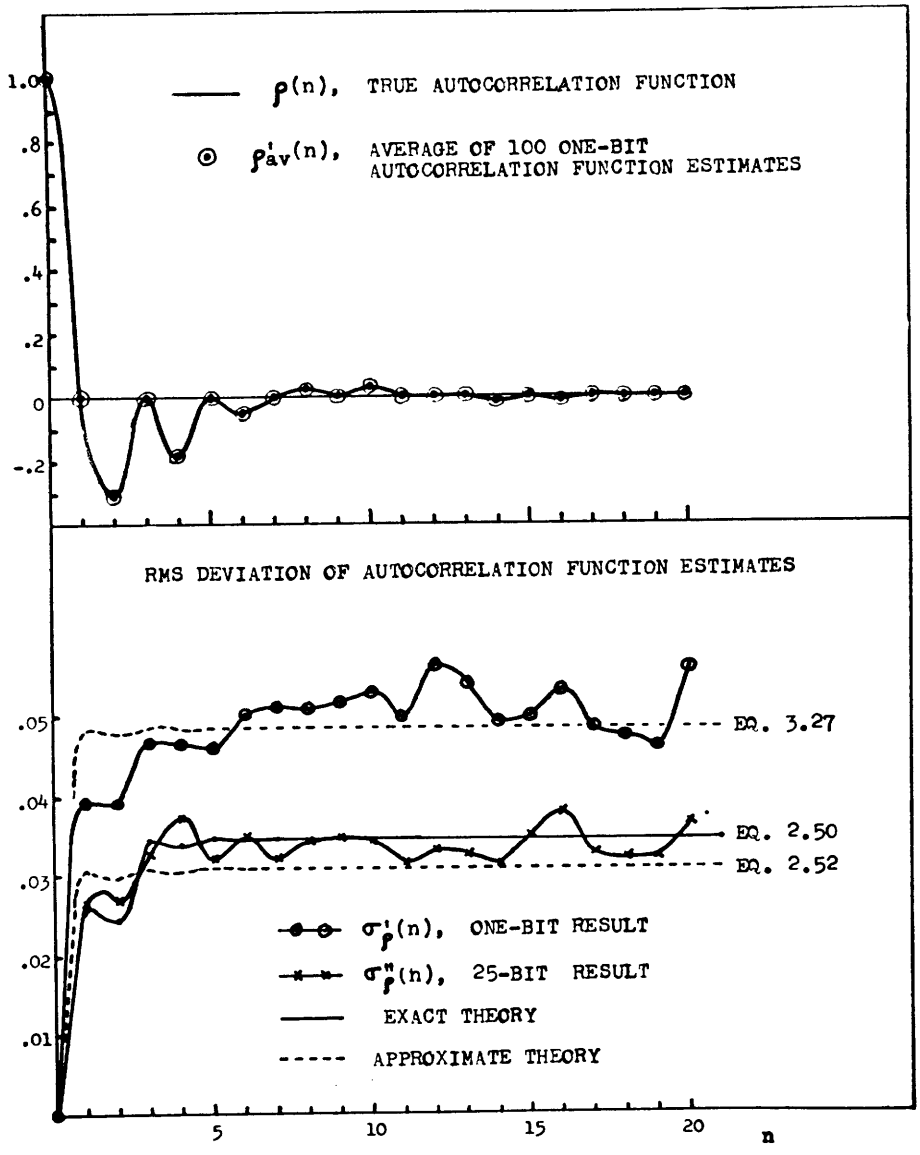

Fig. 21. Results of the computer-simulated autocorrelation-function measurements.

times $\sigma/\sqrt{100}$ of the true mean, where the respective σ of a single estimate is used. The $\sqrt{100}$ term arises because the arithmetic averages are taken over 100 independent estimates. The agreement of the averages of the estimates with the true mean is quite as expected, and is not too illuminating because the theoretical work for

this result is quite clear.

Our major interest is in the estimates of the rms deviations $\sigma''_{\rho}(n)$, $\sigma'_{\rho}(n)$, $\sigma''_{p}(f)$, and $\sigma'_{p}(f)$. It should be kept in mind that these quantities are statistical estimates of the true values $\sigma_{\rho m}(n)$, $\sigma_{\rho 1}(n)$, $\sigma_{pm}(f)$, and $\sigma_{p1}(f)$, and will have an rms error of $1/\sqrt{200} \sim 7$ per cent of the true value as is indicated by Eq. 159.

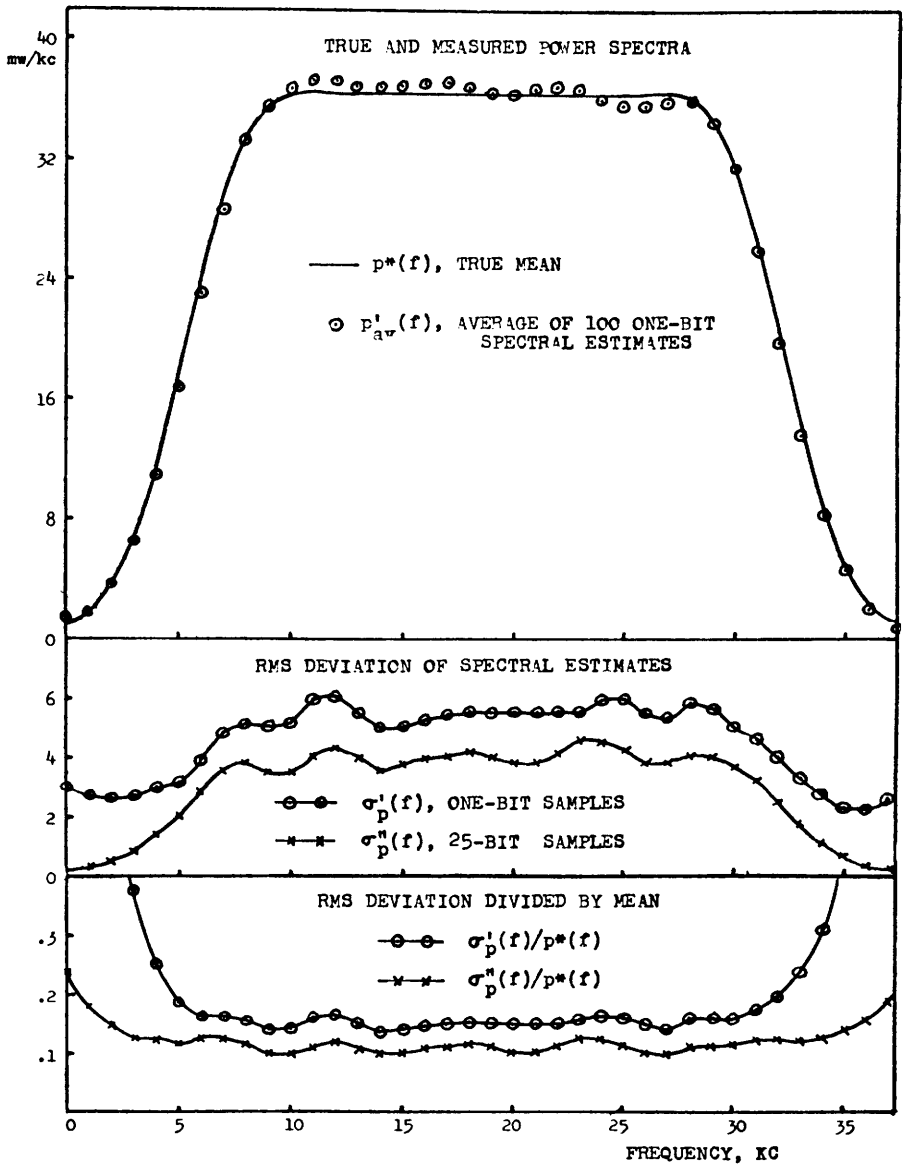

Fig. 22. Results of the computer-simulated spectral measurements.

The many-bit and one-bit rms deviations $\sigma''_{\rho}(n)$ and $\sigma'_{\rho}(n)$, respectively, will be discussed first. Examination of $\sigma''_{\rho}(n)$ in Fig. 22 indicates that it is in good agreement with the "exact" theory (the approximations are well justified) given by Eq. 80. Equation 82, in which linearly independent products of many-bit samples are assumed, gives a value

Table III. Results of computer-simulation experiment autocorrelation functions.

n	$\rho(n)$ x 10,000 True Function	$\rho''_{av}(n)$ x 10,000 Many-Bit Estimate	$\rho'_{av}(n)$ x 10,000 One-Bit Estimate	$\sigma''_{\rho}(n)$ x 10,000 Many-Bit RMS Dev.	$\sigma'_{\rho}(n)$ x 10,000 One-Bit RMS Dev.
0	10000.0	10000.0	10000.0	0.0	0.0
1	-0.3	24.7	43.6	269.8	393.5
2	-3094.2	-3177.1	-3185.3	273.5	389.7
3	-0.4	-9.2	-42.0	338.1	466.9
4	-1801.3	-1702.9	-1766.4	375.8	467.2
5	-0.7	-21.8	44.2	322.3	460.0
6	-501.7	-476.9	-462.3	349.9	502.9
7	-3.0	19.3	41.1	319.2	513.8
8	210.7	194.5	228.1	346.8	486.1
9	-5.8	-9.0	-28.7	350.4	517.8
10	242.8	233.9	285.4	345.8	531.3
11	16.4	-21.0	-36.7	317.7	498.5
12	29.2	31.5	-31.0	343.4	575.0
13	3.9	48.9	107.4	340.0	552.1
14	-74.5	-85.9	-42.4	314.1	493.8
15	-3.3	-40.5	-31.9	357.3	500.1
16	-50.7	-75.5	-92.8	383.8	533.3
17	-10.4	-16.6	-1.2	331.9	486.3
18	7.4	38.0	20.3	326.5	475.8
19	-8.8	26.8	34.3	324.6	462.7
20	9.1	-32.4	-55.0	372.3	570.7

Table IV. Results of computer-simulation experiment power spectra.

f kc	$p^*(f)$ x 5000 True Mean	$p''_{av}(f)$ x 5000 Many-Bit Estimate	$p'_{av}(f)$ x 5000 One-Bit Estimate	$\frac{\sigma''_p(f)}{p^*(f)}$ Many-Bit RMS Dev.	$\frac{\sigma'_p(f)}{p^*(f)}$ One-Bit RMS Dev.
0	4.9	5.2	6.4	0.237	2.882
1	8.1	8.5	9.2	0.181	1.547
2	17.7	18.3	17.9	0.145	0.625
3	34.1	34.4	33.0	0.128	0.375
4	57.5	57.0	55.3	0.122	0.258
5	86.8	85.4	83.9	0.118	0.187
6	118.4	116.3	115.1	0.122	0.166
7	146.8	144.3	143.7	0.126	0.166
8	167.1	164.7	165.1	0.115	0.157
9	178.1	176.1	178.1	0.099	0.144
10	182.1	181.2	184.5	0.096	0.144
11	182.5	183.1	186.6	0.110	0.160
12	182.1	183.6	186.3	0.119	0.167
13	181.8	183.2	185.0	0.109	0.151
14	181.7	182.7	184.5	0.098	0.136
15	181.7	183.2	185.3	0.103	0.139
16	181.7	184.6	186.5	0.108	0.145
17	181.7	185.8	186.3	0.112	0.149
18	181.8	186.1	184.5	0.115	0.154
19	182.0	185.7	182.7	0.112	0.156
20	182.2	185.4	182.6	0.105	0.155
21	182.1	185.5	183.9	0.106	0.155
22	181.8	185.5	184.8	0.116	0.155
23	181.4	184.9	183.7	0.127	0.157
24	181.3	183.4	181.1	0.127	0.163
25	181.6	181.6	178.8	0.116	0.162
26	182.3	180.3	178.6	0.105	0.151
27	183.0	179.5	180.2	0.104	0.149
28	181.4	177.4	180.2	0.111	0.160
29	174.0	170.1	173.8	0.115	0.161
30	157.9	154.1	157.2	0.117	0.161
31	132.8	129.4	130.8	0.123	0.177
32	102.2	99.5	99.2	0.126	0.199
33	71.6	69.6	68.3	0.126	0.236
34	45.2	44.1	42.6	0.131	0.314
35	25.3	24.9	23.3	0.145	0.470
36	12.2	12.2	10.4	0.160	0.941
37	5.7	5.8	3.7	0.190	2.323

for $\sigma_{\rho m}(n)$ that is somewhat low. Similarly, Eq. 114, in which statistically independent products of one-bit samples are assumed, gives a $\sigma_{\rho 1}(n)$ that is somewhat lower than $\sigma'_{\rho}(n)$.

A closer and more compact comparison of the autocorrelation rms deviations can be obtained by averaging along n. For example,

$$\sigma'_{\rho} = \frac{1}{18} \sum_{n=3}^{20} \sigma'_{\rho}(n). \tag{160}$$

Since σ'_{ρ} is the average of 18 approximately independent points, its rms error is reduced by $\sqrt{18}$ to a value of 1.65 per cent. The results concerning autocorrelation-function rms deviations are summarized in Table V.

Table V. Autocorrelation-function rms deviation (average value in interval $3 \leq n \leq 20$).

One-Bit		Many-Bit			Ratio
Results of Computer Simulation σ'_{ρ}	Approx. Theory Eq. 114 $\sigma_{\rho 1}$	Results of Computer Simulation σ''_{ρ}	Approx. Theory Eq. 82 $\sigma_{\rho m}$	Exact Theory Eq, 80 $\sigma_{\rho m}$	Increase Caused by Clipping $\sigma'_{\rho}/\sigma''_{\rho}$
.0500 ±.0008	.0485	.0338 ±.0006	.0309	.0346	1.48 ±.04

The results concerning the rms deviations of the many-bit and one-bit spectral estimates, $\sigma''_p(f)$ and $\sigma'_p(f)$, are indicated in Fig. 22. These results indicate that $\sigma'_p(f)$ is slightly greater than $\sigma''_p(f)$ in the constant passband region of $p^*(f)$. But at the edges of the band, where $p^*(f)$ becomes small, $\sigma'_p(f)$ becomes much greater than $\sigma''_p(f)$. In the many-bit case, $\sigma''_p(f)/p^*(f)$ is fairly constant (except for small increases near $f = 0$ and $f = f_s/2$), and hence a measurement of $p^*(f)$ at a frequency for which $p^*(f)$ is small is just as accurate as at a frequency for which $p^*(f)$ is large. This is not true in the one-bit case; $\sigma'_p(f)/p^*(f)$ becomes large when $p^*(f)$ becomes small. This is the most valuable result of the computer-simulation experiment. Experimental results on actual spectra indicated the same phenomenon; however, it was thought that the increase of $\sigma_{p1}(f)/p^*(f)$ at the edge of the band may have been due to nonideal operation of the sampler and clipper. In actual radio-astronomy measurements, the observations were confined to the constant passband region such as that between 5 kc and 30 kc in Fig. 22.

It is convenient to define β as the ratio of the one-bit spectral rms deviation to the many-bit spectral rms deviation; β is estimated by $\sigma'_p(f)/\sigma''_p(f)$. Strictly speaking, β is

some unknown function of f and depends on p(f) and W(f). Since the spectra that we shall measure in most radio-astronomy applications have the same gross shape as the spectrum of Fig. 22, the estimate of β given by $\sigma_p'(f)/\sigma_p''(f)$ has more general application.

In the midband region where $p^*(f)$ is constant, β appears to be constant. An accurate value can be obtained by averaging the spectral rms deviations in the interval 10 kc $\leq f \leq$ 29 kc; that is,

$$\sigma_p' = \frac{1}{20} \sum_{f=10}^{29} \sigma_p'(f). \tag{161}$$

There are approximately 10 independent points in this interval; thus the rms error is reduced by $\sqrt{10}$ to give a value of 2.4 per cent. The results are given in Table VI.

Table VI. Spectral rms deviation (average value in interval 10 kc $\leq f \leq$ 29 kc).

One-Bit	Many-Bit		Ratio
Results of Computer Simulation σ_p'/p^*	Results of Computer Simulation σ_p''/p^*	Exact Theory Eq. 86 σ_{pm}/p^*	Increase Caused by Clipping $\beta = \sigma_p'/\sigma_p''$
.1534 ±.0036	.1107 ±.0025	.1150	1.39 ±0.04

The most important result here is the value, $\beta = 1.39 \pm .04$, which applies in the constant region of a spectrum similar to that illustrated in Fig. 22. Examination of $\sigma_p'(f)$ and $\sigma_p''(f)$ indicates that the increase in β at the edges of the band follows an empirical law of the form

$$\beta = 1.39\left[p_o^*/p^*(f)\right]^{1/2}, \tag{162}$$

where p_o^* is the value of $p^*(f)$ in the constant midband region. This equation holds only for $p_o^*/p^*(f) < 4$; the increase in β is greater for $p_o^*/p^*(f) > 4$. Thus, at 1-db points, $\beta = 1.56$; at 3-db points, $\beta = 1.95$; and at 6-db points, $\beta = 2.78$.

The increase of β for small $p^*(f)$, in radio-astronomy measurements, implies that the observed frequency band should be in the constant midband region of the receiver power-transfer function $G(f+f_o)$. A correction, of course, is made for the multiplication of the receiver input spectrum $T(f+f_o)$ by $G(f+f_o)$ (see section 4.2a). The uncertainty of the $T(f+f_o)$ measurement will increase, however, at the edges of the band in a manner indicated above.

The spectral rms deviation results discussed in this section will be compared in section 6.5 with the rms deviation of the data taken in the deuterium-line experiment; the results are in excellent agreement.

6.3 MEASUREMENT OF A KNOWN NOISE-POWER SPECTRUM

a. Procedure

The goal of this test was to compare, as accurately as possible, a spectral measurement made by the one-bit digital autocorrelation method with a spectral measurement performed by some other method. The limitation on the accuracy of the comparison lies in the question of how accurately the spectrum can be determined by the "other method." The basic limitation on the accuracy of the autocorrelation method is the statistical uncertainty arising from the finite duration of data; this uncertainty can easily be made less than 0.1 per cent.

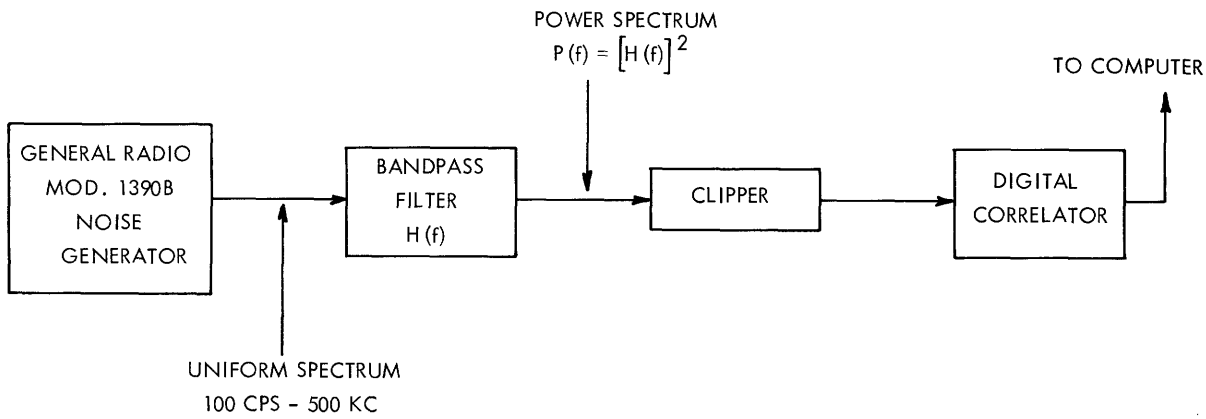

Fig. 23. Procedure for producing the "known" power spectrum.

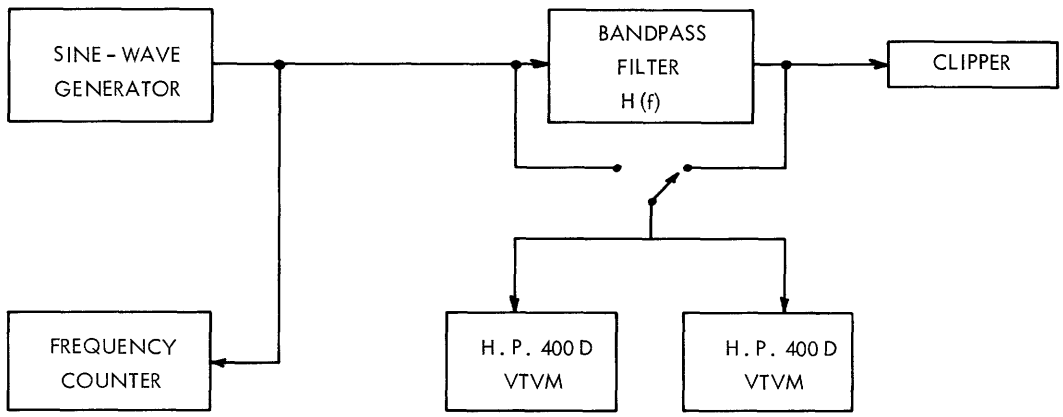

Fig. 24. Procedure for measuring $|H(f)|$.

A spectrum that is "known" with an accuracy of approximately 1 per cent can be produced by passing white noise (uniform spectrum) through a filter whose power transfer function $|H(f)|^2$ is measured (see Figs. 23 and 24). The power spectrum P(f) at the output of the filter is given in terms of the input spectrum $P_o(f)$ by

$$P(f) = |H(f)|^2 P_o(f). \tag{163}$$

Thus if $P_o(f)$ is constant over the region and H(f) is nonzero, then P(f) is proportional to $|H(f)|^2$.

The one-bit autocorrelation-function method of spectral measurement produces a spectral estimate $p_i'(f)$, whose mean is the smoothed and normalized spectrum $p^*(f)$. Ten such estimates (i = 1 to 10) were obtained with the same equipment that was utilized in the deuterium-line experiment; this was one of the early tests of the equipment. A 75-kc sampling rate and 1-hour integration time were used; 21 points on the autocorrelation were determined; and a uniform weighting function was applied in the Fourier transformation. According to Table II and Eq. 121, the frequency resolution Δf is 2.16 kc, and the statistical uncertainty $\sigma_{p1}/p(f)$ is 0.053 per cent.

The arithmetic average of the 10 estimates is defined as $p_{av}'(f)$, where

$$p_{av}'(f) = \frac{1}{10} \sum_{i=1}^{10} p_i'(f). \tag{164}$$

The rms deviation of the spectral estimate $\sigma_{p1}(f)$ is estimated by $\sigma_p'(f)$ which is defined as follows:

$$\sigma_p'(f) = \sqrt{\frac{1}{10} \sum_{i=1}^{10} [p_i'(f) - p_{av}'(f)]^2}. \tag{165}$$

The object of the experiment, then, is to compare $p_{av}'(f)$ or $p_i'(f)$ with the $|H(f)|^2$ measurement. We shall also compare $\sigma_p'(f)$ with the theoretical value $\sigma_{p1}(f)$.

The measured value of $|H(f)|^2$, which we shall call $|H_m(f)|^2$, cannot be compared directly with $p_{av}'(f)$ or $p_i'(f)$, since these spectra have been normalized and smoothed. Therefore $|H_m(f)|^2$ was also smoothed and normalized to give $p_m(f)$, where

$$p_m(f) = \frac{|H_m(f)|^2 * W(f)}{\int_0^{f_s/2} |H_m(f)|^2 * W(f)\, df}. \tag{166}$$

(Here, the asterisk denotes convolution.) Note that even if $|H_m(f)|^2$ were perfectly measured, $p_m(f)$ would not quite be equal to $p^*(f)$ because $p^*(f)$ also contains a modification,

because of sampling (see Eq. 40). As a result, a difference between $p^*(f)$ and $p_m(f)$ should occur for frequencies near half the sampling frequency.

b. Results

The results of the experiment are presented in Fig. 25. In general, the agreement of the spectrum determined by the measurement of $|H(f)|$ and the spectrum measured by the

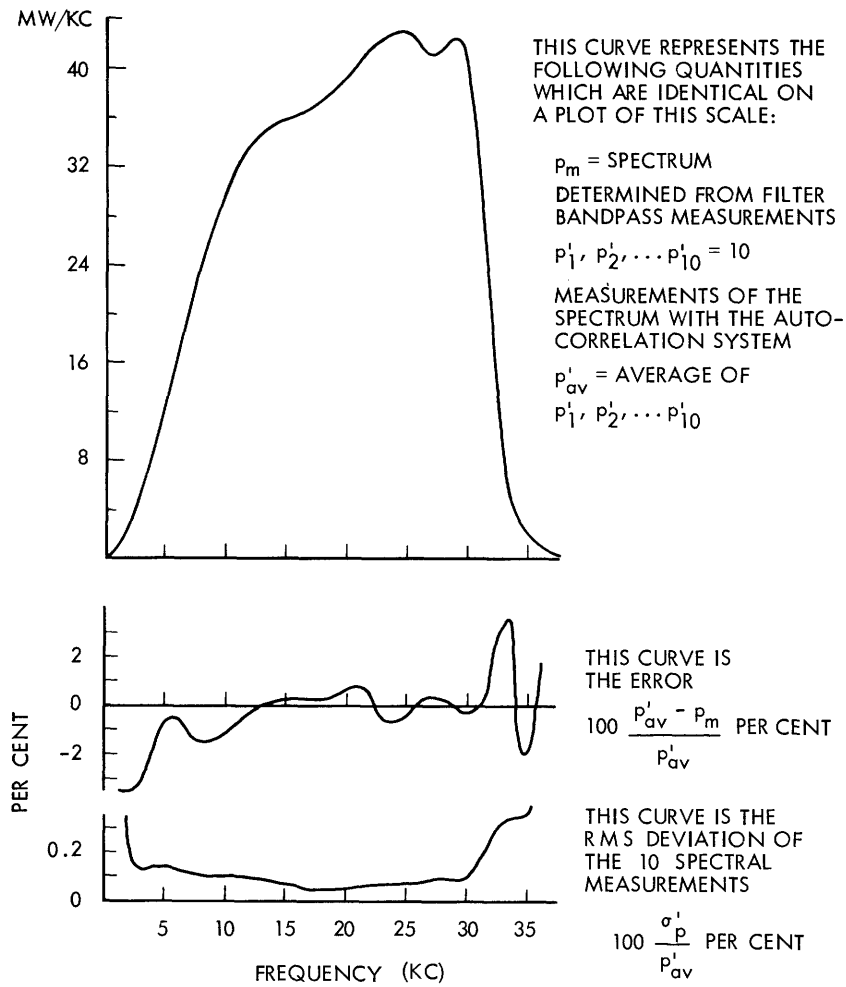

Fig. 25. Results of measurement of known noise-power spectrum.

one-bit autocorrelation system is excellent. Within the region (6-32 kc) between the filter half-power points, the largest error is 1.5 per cent which is probably the result of error in the measurement of $|H(f)|$. The large increase in error for f > 32 kc is due to spectral foldover (an effect of sampling). The increase in the error at very low frequencies may be due to the fact that the noise generator does not have a flat spectrum at these frequencies. The error may also be due to increased rms deviation for small $p^*(f)$ as was discussed in section 6.2c.

The estimate of the rms deviation, $\sigma'_p(f)$, is also shown in Fig. 25, and is of the order of a few tenths per cent. This is higher than the theoretical value of 0.053 per cent (which applies only in the midband region between 6 kc and 32 kc). The reason for the higher experimental value apparently lies in variations in the filter characteristics during the measurement time. The temperature coefficients of the capacitors and inductors used in the filter are of the order of 200 ppm per degree Centigrade. The measurements of the 10 spectra took two days, and it is estimated that the temperature varied ±5°C, thereby causing a ±0.1 per cent change in inductor and capacitor values. This would tend to shift the filter center frequency; this effect can be observed upon examination of the 10 spectra, and is evident both in the shape and magnitude of the experimental rms deviation curve. Subsequent experiments indicate that the system does realize the theoretical rms deviation.

6.4 MEASUREMENT OF ARTIFICIAL DEUTERIUM LINES

The goal of the deuterium-line experiment was to detect the 327-mc deuterium line if the galactic and terrestrial deuterium-to-hydrogen ratios were equal. The search was made for the line in absorption from the Casseopeia A radio source. The spectrum that is expected in this case can be predicted from hydrogen-line observations in this same direction and is shown in Fig. 31. Essentially, 0.01 per cent dip in the noise spectrum, 3 kc wide, near 327 mc must be measured. The receiver noise temperature is approximately 1000°; the background source, Casseopeia A, supplies another 1000°; and the peak deuterium absorption would be approximately 0.2° if the galactic and terrestrial abundance ratios were equal.

A spectrum that is similar to this (a "bump" is produced instead of a "dip") can be generated with the apparatus shown in Fig. 26. A noise spectrum, 3 kc wide, centered at 18 kc, is generated by the noise generator-filter method discussed in section 6.3. This spectrum is heterodyned up to 327 mc through the use of the receiver local oscillators. Care was taken to prevent the generation of spurious signals. The signal is passed through a calibrated (±.5 db) high-frequency attenuator and then coupled through the -20 db ports of two-directional couplers to give two outputs. The radio source, Casseopeia A, is simulated by high-frequency broadband noise generators attenuated to a proper level.

Two sources of the signal are needed, since both polarizations are observed by the deuterium-line equipment. In the acutal experiment, each polarization gives an independent but statistically alike signal; this doubles the effective observation time and, hence, increases the sensitivity by $\sqrt{2}$. In our artificial experiment, two separate high-frequency noise generators (each simulating a component of the random polarization of Casseopeia A) were used, and hence the 1000° broadband noise signals are independent. In contrast to this, the weak, 3 kc-wide, artificial deuterium-line signals arise in a common source, and therefore are not independent. As long as these signals are

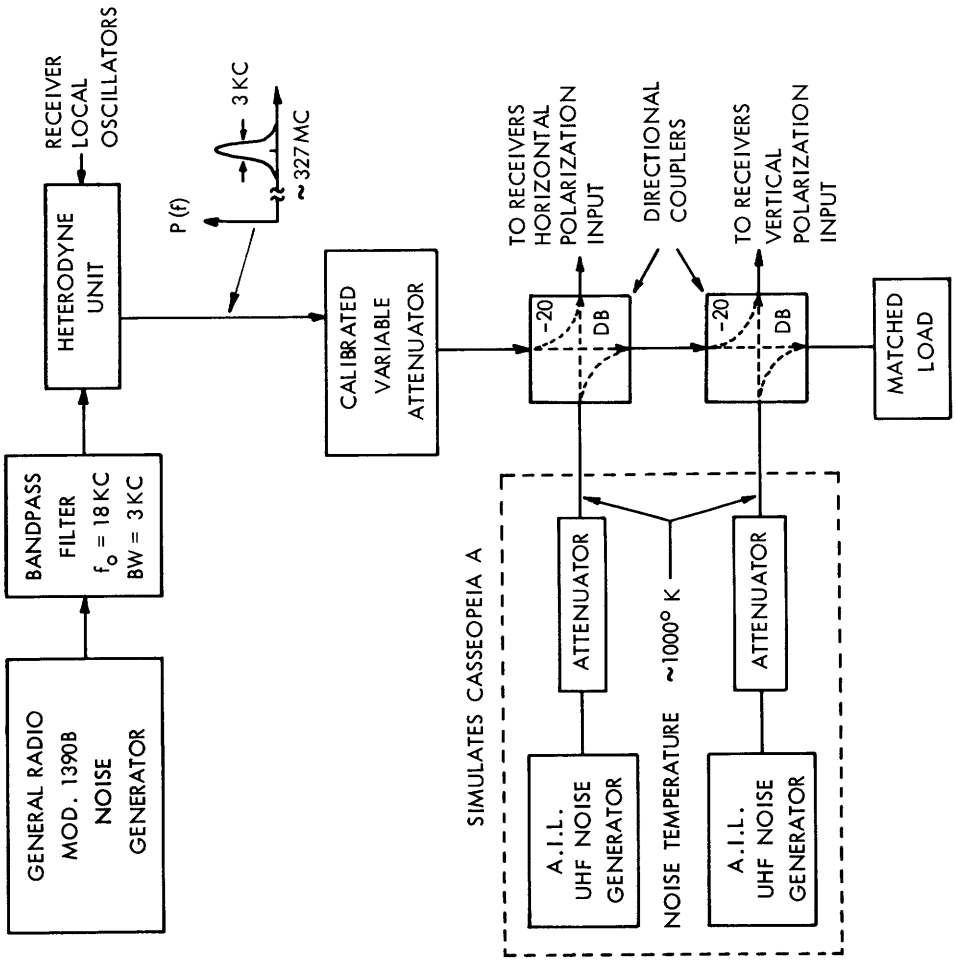

Fig. 26. Artificial deuterium-line generator.

small (« 1000°), there will not be an increase in rms fluctuation, because of the coherence of the two artificial signals.

The ratio of the artificial signal power to the broadband noise power can be determined by observing (on a meter) the change in total receiver output power as the artificial signal is increased by varying the calibrated attenuator. By knowing the shape of the artificial line and the shape of the receiver bandpass, the peak artificial signal temperature can be found. The attenuator then provides a means of adjusting the strength of the artificial deuterium line.

The results of some artificial deuterium-line observations are shown in Fig. 27. Two observations of an artificial line, which is 1 per cent of the total noise temperature (2000°), are shown in the top part of Fig. 27. The two observations were performed two weeks apart and illustrate the repeatability of the measurement.

The lower part of Fig. 27 shows the results of an observation of a 0.02 per cent,

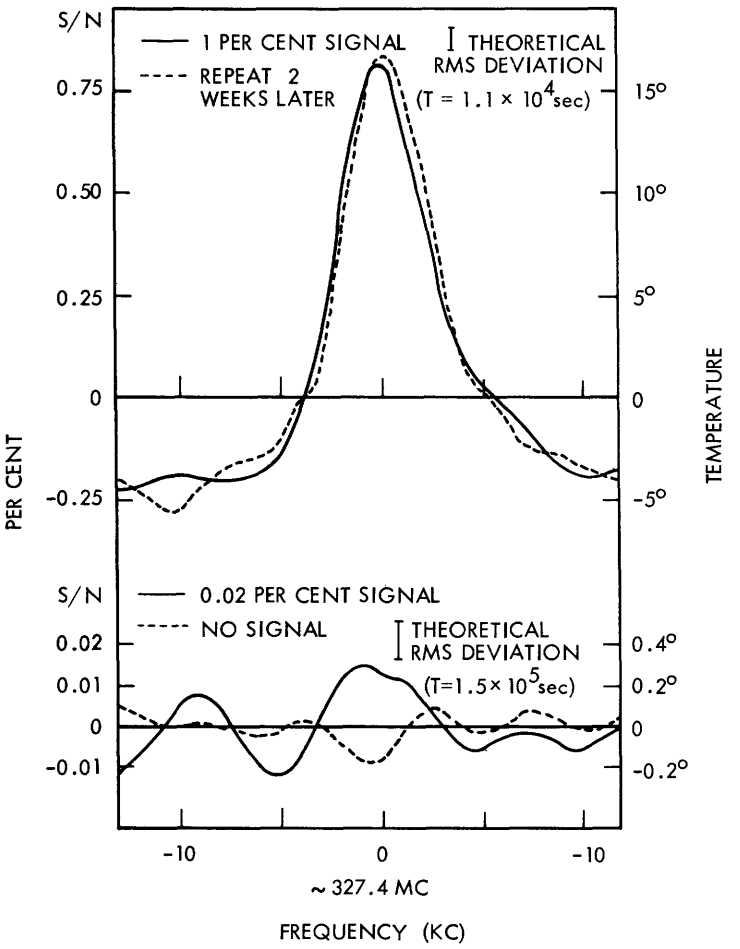

Fig. 27. Artificial deuterium-line results. Ordinates are expressed as a temperature difference from T_{av}, the total noise temperature (~2000°) averaged over the receiver bandpass.

0.4°, artificial line and, for comparison, an observation with no line. The 0.02 per cent line is just at the borderline of detectability, being just twice the theoretical rms deviation for the integration time of 1.5×10^5 seconds.

6.5 ANALYSIS OF THE RMS DEVIATION OF THE DEUTERIUM-LINE DATA

a. Theoretical RMS Deviation

The deuterium-line data were processed slightly differently from the procedure used to specify antenna temperature (see Section IV), and thus an rms deviation equation slightly different from that given by Eq. 148 results. The quantity that was examined is the measured difference spectrum $\delta p'(f) = p'(f) - p'_c(f)$ divided by the measured receiver bandpass function $p'_o(f)$. This dimensionless quantity, $\delta p'(f)/p'_o(f)$, will be designated s(f), and has physical significance in that it is simply related to the deuterium optical depth.

Under the assumption (discussed in section 5.1b) that the receiver is balanced ($\delta T_{av} = 0$), the mean of s(f) is given by Eq. 142 as

$$\overline{s(f)} = \overline{\left[\frac{\delta p'(f)}{p'_o(f)}\right]} = \frac{T^\dagger(f+f_o) - T_{av}}{T_{av}}, \tag{167}$$

where $T^\dagger(f+f_o)$ is the smoothed input temperature spectrum, and T_{av} is $T^\dagger(f+f_o)$ averaged in frequency over the receiver bandpass. $T^\dagger(f+f_o)$ is the sum of the smoothed antenna temperature spectrum $T_a^\dagger(f+f_o)$ and the receiver noise temperature T_r. (All of these terms were defined and discussed in Section IV.) If Eq. 167 is solved for $T^\dagger(f+f_o)$, Eq. 140 (with $\delta T_{av} = 0$) results. The rms deviation of $T_a^\dagger(f+f_o)$ is then given by Eq. 148.

The rms deviation of s(f) is found upon application of Eq. 143; this gives the rms deviation of a normalized spectral estimate, such as p'(f), $p'_c(f)$ or $p'_o(f)$. As explained in section 4.4, the rms deviation of $p'_o(f)$ can be neglected. The rms deviation of $\delta p'(f) = p'(f) - p'_c(f)$ is twice that of p'(f) or $p'_c(f)$ (a factor of $\sqrt{2}$ arises because $\delta p'(f)$ is the difference of two random quantities; another factor of $\sqrt{2}$ arises because only half the total observation time τ is spent on each measurement). The result is

$$\Delta s(f) = \frac{2\alpha\beta}{\sqrt{\tau \Delta f}} \cdot \sqrt{1 - \Delta f/b} \tag{168}$$

where α, β, Δf, and b are defined after Eq. 143. The numerical values that apply in the deuterium-line experiment are $\alpha = 0.866$, $\beta = 1.39$, $\Delta f = 3.75$ kc, and b = 30 kc.

The time τ in Eq. 168 is equal to the actual observation time only if a single switched receiver is used, and if no blanking time is allowed in the switching cycle. As previously explained, four switched receivers, each monitoring an independent signal, were used in the deuterium-line experiment. The time τ then becomes the observation

time per receiver and, except for blanking, would be equal to 4 times the actual observation time. The blanking time is 1/4 of the total time; thus τ is equal to 3 times the actual deuterium-line observation time τ_a. In the course of the experiment, τ was recorded (it is proportional to the number of counts accumulated in the first counter of the correlator), and whenever observation times are quoted, τ (and not τ_a) is meant. In the deuterium-line experiment a τ of 76.5 days was achieved, even though the antenna was in use only 68 days and the source was observable only 12 hours a day.

One further step was taken in the processing of the deuterium-line data. A linear (with frequency) correction was applied to the measured spectrum to remove any slope that was present (typical slope correction, 1.5×10^{-5}/kc). In other words, the slope-corrected function c(f) is given by

$$c(f) = s(f) - (a+bf), \tag{169}$$

where a and b are chosen to minimize the mean-square value of c(f). The reason that this correction is needed is that there are imperfections in the front-end switch and noise source (see section 5.1a).

Some of the statistical error is removed by the slope correction, and the theoretical rms deviation of c(f) is lower than that of s(f). It can be shown (Kenney and Keeping,[21] Section 8.7) that the reduction is a factor of $\sqrt{1 - 2/N}$, where N is the number of independent points on the curve. Assuming that points $\Delta f/2 = 1.87$ kc apart are independent, N = 13.4 for the 25-kc bandwidth that was analyzed. Thus the rms deviation should be reduced by a factor of 0.92. The result of applying this correction and substituting numerical values for α, β, and b is

$$\Delta c(f) = \frac{2.05}{\sqrt{\tau \Delta f}}. \tag{170}$$

It is convenient at times to give a temperature scale to s(f) and c(f) by multiplying them by T_{av} which was approximately 2000°. The quantity $\Delta T \equiv T_{av} \Delta c(f)$ then can be interpreted as the rms deviation of the measurement of $T^{\dagger}(f+f_o) - T_{av}$, and is given by

$$\Delta T = \frac{2.05}{\sqrt{\tau \Delta f}} T_{av} \tag{171}$$

$$= \frac{1.1°}{\sqrt{(\tau)_{HRS}}}. \tag{172}$$

b. Experimental Results

The deuterium-line data consist of 169 spectral estimates, each accumulated with an average observation time, τ, of 10.8 hours. These estimates will be labeled $c_i(f)$ (i goes from 1 to 169). The mean of each estimate is given by Eq. 167 (with a slope correction), and the rms deviation is given by Eqs. 170, 171 or 172. The computer

program that was used to produce each $c_i(f)$ from the output of the digital correlator is listed in Appendix D.

Each spectral estimate was plotted and examined for interference. A few spectra were discarded because of their unusual appearance. The remaining 169 spectra were averaged into weekly averages, three-week averages, and a final, over-all, nine-week average. The results of the three-week and nine-week averages are shown in Fig. 31.

An experimental estimate of the frequency-averaged rms deviation of each $c_i(f)$ is given by Δc_i, computed as follows:

$$\Delta c_i = \sqrt{\frac{1}{26} \sum_{f=5}^{30} c_i^2(f)}. \tag{173}$$

(It is assumed in this computation that the mean of each $c_i(f)$ is zero, which means that the deuterium line is not present. Unfortunately, this proved to be the case.) The rms error of an estimate of the rms deviation computed in this manner is equal to $100/\sqrt{2I}$ per cent (Burington and May,[20] p. 149), where I is the number of independent points on the spectrum. Assuming that points $\Delta f/2 = 1.87$ kc apart are independent, $I = 13.4$, and the error is approximately 19 per cent. If the Δc_i from L different records are averaged together, the rms error will be $19/\sqrt{L}$ per cent.

In addition to computing the Δc_i for each 10.8-hour record, the frequency-averaged rms deviation was also computed for longer records formed by averaging the 10.8-hour records. The results are presented in Table VII and, in somewhat different form, in Fig. 28.

Table VII. Analysis of rms deviation of the deuterium-line data.

Average Record Length τ	Number of Records L	Theoretical rms Deviation $T_{av}\Delta c$	Experimental rms Deviation $T_{av}\Delta c_i$
10.8 hrs	169	0.340°	0.340°±0.010°
229 hrs	8	0.073°	0.087°±0.012°
612 hrs	3	0.045°	0.066°±0.014°
1835 hrs	1	0.026°	0.042°±0.016°

These results indicate that the departure from the theoretical sensitivity is not large, even for integration times of the order of 10^6-10^7 seconds. This result should be compared with those from the conventional Dicke radiometer, for which the theoretical rms deviation is usually not achieved for integration times longer than from 10^2 to 10^3 seconds.

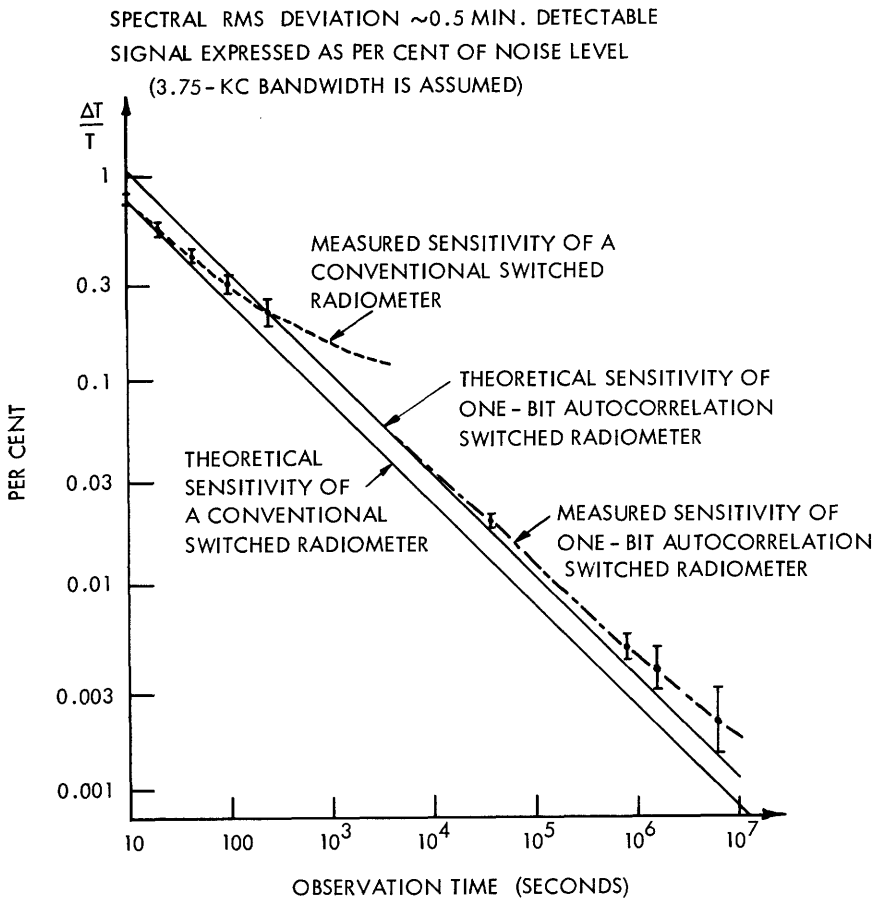

Fig. 28. Experimental and theoretical sensitivity of a conventional Dicke radiometer compared with a one-bit autocorrelation radiometer. (The measurements on the Dicke radiometer were made by Cohen and Orhaug.[22])

The stability advantage of the one-bit autocorrelation system is clearly in evidence in Fig. 28.

VII. THE DEUTERIUM-LINE EXPERIMENT

7.1 INTRODUCTION

At present, only one spectral line has been observed in radio astronomy. This is the 1420-mc (21-cm) hydrogen line, detected by Ewen and Purcell, in 1951. This line is caused by hyperfine splitting of the ground state of cold, neutral, atomic hydrogen that is in the interstellar space of a galaxy. During the past 11 years, extensive studies of the hydrogen line have been made (see Shklovsky,[23] Chapter 4), and valuable physical characteristics of the interstellar medium, such as density, temperature, and line-of-sight velocity, have been measured. Indeed, it has been found that a large fraction of the total mass of our galaxy consists of this neutral atomic hydrogen, which, at present, is not observable by any other means.

Deuterium, an isotope of hydrogen (sometimes called "heavy hydrogen") exhibits a similar hyperfine transition occurring at approximately 327 mc. In 1952, Shklovsky[24] predicted that it might be possible to detect this line. Since 1952, there have been at least four attempts to detect the deuterium line, and all have given negative results.[25-28] In the most recent of these attempts, by Adgie at Jodrell Bank, the experimental sensitivity was not quite sufficient to detect the line if the interstellar deuterium-to-hydrogen ratio, N_D/N_H, was equal to the terrestrial value 1/6600. Consequently, the goal of our experiment was to detect the deuterium line if the interstellar and terrestrial deuterium-to-hydrogen ratios were equal.

The interstellar deuterium-to-hydrogen ratio is of astrophysical importance because it gives information concerning the nucleogenesis of the interstellar medium.[29, 30] The role that N_D/N_H plays in nucleogenesis will be very briefly outlined here.

The relative abundances of elements formed by the nuclear burning in a star can be predicted by stellar nuclear theory. For most of the elements, these abundances agree remarkably well with the abundances found on earth and in meteorites. But, an outstanding anomaly exists for deuterium. The predicted value of N_D/N_H is 10^{-17}, which is approximately 10^{13} times less than the measured terrestrial ratio.

Fowler, Greenstein, and Hoyle[31] have attempted to explain the high terrestrial N_D/N_H ratio in terms of nuclear processes that occurred on the primordial earth. According to this theory, the N_D/N_H ratio 1/6600 would appear to be a purely terrestrial phenomenon, and there would be no reason to expect this value to be true in interstellar space. If the interstellar medium consists primarily of the debris of stars, an interstellar N_D/N_H of 10^{-17} would be expected. An interstellar N_D/N_H of 1/6600 would tend to imply that both the earth and the interstellar medium were formed from material which had never been through the stellar-burning process.

Some background material concerning the deuterium-line experiment was presented in the author's Bachelor's thesis.[32] The major topics discussed there are:

1. The bandwidth and magnitude of the expected deuterium line are derived in terms

of N_D/N_H. (This will be discussed in this report.)

2. The choice of a direction of observation is discussed. Under the assumption that N_D/N_H is constant in the interstellar medium, a prediction of the best signal-to-noise ratio for an attempt to detect the line in absorption from the Cas A radio source is made.

The deuterium-line observations were performed with the 85-ft Howard Tatel Radio Telescope at the National Radio Astronomy Observatory, Green Bank, West Virginia. The receiving system has already been discussed in this report. The basic steps in the signal-processing system are given in Figs. 7 and 11. A detailed block diagram of the deuterium-line receiver is given in Fig. 13, and the components of the system are discussed in Section V. The treatment of the data and the theoretical and experimental sensitivities are discussed in section 6.5.

7.2 PHYSICAL THEORY AND ASSUMPTIONS

The relation between the antenna temperature spectrum, $T_a(f)$, and the interstellar deuterium-to-hydrogen ratio, N_D/N_H, will be discussed now. This relationship can be written very simply if some very important assumptions are made. These assumptions have been made, but not stated, by past researchers who were looking for the deuterium line. Indeed, these same assumptions are included in the basic statement of the results of our work – The galactic deuterium-to-hydrogen ratio is less than 1/2 the terrestrial value. A few of these assumptions are not well justified and a reinterpretation of our measurements, based upon future theoretical and experimental work in astrophysics, may be necessary.

In light of the statements above, the three basic steps relating the antenna temperature to N_D/N_H will be briefly reviewed. The simple relation between $T_a(f)$ and N_D/N_H will then be stated, and the important assumptions included in this statement will be listed.

Step 1

The antenna temperature, $T_a(f)$, is equal to a weighted spatial average of the sky brightness temperature, $T_b(f, \theta, \phi)$.

$$T_a(f) = \frac{1}{4\pi} \int_{4\pi} T_b(f, \theta, \phi)\, g(\theta, \phi)\, d\Omega, \tag{174}$$

where $g(\theta, \phi)$ is the antenna gain function, and $d\Omega = \sin\theta\, d\theta d\phi$ is the solid-angle increment.

Step 2

The sky brightness temperature, $T_b(f, \theta, \phi)$, is related by the classical equation of transfer (see Chandrasekhar[33]) to the optical depth of the gas (deuterium or hydrogen), $\tau(f, \theta, \phi)$, the spin temperature of the gas, T_g (assumed to be constant in space and frequency), and the background brightness temperature, $T_{bg}(\theta, \phi)$ (assumed to be

independent of frequency). The relation is

$$T_b(f, \theta, \phi) = T_{bg}(\theta, \phi)\, e^{-\tau(f, \theta, \phi)} + T_g[1-e^{-\tau(f, \theta, \phi)}]. \tag{175}$$

Step 3

The optical depth of the gas is related to $n(\theta, \phi)$, the number of gas atoms (in both of the hyperfine states) in a column of unit cross section extending from the observer to infinity in the direction of θ and ϕ. The relation[32] is

$$\tau(f, \theta, \phi) = \frac{hc^2}{8\pi k} \cdot \frac{A}{T_g f_o \Delta f} \cdot \frac{g_1}{g_1+g_o} \cdot u(f) \cdot n(\theta, \phi), \tag{176}$$

where $hc^2/8\pi k$ is a constant, A is the spontaneous emission probability, T_g is the spin temperature, f_o is the line frequency, Δf is the Doppler-broadened linewidth, g_1 and g_o are the statistical weights of the upper and lower states, and u(f) is the line-shape function $[u(f_o)=1]$.

The problem is to apply these equations to the physical situation shown in Fig. 29, and to interpret a deuterium-to-hydrogen ratio from our deuterium results, previous

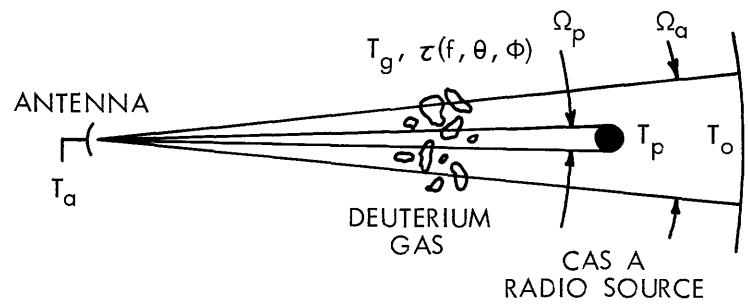

Fig. 29. Configuration for the deuterium-line experiment.

hydrogen-line observations made in the same direction, and measurements and calculations of the physical properties of deuterium and hydrogen.

In the configuration of Fig. 29, the background brightness temperature distribution, $T_{bg}(\theta, \phi)$, consists of a term, T_o, which is constant within the antenna beam and a term, $T_p(\theta, \phi)$, representing the contribution of the discrete source. It is convenient to describe the antenna temperature in terms of measurable spatial averages of $T_p(\theta, \phi)$ and $e^{-\tau(f, \theta, \phi)}$. These spatial averages are T_p', $e^{-\tau'(f)}$, and $e^{-\tau''(f)}$, defined as follows:

$$T_p' \equiv \frac{1}{4\pi} \int_{4\pi} T_p(\theta, \phi)\, g(\theta, \phi)\, d\Omega \tag{177}$$

$$e^{-\tau'(f)} \equiv \frac{1}{4\pi} \int_{4\pi} e^{-\tau(f, \theta, \phi)} \cdot \frac{T_p(\theta, \phi)}{T_p'} \cdot g(\theta, \phi)\, d\Omega \tag{178}$$

$$e^{-\tau''(f)} \equiv \frac{1}{4\pi} \int_{4\pi} e^{-\tau(f,\theta,\phi)} \cdot g(\theta,\phi)\, d\Omega. \tag{179}$$

In words, T'_p is the contribution to antenna temperature from the discrete source; $\tau'(f)$ is minus the logarithm of the average of $e^{-\tau(f,\theta,\phi)}$ taken over the solid angle subtended by the discrete source; and $\tau''(f)$ is minus the logarithm of the average of $e^{-\tau(f,\theta,\phi)}$ taken over the entire antenna beam. It is important to note that $\tau'(f)$ and $\tau''(f)$ are not just simple averages of $\tau(f)$.

Equations 174 and 175 can be combined to specify the antenna temperature in terms of the quantities defined above,

$$T_a(f) = T'_p e^{-\tau'(f)} + T_o e^{-\tau''(f)} + T_g[1-e^{-\tau''(f)}]. \tag{180}$$

The first term in this equation represents the contribution to antenna temperature from the discrete source attenuated by the gas, the second represents the background contribution attenuated by the gas, and the last represents emission by the gas.

For the deuterium-line case, $\tau'(f) = \tau'_D(f)$ and $\tau''(f) = \tau''_D(f)$ are much less than one. The exponentials can be expanded to give

$$T_a(f) = T'_p - \tau'_D(f)\, T'_p + T_o + \tau''_D(f)\, [T_s - T_o]. \tag{181}$$

In the direction of the Cas A radio source, the last term can be neglected, since $\tau''_D(f)$ will be of the same order as $\tau'_D(f)$ and $T'_p \sim 1000°$ (with an 84-ft telescope) is much larger than $T_g - T_o \sim 45°$ (under the assumption that T_g for deuterium is the same as T_g for hydrogen, ~125°K). Thus the final result for the antenna temperature is

$$T_a(f) = T'_p + T_o - \tau'_D(f)\, T'_p. \tag{182}$$

The relation between the peak optical depth $\tau'_D(f_D)$ and N_D/N_H can be calculated with the aid of Eq. 176 evaluated for both deuterium and hydrogen. We find

$$\frac{\tau'_D(f_D)}{\tau'_H(f_H)} = 0.30\, \frac{N_D}{N_H}. \tag{183}$$

The following assumptions, listed in order of increasing degree of justification, are included in Eq. 183.

1. The value of N_D/N_H that is interpreted from the measurement of $\tau'_D(f_D)/\tau'_H(f_H)$ really depends on the angular distribution of hydrogen, $n_H(\theta,\phi)$, within the solid angle, Ω_p, subtended by the discrete source. It also depends on the discrete source temperature distribution, $T_p(\theta,\phi)$. These statements are illustrated in Fig. 30.

The ratio $\tau_D(f_D,\theta,\phi)/\tau_H(f_H,\theta,\phi)$ does not depend on $n_H(\theta,\phi)$ if the deuterium spatial distribution is the same as that of hydrogen (that is, $n_D(\theta,\phi) = (N_D/N_H)\, n_H(\theta,\phi)$). Even if the distributions are the same, the measured ratio $\tau'_D(f_D)/\tau'_H(f_H)$ depends on $n_H(\theta,\phi)$. This results from the peculiar way in which $\tau'_H(f_H)$ depends on $\tau_H(f_H,\theta,\phi)$ in Eq. 178.

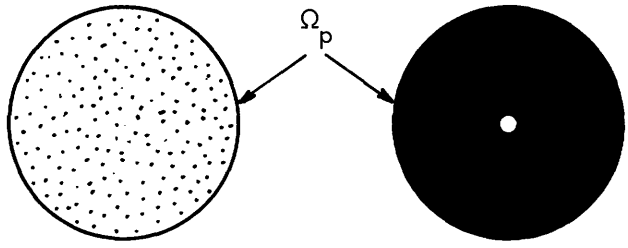

Fig. 30. Two extremes of the possible distributions of hydrogen optical depth in front of the Cas A radio source are shown. Both configurations would give the same measured, spatially averaged, hydrogen optical depth, $\tau'_H(f_H)$, defined by Eq. 183. The distribution at right, however, would give a measured, spatially averaged, deuterium optical depth, $\tau'_D(f_D)$, which would be 100 times greater than that given by the uniform distribution with the same N_D/N_H ratio. The major point is that the assumption of uniform hydrogen optical depth is the most conservative distribution that can be chosen as far as setting an upper limit on the N_D/N_H ratio is concerned.

If $\tau'_H(f_H)$ were a simple spatial average of $\tau_H(f_H, \theta, \phi)$, then $\tau'_D(f_D)/\tau'_H(f_H)$ would be directly related to N_D/N_H in a manner independent of $n_H(\theta, \phi)$ [assumed to be proportional to $n_D(\theta, \phi)$].

Because of the high resolution that is required, neither $n_H(\theta, \phi)$ nor $T_p(\theta, \phi)$ were measured. The assumption in Eq. 183 is that both $n_H(\theta, \phi)$ [and hence $\tau_H(f_H, \theta, \phi)$] and $T_p(\theta, \phi)$ are constant over Ω_p. It appears (see Fig. 30) that this is the most conservative distribution that can be assumed. In other words, any other distribution would allow a lower upper limit of N_D/N_H to be interpreted from our results. Future measurements of $n_H(\theta, \phi)$ and $T_p(\theta, \phi)$ for the Cas A radio source will allow a more sensitive interpretation of our results.

2. The spin temperatures for deuterium and hydrogen are assumed to be equal. Justification of this assumption is uncertain, since it depends on estimates of the intensity and detailed profile of the interstellar radiation field at the frequency of deuterium Lyman α radiation. This problem has been discussed by Field.[34]

3. The ratio of the Doppler-broadened linewidths of deuterium and hydrogen, $\Delta f_D/\Delta f_H$, would be equal to the ratio of the line frequencies, f_D/f_H, if the atoms had the same rms velocity. A portion of the rms velocity, however, is due to thermal motion in which the deuterium atoms, having twice the mass, would have $1/\sqrt{2}$ of the rms thermal velocity of the hydrogen atoms. The other component of rms velocity is believed to result from random cloud motion that would give the same velocity to deuterium and hydrogen atoms. These velocities are independent, and hence the total rms velocity is the square root of the sum of the squares of the rms thermal and random velocities.

Approximately 0.5 Δf_H is due to thermal motion, and thus 0.866 Δf_H must be due to random cloud motion. These numbers give $\Delta f_D/\Delta f_H = 0.935\, f_D/f_H$.

4. The value of the deuterium transition probability, $A_D = 4.65 \times 10^{-17}$ sec^{-1} (given by Field[34]) is correct. (This same value was computed independently by Alan H. Barrett of the Massachusetts Institute of Technology.) The value, $A_D = 6.6 \times 10^{-17}$, given by Shklovsky,[23] is incorrect (Eqs. 14-6, 15-4, 18-3, and 18-4 appear to be incorrect). The value of $A_H = 2.85 \times 10^{-15}$ sec^{-1} is not in doubt.

5. The value of the peak hydrogen optical depth, $\tau'_H(f_H)$, in the Cas A radio source is also the subject of some controversy, its large value being difficult to measure. The first observers, Hagen, Lilley, and McClain,[35] using a 50-ft paraboloid, report $\tau'_H(f_H) = 2.6$. Muller,[36] using an 83-ft reflector, gives 4.0, and observers at California Institute of Technology,[37] using a single 90-ft telescope, report $\tau'_H(f_H) > 4.7$, and 3.4±.4 when using two 90-ft telescopes as an interferometer. We shall assume that a value, $\tau'_H(f_H) = 4.0$, is correct, and thus Eq. 183 gives

$$\tau'_D(f_D) = 1.8 \times 10^{-4} \tag{184}$$

for $N_D/N_H = 1/6600$.

7.3 RESULTS AND CONCLUSION

The final result of the deuterium-line data analysis described in section 6.5 is the normalized spectral function, c(f). The mean or expected value of this function is given by

$$\overline{c(f)} = \frac{T_a^{\dagger}(f+f_o) + T_r - T_{av}}{T_{av}}, \tag{185}$$

where $T_a^{\dagger}(f+f_o)$ is the smoothed (by an equivalent scanning filter of 3.75-kc bandwidth) antenna-temperature spectrum, T_r is the receiver noise temperature, and T_{av} is the frequency-averaged value of $T_a^{\dagger}(f+f_o) + T_r$ (see Eq. 134).

The antenna temperature spectrum is specified by Eq. 182 in terms of the deuterium optical depth $\tau'_D(f)$, the sky background temperature T_o, and the contribution to antenna temperature from the discrete source T'_p. The substitution of Eq. 182 in Eq. 185 gives

$$c(f) = \frac{T'_p}{T'_p + T_o + T_r} \cdot \left[\tau_{av} - \tau_D^{\dagger}(f)\right], \tag{186}$$

where τ_{av} is the frequency-averaged value of $\tau'_D(f)$, and $\tau_D^{\dagger}(f)$ is the smoothed version of $\tau'_D(f)$. (A term, $-\tau_{av}T'_p$, has been neglected in the denominator of Eq. 186.) The ratio $T'_p/(T'_p+T_o+T_r)$ was measured directly each day by noting the change in total power as the antenna was moved on and off Cas A; its value is 0.46±.02. (The individual temperatures were $T'_p \sim 920°$, $T_o \sim 80°$, and $T_r \sim 1000°$.)

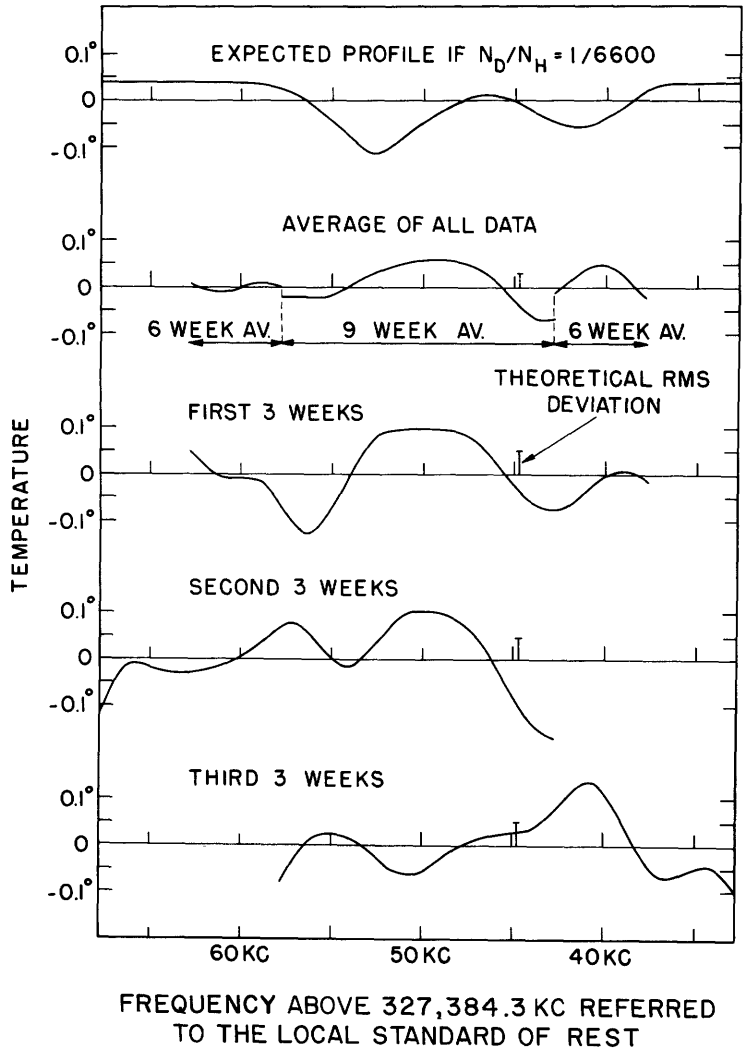

Fig. 31. Results of the deuterium-line search in the Cas A radio source. The temperature on the ordinate is with respect to the total noise temperature (~2000°) averaged over the receiver bandpass. The quantity c(f) is defined by Eq. 185.

The value of $\overline{c(f)}$ that is expected if $N_D/N_H = 1/6600$ is shown at the top of Fig. 31, and the measured results are shown beneath it. The shape of $\tau'_D(f)$ can be predicted from the measured hydrogen profile, $\tau'_H(f)$.[32] The value of the peak deuterium absorption dip, $\tau'_D(f_D)$, is given by Eq. 189. A reduction by a factor of 0.9 was allowed because of the smoothing effect of the spectral measurement system (that is, $\tau'^{\dagger}_D(f_D) = 0.9\,\tau'_D(f_D)$).

The theoretical rms deviations of the measurement are given by Eqs. 170, 171 or 172, and are indicated in Fig. 31. The theoretical rms deviation of the average of all data equals the peak spectral dip expected from an N_D/N_H of 1/36,000. If a detection criterion of twice the theoretical rms deviation (97.7 per cent confidence) is used, the minimum detectable N_D/N_H is 1/18,000. Examination of the data in section 6.5b indicates that the experimental rms deviation is approximately 1.4 times the theoretical value; thus the minimum detectable N_D/N_H should be raised to 1/13,000.

Our conclusion is that the deuterium-to-hydrogen ratio in the region examined, with probability 0.977 and within the stated assumptions, is less than half the terrestrial value.

VIII. AN ATTEMPT TO MEASURE ZEEMAN SPLITTING OF THE 21-cm HYDROGEN LINE

8.1 INTRODUCTION

The existence of a galactic magnetic field is presupposed from theories concerning the polarization of starlight, the emission of galactic radio noise, and the behavior of cosmic rays. The magnitude of the field cannot be measured directly from these effects, although estimates of from 10^{-5} gauss to 10^{-6} gauss are common. These facts have been discussed and referenced by Shklovsky,[23] and also in two papers[38, 39] that describe previous attempts to measure the field by measuring the Zeeman splitting of the 21-cm hydrogen line. The experiment was first suggested by Bolton and Wild.[40]

A brief description of the Zeeman effect on hydrogen-line radiation will now be given. The line-of-sight component of the galactic magnetic field causes a splitting of the radiation into left-hand and right-hand circularly polarized waves with a difference in frequency of 2.8 cps per 10^{-6} gauss. The sharpest hydrogen lines found in absorption of the strong discrete sources are ~10-20 kc wide, and thus the expected splitting of 3-30 cps is quite difficult to measure. The procedure consists of measuring alternately the hydrogen profile with feeds that are receptive to circular polarization of opposite sense and recording the difference profile. This difference profile, $\Delta T(f)$, is related to the observed (either polarization) profile, $T(f)$, by the following relation, which holds if the frequency splitting, Δf, is small compared with the width of the observed line:

$$\Delta T(f) = \Delta f \cdot T'(f) = 2.8 \times 10^{6}\, H \cdot T'(f), \qquad (187)$$

where H is the magnetic field, and the prime denotes derivative with respect to frequency. The observed profile and the expected difference profile for the two observed sources, Cas A and Taurus A, are shown in Figs. 32 and 33.

8.2 EXPERIMENTAL PROCEDURE

Observations of Cas A and Taurus A were performed with the use of the 85-ft Howard Tatel Radio Telescope at the National Radio Astronomy Observatory, Green Bank, West Virginia, in conjunction with a dual circular-polarization feed built by Jasik Laboratories. The receiving system that was used and the treatment of data were the same as in the deuterium-line experiment except for the following changes:

1. Instead of switching between the antenna feed and a comparison noise source, switching was performed between an antenna feed receptive to right-hand circular polarization and another feed receptive to left-hand circular polarization. Thus, a measure of the difference spectrum, $\Delta T(f)$, given by Eq. 187, is obtained. Switching between polarizations at a 1/14 cps rate was performed by using a mechanical coaxial switch. Double stub tuners were inserted between each arm of the switch and the feed, and were adjusted so that the standing-wave ratio of each polarization feed was less than 1.01 when measured through the switch.

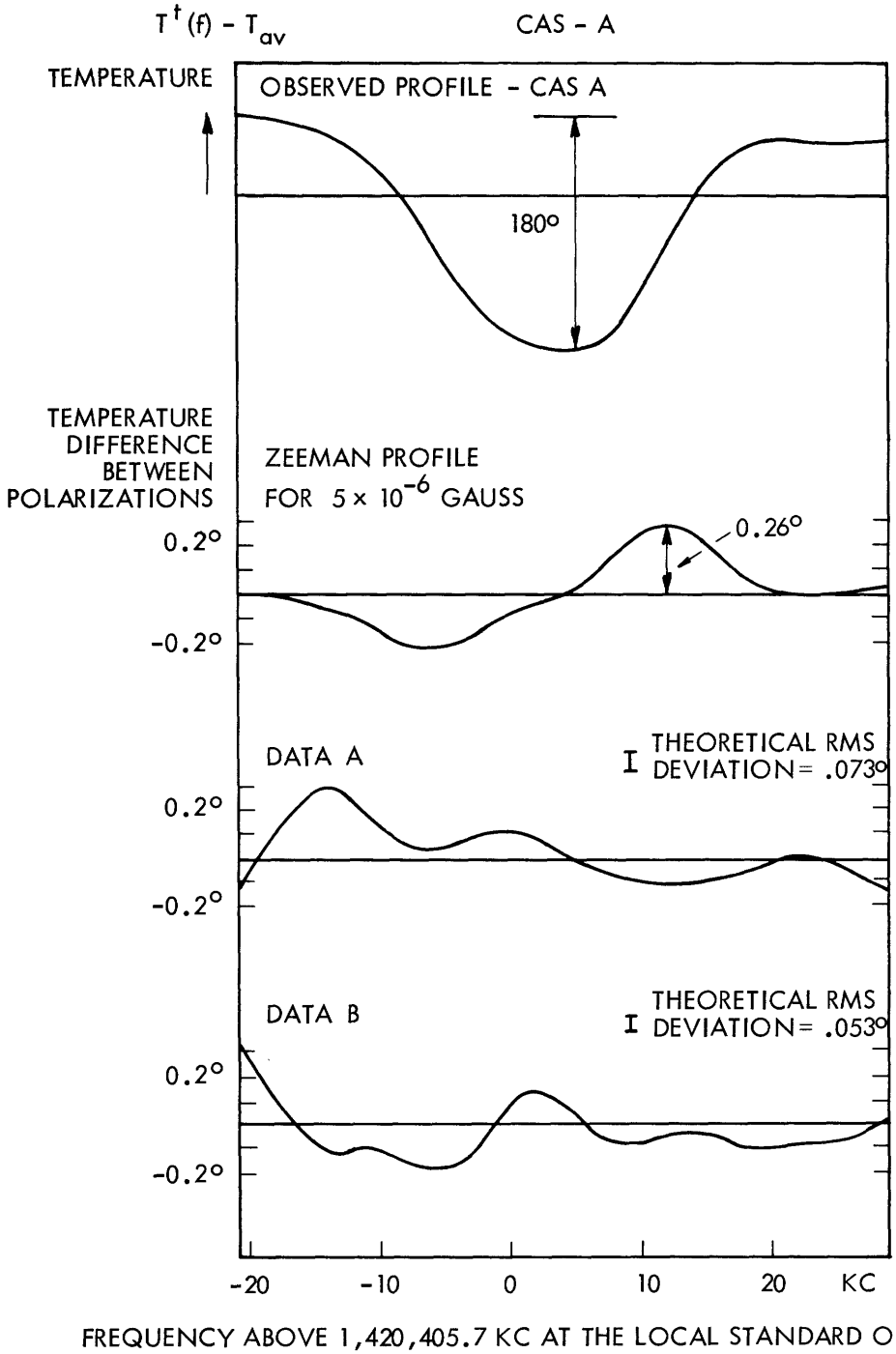

Fig. 32. Results of the attempt to measure Zeeman splitting of the 21-cm galactic hydrogen line of the Cas A radio source observed in absorption.

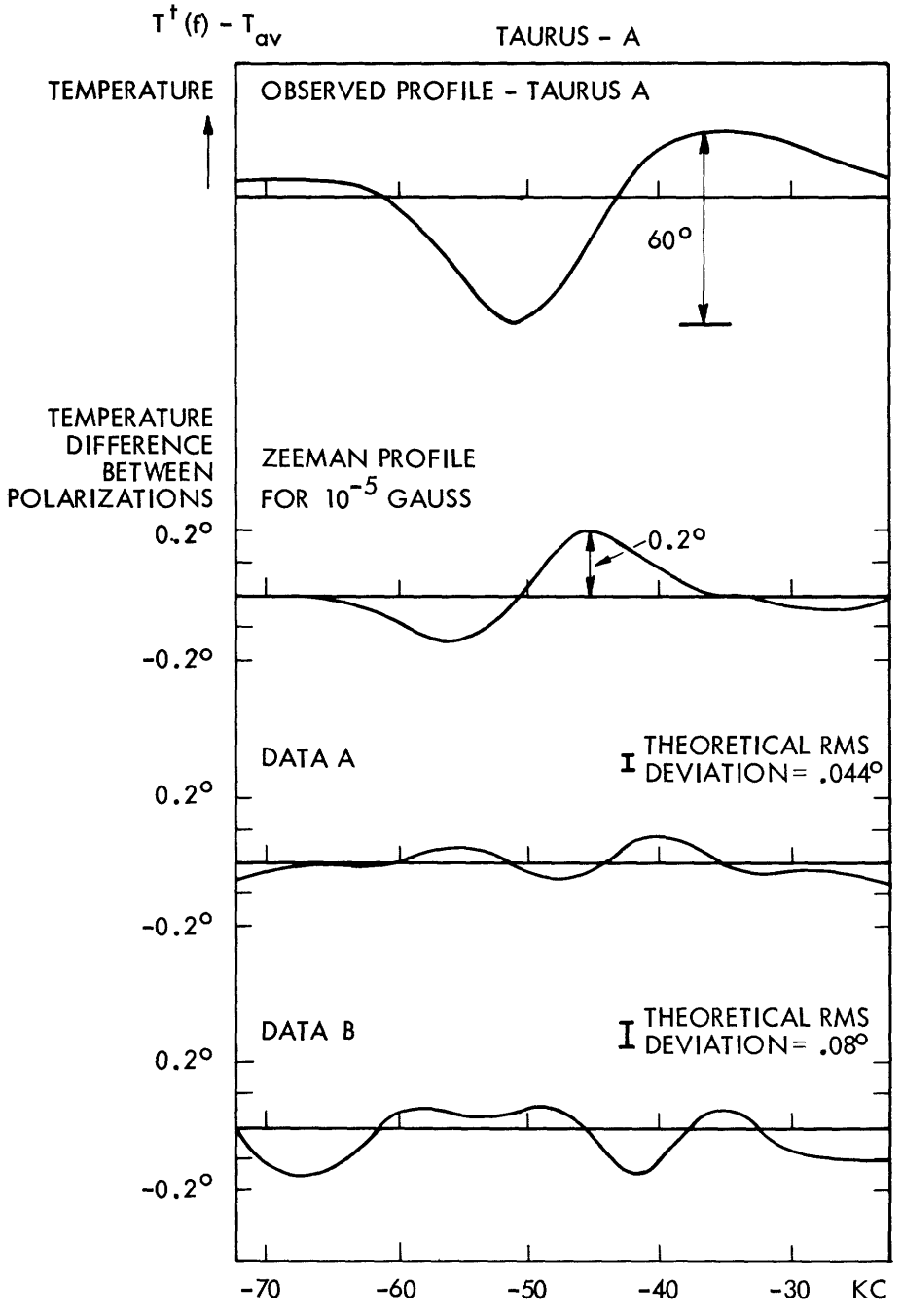

Fig. 33. Results of the attempt to measure Zeeman splitting of the galactic hydrogen line of the Taurus A radio source observed in absorption.

Table VIII. Results of Zeeman-effect experiments.

	Theoretical RMS Fluctuation*	Actual RMS Fluctuation	Total Noise Temperature T	Profile Depth	Observ. Time τ (sec)	Treatment of Data
Cas Data A	0.073° 1.4	0.099° 1.9	1060°	180°	1.2×10^5	No correction to data
Cas Data B	0.053° 1.0	0.12° 2.3	1060°	180°	2.1×10^5	Absorption profile of 1.37° peak subtracted from raw data
Taurus Data A	0.044° 2.2	0.04° 2.0	850°	60°	2.2×10^5	Small slope correction of 0.12°/10 kc
Taurus Data B	0.08° 4.0	0.05° 2.5	1330°	60°	1.6×10^5	Absorption profile of 1.15° peak subtracted from raw data

*$\Delta T = 2.1\,T/\sqrt{B\tau}$, where T = Antenna + Receiver Noise Temperature, $B = 7.5 \times 10^3$, and τ is the Observation Time. (The quantity below ΔT is the magnetic field in units of 10^{-6} gauss which will give a peak signal = ΔT.)

$\Delta T'$ = RMS value of data, with the mean taken over frequency.

2. Of course, it was necessary to change the receiver front-end and first local oscillator. An electron-beam, traveling-wave, parametric amplifier was used for all observations except for those of Taurus, data B, for which a crystal mixer was used. The single-channel noise temperature, including switch and stub losses, was 600° for the parametric amplifier, and 1080° for the crystal mixer.

3. The filter and phase-shift networks (items 20, 18, and 17 in the block diagram of Fig. 13) were changed so that the receiver bandwidth was doubled. The 1-db bandwidth became 50 kc, and the 20-db bandwidth became 75 kc. The correlator clock frequency was changed so that the sampling frequency became 150 kc. The frequency resolution, Δf, is therefore 7.5 kc.

The observational procedure consisted, first, of making a 10-minute observation of the absorption profile, with the use of the right-hand circular polarization feed. Typical results are the top curves in Figs. 32 and 33. A loss in sensitivity, or a frequency error, could be found in this manner. After this run, a 5-hour run was made for measuring the difference profile. The local oscillator was reset every half hour to correct for Doppler shift resulting from the earth's motion. One or two 5-hour runs were made on Cas A and Taurus A each day for approximately 35 days.

8.3 RESULTS AND CONCLUSION

A difficulty that arises in performing the Zeeman experiment is due to small differences in gain between the right-hand and left-hand circular polarization feeds. If the gain of one feed is $1 + \alpha$ times the gain of the other feed, then the difference profile, $\Delta T(f)$, will contain a term $\alpha \cdot T(f)$; the absorption profile will appear in the data. Since the absorption profile is known, it may be removed from the difference profile. Care must be taken, however, to see that the correction is not shifted in frequency, for this would cause a false Zeeman effect. If an unbalance signal, $\alpha \cdot T(f)$, is corrected by subtraction of a profile, $\alpha \cdot T(f+\delta f)$, then the result is the same as would be found for a Zeeman splitting of value $\alpha \cdot \delta f$.

Approximately 20 per cent of the data that were taken showed values of α less than 0.003 (data A); 40 per cent had α between 0.003 and 0.03 (data B); and the rest had α greater than 0.03 and were not used. The variations in α are probably due to temperature effects on the feed, stubs, and switch, and to tracking errors and flexure of the telescope. The largest error in the local oscillators was less than 100 cps; thus, even with $\alpha = 0.03$, the largest spurious Zeeman effect would be 3 cps, or $\sim 10^{-6}$ gauss.

The averages of the data A and data B runs for Cas A and Taurus A are plotted in Figs. 32 and 33. The data A runs require no correction for feed unbalance, while the data B runs have been corrected as indicated in Table VIII. Our conclusion is that the line-of-sight component of the magnetic field is less than 3×10^{-6} gauss for Cas A, and less than 5×10^{-6} for Taurus A. This result includes the important assumption that the line-of-sight component of the magnetic field is constant within the absorbing hydrogen gas.

APPENDIX A

EQUIVALENCE OF THE FILTER METHOD AND THE AUTOCORRELATION METHOD OF SPECTRAL ANALYSIS

Two methods of measuring the power spectrum are presented in Fig. 2, the filter method having output $P'_F(i\delta f)$, and the autocorrelation method having output $P'_A(i\delta f)$. Each of these outputs is a set of N numbers (i=0, N-1) which estimate the power spectrum at N frequencies spaced δf apart. It will be shown here that the two methods are equivalent if the filter impulse responses, $h_i(t)$, are related to the autocorrelation weighting function, $w(\tau)$, in a certain manner. The equivalence of the two systems simply means that for any common input, x(t), the outputs are equal, $P'_F(i\delta f) = P'_A(i\delta f)$.

The input-output relations of the two systems are,

$$P'_A(i\delta f) = 2\Delta\tau\, w(0)\frac{1}{T}\int_0^T x^2(t)\,dt + 4\Delta\tau \sum_{n=1}^{N-1} w(n\Delta\tau)\cos(2\pi\, i\delta f\, n\Delta\tau)$$

$$\cdot \frac{1}{T}\int_0^T x(t)\,x(t+n\Delta\tau)\,dt \qquad (A.1)$$

$$P'_F(i\delta f) = \frac{1}{T}\int_0^T \left[\int_0^T x(t)\,h_i(\lambda-t)\,dt\right]^2 d\lambda. \qquad (A.2)$$

We shall manipulate Eq. A.2 so that it takes the form of Eq. A.1. In order to do so, we must make approximations that are quite valid, provided that the observation time, T, is much greater than the filter time constants. In other words,

$$T \gg \tau_m, \qquad (A.3)$$

where $h_i(\tau) = 0$ for $\tau \gtrsim \tau_m$. This condition is necessary in practice in order to give a meaningful spectral estimate.

After expanding the square of the integral in Eq. A.2 and interchanging the order of integration, we obtain

$$P'_F(i\delta f) = \frac{1}{T}\int_0^T \int_0^T x(t)\,x(s) \int_0^T h_i(\lambda-t)\cdot h_i(\lambda-s)\,d\lambda\,ds\,dt. \qquad (A.4)$$

A change of variable, $\tau = s-t$, gives

$$P'_F(i\delta f) = \frac{1}{T}\int_0^T \int_{-t}^{T-t} x(t)\,x(t+\tau) \int_0^T h_i(\lambda-t)\cdot h_i(\lambda-t-\tau)\,d\lambda\,d\tau\,dt. \qquad (A.5)$$

If the condition of Eq. A.3 is used, the integral on λ can be very closely approximated by

$$g_i(\tau) = \int_0^\infty h_i(\lambda)\, h_i(\lambda-\tau)\, d\lambda \tag{A.6}$$

to give

$$P'_F(i\delta f) = \frac{1}{T} \int_0^T \int_{-t}^{T-t} x(t)\, x(t+\tau)\, g_i(\tau)\, d\tau\, dt. \tag{A.7}$$

Upon examination of Eqs. A.1 and A.7 we notice that they will be similar if we require

$$g_i(\tau) = 2\Delta\tau \sum_{n=-(N-1)}^{N-1} w(n\Delta\tau) \cos(2\pi\, i\delta f\, n\Delta\tau)\, \delta(\tau-n\Delta\tau). \tag{A.8}$$

If Eq. A.8 is substituted in Eq. A.7, the integral on τ becomes

$$\int_{-t}^{T-t} x(t+\tau)\, \delta(\tau-n\Delta\tau)\, d\tau = x(t+n\Delta\tau). \tag{A.9}$$

An approximation based on condition (A.3) has again been used in Eq. A.9; the argument of the impulse function will be between the limits of integration for the range of interest, $-(N-1)\,\Delta\tau < n\Delta\tau < (N-1)\,\Delta\tau$, if (A.3) is valid.

The result, then, of the substitution of Eq. A.8 in Eq. A.7 is

$$P'_F(i\delta f) = P'_A(i\delta f) \tag{A.10}$$

which is what we wished to prove.

The equality required by Eq. A.8 can be more easily understood if Fourier transforms are taken of both sides of the equation. The quantity $g_i(\tau)$ is the autocorrelation of the filter impulse response, $h_i(t)$; its Fourier transform is simply the power transfer function of the filter, $G_i(f)$. The Fourier transform of the right-hand side of Eq. A.8 can be expressed in terms of the Fourier transform, $W(f)$, of the autocorrelation weighting function, $w(\tau)$. We obtain, then,

$$G_i(f) = \sum_{k=-\infty}^{\infty} \left[W(f-i\delta f-kf_s) + W(f+i\delta f+kf_s)\right]. \tag{A.11}$$

This result is illustrated in Fig. 3. $G_i(f)$ consists of narrow lobes centered at $\pm i\delta f$, $f_s \pm i\delta f$, $2f_s \pm i\delta f$, ... If the true power spectrum is zero for $|f| > f_s/2$ (in practice we shall force this to be the case), then only the lobes of $G_i(f)$ at $\pm i\delta f$ are of any importance, and an equivalent filter bandpass is given by

$$G_i(f) = W(f-i\delta f) + W(f+i\delta f). \tag{A.12}$$

Finally, if we only consider positive frequencies that are not close to dc (see Fig. 3), then,

$$G_i(f) = W(f-i\delta f). \tag{A.13}$$

APPENDIX B

THE E1B METHOD OF AUTOCORRELATION FUNCTION MEASUREMENT

The material presented here is based on papers by Veltmann and Kwackernaak,[9] and Jespers, Chu, and Fettweis.[10] The first paper is in German and not readily available. The second paper was presented at a conference in Belgium, and only the conference abstracts are available. For these reasons, and in view of the importance of these papers to spectral measurements, a summary of the results is given here. See Table I for a comparison of the method presented in this section with that (A1B) of most of this report.

Suppose we wish to measure the crosscorrelation functions of $x_1(t)$ and $x_2(t)$, stationary, ergodic, random signals bounded by $\pm A_1$ and $\pm A_2$, respectively. [For autocorrelation, $x_1(t) = x_2(t)$.] Two auxiliary functions, $z_1(t)$ and $z_2(t)$, having uniform probability density of $1/(2A_1)$ and $1/(2A_2)$ between $\pm A_1$ and $\pm A_2$, respectively, must be introduced. These auxiliary functions must be stationary, ergodic, and statistically independent of each other, $x_1(t)$ and $x_2(t)$; that is, the joint probability density function factors are

$$p(x_1, x_2, z_1, z_2) = p(x_1, x_2)\, p(z_1)\, p(z_2) \tag{B.1}$$

$$= \begin{cases} \dfrac{p(x_1, x_2)}{2A_1 \cdot 2A_2} & \begin{matrix} |z_1| < A_1 \\ |z_2| < A_2 \end{matrix} \\ 0 & \begin{matrix} |z_1| > A_1 \\ |z_2| > A_2 \end{matrix} \end{cases} \tag{B.2}$$

for all arguments of x_1, x_2, z_1, and z_2.

The auxiliary functions are used as variable clipping levels for $x_1(t)$ and $x_2(t)$. The outputs of these "variable clippers" are $y_1(t)$ and $y_2(t)$, where

$$\begin{aligned} y_1(t) &= 1 \qquad \text{when } x_1(t) > z_1(t) \\ y_1(t) &= -1 \qquad \text{when } x_1(t) < z_1(t) \end{aligned} \tag{B.3}$$

with identical equations for y_2, x_2, and z_2.

Since $y_1(t)$ and $y_2(t)$ are either one of two values, their crosscorrelation functions are easily calculated with a one-bit digital correlator which computes

$$\rho'_y(n\Delta\tau) = \frac{1}{K} \sum_{k=1}^{K} y_1(k\Delta t)\, y_2(k\Delta t + n\Delta\tau) \tag{B.4}$$

for n = 0 to N-1. An estimate, $R'_{12}(n\Delta\tau)$, of a point on the true crosscorrelation

function, $R_{12}(\tau)$, is then given as

$$R'_{12}(n\Delta\tau) = A_1 A_2 \rho'_y(n\Delta\tau). \tag{B. 5}$$

We shall now prove that $R'_{12}(n\Delta\tau)$ is an unbiased estimate of a point on the true crosscorrelation function, that is,

$$\overline{R'_{12}(n\Delta\tau)} = R_{12}(n\Delta\tau). \tag{B. 6}$$

Thus, a method is provided for estimating the crosscorrelation or autocorrelation functions of bounded signals through the use of a one-bit digital correlator.

The proof follows from simple manipulations of probability density functions. For convenience, we set $y_1(k\Delta t) = y_1$, $y_2(k\Delta t+n\Delta\tau) = y_2$, and do likewise for $x_1(k\Delta t)$, $x_2(k\Delta t+n\Delta\tau)$, $z_1(k\Delta t)$, and $z_2(k\Delta t+n\Delta\tau)$. Equation B. 4 can be substituted in Eq. B. 5 which, in turn, is substituted in Eq. B. 6 to give

$$\overline{R'_{12}(n\Delta\tau)} = A_1 A_2 \overline{y_1 y_2}, \tag{B. 7}$$

where the stationariness of $y_1(k\Delta t)$ and $y_2(k\Delta t+n\Delta\tau)$ has been used.

The product, $y_1 y_2$, is either +1 or -1, and thus $\overline{y_1 y_2}$ can be written

$$\overline{y_1 y_2} = (1)\, P[y_1 y_2 = 1] + (-1)\, P[y_1 y_2 = -1] \tag{B. 8}$$

$$= 2P[y_1 y_2 = 1] - 1 \tag{B. 9}$$

$$= 2P[y_1 = 1, y_2 = 1] + 2P[y_1 = -1, y_2 = -1] - 1 \tag{B. 10}$$

$$= 2P[z_1 < x_1, z_2 < x_2] + 2P[z_1 > x_1, z_2 > x_2] - 1 \tag{B. 11}$$

($P[y_1 y_2 = 1]$ means "probability $y_1 y_2 = 1$"). The term $P[z_1 < x_1, z_2 < x_2]$ can be written as an integral over the joint probability density function $p(x_1, x_2, z_1, z_2)$.

$$P[z_1 < x_1, z_2 < x_2] = \int_{-\infty}^{\infty} \int_{-\infty}^{\infty} \int_{-\infty}^{x_1} \int_{-\infty}^{x_2} p(x_1, x_2, z_1, z_2)\, dz_1 dz_2 dx_1 dx_2. \tag{B. 12}$$

Substitution of Eq. B. 2 in Eq. B. 12 and the use of the boundedness of x_1 and x_2 yields

$$P[z_1 < x_1, z_2 < x_2] = \frac{1}{4A_1 A_2} \int_{-A_1}^{A_1} \int_{-A_2}^{A_2} \int_{-A_1}^{x_1} \int_{-A_2}^{x_2} p(x_1, x_2)\, dz_1 dz_2 dx_1 dx_2 \tag{B. 13}$$

$$= \frac{1}{4A_1 A_2} \int_{-A_1}^{A_1} \int_{-A_2}^{A_2} (x_1+A_1)(x_2+A_2) \cdot p(x_1, x_2)\, dx_1 dx_2 \tag{B. 14}$$

$$= \frac{1}{4A_1 A_2} [\overline{x_1 x_2} + \overline{x_1} A_2 + \overline{x_2} A_1 + A_1 A_2]. \tag{B. 15}$$

A similar manipulation of $p[z_1>x_1, z_2>x_2]$ gives

$$P[z_1>x_1, z_2>x_2] = \frac{1}{4A_1A_2}[\overline{x_1x_2}-\overline{x}_1A_2-\overline{x}_2A_1+A_1A_2]. \tag{B. 16}$$

Equations B. 15 and B. 16 can be substituted in Eqs. B. 11 and B. 7 to give the desired result,

$$\overline{R'_{12}(n\Delta\tau)} = \overline{x_1x_2} \tag{B. 17}$$

$$= \overline{R_{12}(n\Delta\tau)}. \tag{B. 18}$$

APPENDIX C

CALCULATION OF THE COVARIANCES OF MANY-BIT ESTIMATES OF THE AUTOCORRELATION FUNCTION AND POWER SPECTRUM

The covariances $\sigma^2_{Pm}(f_1, f_2)$ and $\sigma^2_{Rm}(n, m)$, defined in section 2.3a, are calculated here. The results have been discussed in section 2.3b.

Calculation of $\sigma^2_{Rm}(n, m)$ proceeds by substituting the definition of $R''(n\Delta\tau)$ (Eq. 34) in Eq. 53 to give

$$\sigma^2_{Rm}(n, m) = \frac{1}{K^2} \sum_{k=1}^{K} \sum_{g=1}^{K} \overline{x(k\Delta t)\, x(k\Delta t + |n|\Delta\tau)\, x(g\Delta t)} \cdot \overline{x(g\Delta t + |m|\Delta\tau)} - R(n\Delta\tau)\, R(m\Delta\tau). \tag{C.1}$$

Fortunately, for a Gaussian random process, the joint fourth moment of the process can be expressed in terms of products of autocorrelation functions (see Davenport and Root[42]):

$$\begin{aligned}\overline{x(k\Delta t)\, x(k\Delta t + |n|\Delta\tau)\, x(g\Delta t)\, x(g\Delta t + |m|\Delta\tau)} &= R(n\Delta\tau)\, R(m\Delta\tau) \\ &+ R(i\Delta t + |n|\Delta\tau - |m|\Delta\tau)\, R(i\Delta t) \\ &+ R(i\Delta t + |n|\Delta\tau)\, R(i\Delta t - |m|\Delta\tau).\end{aligned} \tag{C.2}$$

Here, we have set $i = k - g$.

Substitution of Eq. C.2 in Eq. C.1 gives

$$\begin{aligned}\sigma^2_{Rm}(n, m) = \frac{1}{K^2} \sum_{i=-K}^{K} (K - |i|)[&R(i\Delta t + |n|\Delta\tau - |m|\Delta\tau)\, R(i\Delta t) \\ &+ R(i\Delta t + |n|\Delta\tau)\, R(i\Delta t - |m|\Delta\tau)].\end{aligned} \tag{C.3}$$

Here, a change of variable (i=k-g) has eliminated one summation. Thus we have found the autocorrelation covariance in terms of the autocorrelation function.

Equation C.3 can be simplified if it is assumed that $R(i\Delta t) = 0$ for $i > i_{max}$, where $i_{max} \ll K$. This will be true in the practical case of interest, and we obtain

$$\begin{aligned}\sigma^2_{Rm}(n, m) = \frac{1}{K} \sum_{i=-K}^{K} [&R(i\Delta t + |n|\Delta\tau - |m|\Delta\tau)\, R(i\Delta t) \\ &+ R(i\Delta t + |n|\Delta\tau)\, R(i\Delta t - |m|\Delta\tau)].\end{aligned} \tag{C.4}$$

Equation C.4 will be used to calculate the spectral variance. For this purpose, it is convenient to express $\sigma^2_{Rm}(n, m)$ in terms of $P(f)$ instead of $R(\tau)$. This is done by substituting the inverse transform relation (Eq. 14) in Eq. C.4. The result is

$$\sigma^2_{Rm}(n, m) = \frac{1}{4K} \sum_{i=-K}^{K} \int_{-\infty}^{\infty} \int_{-\infty}^{\infty} P(f)\ P(a)\ e^{j2\pi(f+a)\, i\Delta t}$$

$$\cdot\, e^{j2\pi f n\Delta\tau} \cdot \left[e^{-j2\pi f m\Delta\tau} + e^{-j2\pi a m\Delta\tau}\right] df da. \qquad (C.5)$$

The summation on i can be expressed in closed form as (see Reference Data for Radio Engineers[43])

$$\sum_{i=-K}^{K} e^{j2\pi(f+a)\, i\Delta t} = \frac{\sin\left[\pi(f+a)(2K+1)\Delta t\right]}{\sin\left[\pi(f+a)\Delta t\right]} \qquad (C.6)$$

$$\approx \frac{1}{\Delta t} \sum_{k=-\infty}^{\infty} \delta(f+a-kf_t), \qquad (C.7)$$

where $f_t = 1/\Delta t$. The approximation is valid for the purpose of carrying out the integration on a in Eq. C.5, since the other terms in Eq. C.5 can be considered constant over regions of width $1/K\Delta t$. The result of this operation is

$$\sigma^2_{Rm}(n, m) = \frac{1}{4K\Delta t} \sum_{k=-\infty}^{\infty} \int_{-\infty}^{\infty} P(f)\ P(kf_t - f)\ e^{j2\pi f|n|\Delta\tau}$$

$$\cdot \left[e^{-j2\pi f|m|\Delta\tau} + e^{-j2\pi(kf_t - f)|m|\Delta\tau}\right] df. \qquad (C.8)$$

The spectral covariance, $\sigma^2_{Pm}(f_1, f_2)$, is given in terms of $\sigma^2_{Pm}(n, m)$ by Eq. 54. Before making this substitution, a great deal of complexity can be avoided by making an assumption that removes the absolute-value signs in Eq. C.8. The absolute-value signs arose in the definition of $R''(n\Delta\tau)$ in Eq. 34. They can be removed if $|n|$ can be replaced by $-n$ in Eq. 34 without a change; that is, we must show that

$$R''(n\Delta\tau) = \frac{1}{K} \sum_{k=1}^{K} x(k\Delta t)\, x(k\Delta t - n\Delta\tau). \qquad (C.9)$$

This can be done if we assume $\Delta\tau = h\Delta t$, where h is an integer, and $K \gg nh$. This assumption applies in the practical case of interest (the correlator is more complex if h is not an integer and the statistical uncertainty is large if K is not much greater than nh), and the substitution $k' = k - nh$ leads to the proof.

Equation C.8 (with absolute-value signs removed) can now be substituted in Eq. 54 along with the following Fourier transform relations for $w(n\Delta\tau)\, w(m\Delta\tau)$:

$$w(n\Delta\tau)\, w(m\Delta\tau) = \int_{-\infty}^{\infty} \int_{-\infty}^{\infty} W(\beta)\, W(\gamma) \cdot e^{j2\pi\Delta\tau(n\beta+m\gamma)}\, d\beta d\gamma. \qquad (C.10)$$

The resulting expression for $\sigma^2_{Pm}(f_1, f_2)$ is rather long, as it involves three summations (indices: k, n, and m) and three integrations (variables: f, β, and γ). However, two of the summations (n and m) can be expressed in terms of sums of impulses (new indices: μ and ν); this operation allows the integrations on β and γ to be performed. The result of these operations is

$$\sigma^2_{Pm}(f_1, f_2) = \frac{1}{K\Delta t} \sum_{k=-\infty}^{\infty} \sum_{\mu=-\infty}^{\infty} \sum_{\nu=-\infty}^{\infty} \int_{-\infty}^{\infty} P(f)\, P(kf_t - f)$$

$$\cdot\, W(f+f_1-\mu f_s)\, [W(f-f_2+\nu f_s) + W(f+f_2-\nu f_s-kf_t)]\, df. \qquad (C.11)$$

In order to obtain minimum variance, f_t should be chosen high enough so that

$$P(f) = 0 \qquad \text{for } |f| > f_t/2. \qquad (C.12)$$

In this case, only the k=0 term is nonzero in the summation on k in Eq. C.11. The μ and ν summations can be reduced similarly if f_s is chosen large enough to avoid the spurious responses that are due to sampling of the autocorrelation function. The exact requirement is that f_s be chosen large enough so that

$$\int_{-\infty}^{\infty} P^2(f)\, W(f+a)\, W(f+b)\, df = 0 \qquad \text{for } |a| \text{ and } |b| > f_s/2. \qquad (C.13)$$

If the requirements of Eqs. C.12 and C.13 are met, and we consider only $|f_1|$ and $|f_2| < f_s/2$, then Eq. C.11 can be simplified.

$$\sigma^2_{Pm}(f_1, f_2) = \frac{1}{K\Delta t} \int_{-\infty}^{\infty} P^2(f)\, W(f+f_1)\, [W(f+f_2) + W(f-f_2)]\, df. \qquad (C.14)$$

In practice, f_t and f_s should both be chosen equal to 2B, which is twice the highest frequency of a component in the power spectrum. This choice gives minimum variance and no spurious responses arise from sampling. In this case conditions (C.12) and (C.13) are approximately obeyed and Eq. C.14 gives an accurate description of the spectral variance.

APPENDIX D

COMPUTER PROGRAMS

Some of the computer programs developed for this work are given here. The programs may be helpful to a reader concerned with some specific detail of the Zeeman, deuterium-line or computer-simulation experiments, and may also be of some aid to people who wish to write similar programs in the future. The programs are written in the Fortran language for use with the IBM 1620 computer.

D.1 DOPPLER CALCULATION PROGRAM

The frequency of a spectral line received from galactic sources is Doppler shifted from the rest frequency of the line because of the following motions:

1) Rotation of the earth about its axis.

2) The orbital motion of the earth around the sun.

3) The motion of the sun with respect to a group of nearer stars which form a velocity reference point called the local standard of rest.

4) The motion of the sources of the spectral line with respect to the local standard of rest.

The program presented below calculates the line-of-sight component of the first three of these velocities. The line-of-sight component of the fourth velocity is specified as data (VLSR) to the program which then gives the observed frequency, F, for a given rest frequency, FO. The calculation method is that given by MacRae and Westerhout.[41] For convenience in setting local oscillators, the program will calculate two linear functions of F. These are, F1 = F · Y1 + Z1 and F2 = F · Y2 + Z2, where Y1, Z1, Y2, and Z2 are constants that are specified as data to the program. The following additional data must also be supplied to the program:

1) The right ascension (RA HR, RA MIN, RA SEC) and declination (D DEG, D MIN) of the observed direction.

2) The date in units of sidereal days from November 5, 1961. The program will then calculate the number of mean solar days from November 5, 1961, and will specify the Eastern Standard Time when the source is at transit (right ascension equals sidereal time). The frequency correction will then be calculated for hour angles of -6 to +6 in increments of HT hours, where HT is supplied as data.

3) The program assumes that the observation point is Green Bank, West Virginia. If a different observation point is used, the correct latitude must be used in the statement specifying CAT, and the correct relation between local time and sidereal time must be used in the statement specifying EST1.

A sample of the Doppler Calculation program follows.

```
C  DOPPLER CALCULATION PROGRAM

      CL=2.998E+5
      CAT= 3.1415926*(36.+26./60.+11./3600.)/180.
      C1=(23.+56./60.+4.099/3600.)/24.
      C2=(21.+40./60.+32.5/3600.)/24.
      C3=3.1415926*(280.+6./60.+33.9/3600.)/180.
      E=.0167268
      P=3.1415926*(282.+15./60.+5./3600.)/180.
    5 READ 100, RAHR, RAMIN, RASEC, DDEG, DMIN
      PRINT 105, RAHR, RAMIN, RASEC, DDEG, DMIN
      READ 101, F0, VLSR, T, HT, Y1, Z1, Y2, Z2, F01
      PRINT 106, F0, VLSR, T, HT, Y1, Z1, Y2, Z2, F01
      KT=6./HT
      K1=KT+1
      K2=2*KT+1
      RA1=(RAHR+RAMIN/60. +RASEC/3600.)/24.
      RA=2.*3.1415926*RA1
      DEC=3.1415926*(DDEG/180.+DMIN/10800.)
      CC=COSF(DEC)*COSF(RA)
      CS=COSF(DEC)*SINF(RA)
      S=SINF(DEC)
      PRINT 107, CC, CS, S
      PAUSE
    1 RAT=T+RA1
      EST1=19./24.+C1*(RAT-C2)
      ND=EST1
      D=ND
      NH=(EST1-D)*24.
      H=NH
      NM=(EST1-D-H/24.)*1440.
      DM=NM
      NS=(EST1-D-H/24.-DM/1440.)*86400.
      PRINT 102, ND, NH, NM, NS
      PRINT 108, RAHR, RAMIN, RASEC
      PRINT, DDEG, DMIN
      PRINT, F0, VLSR
      PRINT,
      PRINT,
      DO 4 K=1,K2
      XK=K-K1
      XK=HT*XK
      EST2=C1*(T+RA1+XK/24.-C2)
      XL=(2.*3.1415926/365.2564)*(EST2+1405.)+C3
      XLAM=XL+2.*E*SINF(XL-P)+1.25*E*E*SINF(2.*(XL-P))
      A=-29.804*SINF(XLAM)+.319
      B=27.344*COSF(XLAM)+17.417
      C=11.858*COSF(XLAM)-9.958
      V=A*CC+B*CS+C*S
      VE=+.465*COSF(CAT)*COSF(DEC)*SINF(3.14159*XK/12.)
      V1=V+VLSR+VE
      DELF=-(F0/CL)*V1
      F=F01+DELF
      F1=Y1*F+Z1
```

```
C  DOPPLER CALCULATION PROGRAM CONTINUED

      F2=Y2*F+Z2
      IF (SENSE SWITCH 1) 2,3
    2 PRINT 103, XK, F1, V1, VE, V
      GO TO 4
    3 PRINT 104, XK, F1, F2
    4 CONTINUE
      PRINT,
      PRINT,
      IF (SENSE SWITCH 2) 5,6
    6 T=T+1.
      GO TO 1
      END


C DATA CARDS

C NEXT TWO CARDS FOR CAS A
23.  21.  38.  58.  35.2
1420405.73  -.8  33.  .5  1.  1400000.  .1  0.  20405.73
C  NEXT TWO CARDS FOR TAURUS A
5.  32.  6.  22.  00.1
1420405.73  10.1  25.  .5  1.  1400000.  .1  0.  20405.73
C  NEXT TWO CARDS FOR SAG A
17.  43.  22.  -28.  57.2
1420405.73  6.  27.  .5  1.  1400000.  .1  0.  20405.73
```

TOTAL

D.2 DEUTERIUM AND ZEEMAN DATA ANALYSIS PROGRAM

The program that is now to be described takes in as data the output of the one-bit digital correlator and produces the spectral estimate, c(f), which was described in section 6.5a. The program is broken up into five steps.

1. The cos weighting function described in section 2.2b is generated.

2. The computer reads in the digital correlator output on punch cards. The correlator output consists of 21 numbers that have accumulated in a combination of binary and decimal counters. After read-in, these numbers are converted to the computer's binary-coded-decimal number system.

3. The correlator output is normalized according to Eq. 153 when the radiometer is operated in the switched mode of operation (MODE = 2 in the program), or according to Eq. 154 when operated in the unswitched mode of operation (MODE = 1 in the program). The switched mode of operation was used for the actual data, while the unswitched mode was used to determine the receiver bandpass function, $p'_o(f)$. The autocorrelation function correction (for the effect of clipping) is programmed according to Eq. 148 for the switched mode and Eq. 115 for the unswitched mode.

4. The sampled-data Fourier transform is performed as indicated by Eq. 129.

5. The resulting difference spectrum, $\delta p'(f)$, is divided by the receiver bandpass function, $p'_o(f)$ [SBP(I) in the program], to give the normalized spectral estimate, s(f). The slope of this spectrum is adjusted to be zero as was discussed in section 6.5a. The final output spectrum is then typed out and punched on cards.

A sample of the Deuterium and Zeeman Data Analysis program follows.

```
C DEUTERIUM - ZEEMAN DATA ANALYSIS PROGRAM

C  SENSE SWITCH 1 ON FOR PUNCH OUTPUT
C  SENSE SWITCH 2 ON FOR PRINT OUTPUT
DIMENSION W(21),A(21),B(21),RBP(21),R(21),S(38),SBP(38),D(21)

C  GENERATION OF WEIGHTING FUNCTION,W(K)

DO 1 K=1,21
FLO=K-1
1 W(K)=.5+.5*COSF(3.14159265*FLO/21.)

C  DATA INPUT AND OCTAL - FRACTION CONVERSION.

5 READ,NRUN,MODE,SIGN
DO 6 K=1,21
6 READ,A(K),B(K)
PUNCH,NRUN,MODE,A(1),SIGN
PRINT,NRUN,MODE,A(1),SIGN
PRINT,
7 DO 14 K=1,21
OC1=0.
OC2=0.
OC3=0.
8 IF(B(K)-100.)10,9,9
```

```
9 OC1=OC1+1.
B(K)=B(K)-100.
GO TO 8
10 IF(B(K)-10.)12,11,11
11 OC2=OC2+1.
B(K)=B(K)-10.
GO TO 10
12 IF(B(K)-1.)14,13,13
13 OC3=OC3+1.
B(K)=B(K)-1.
GO TO 12
14 D(K)=OC1/8.+OC2/64.+OC3/512.+A(K)

C  NORMALIZATION AND CORRECTION

C=1.5707963
IF(MODE-1)15,15,17
C  MODE 1
15 DO 16 K=1,21
RBP(K)=(2.*D(K)-D(1))/D(1)
16 R(K)=SINF(C*RBP(K))
GO TO 19
C  MODE 2
17 D1=D(1)
DO 18 K=1,21
18 R(K)=2.*SINF(C*(D(K)-D1)/D1)*COSF(C*RBP(K))*SIGN
19 IF(SENSE SWITCH 2) 20,220
20 DO 21 K=1,21,3
21 PRINT,R(K),R(K+1),R(K+2)
PRINT,
```



```
C DEUTERIUM - ZEEMAN DATA ANALYSIS PROGRAM CONTINUED

220 IF (SENSE SWITCH 1) 22,24
22 DO 23 K=1,21,3
23 PUNCH,R(K),R(K+1),R(K+2)

C  FOURIER TRANSFORM  S I  OF W K R K

24 T=1./75.
      DF=1.0
AA=2.*T
BB=6.2831853*T*DF
DO 25 K=1,21
25 R(K)=R(K)*W(K)
CC=R(1)*T
J=0
      DO 30 I=1,38
S(I)=CC
DO 26 K=2,21
DD=(K-1)*(I-1)
26 S(I)=S(I)+AA*R(K)*COSF(BB*DD)
S1=10000.*S(I)
IF (SENSE SWITCH 2) 28,290
   28 PRINT,J,S1
```

```
290 IF (SENSE SWITCH 1) 29,30
   29 PUNCH,J,S1
PRINT,

C FINISHING OPERATIONS

IF(MODE-1)31,31,33
C MODE 1
   31 DO 32 I=1,38
32 SBP(I)=S(I)
GO TO 5
C MODE 2
   33 J=0
      DO 39 I=1,38
34 S(I)=100.*S(I)/SBP(I)
IF (SENSE SWITCH 2) 36,380
   36 PRINT,J,S(I)
380 IF (SENSE SWITCH 1) 38,39
   38 PUNCH,J,S(I)
39 J=J+1
PRINT,
IF (SENSE SWITCH 3) 141,140
141 READ,C1,C2
B1=C1/60.
A1=C2-34.*B1
PRINT,C1,C2
GO TO 142
  140 U=0
V=0.
W1=0.
```

```
C DEUTERIUM - ZEEMAN DATA ANALYSIS PROGRAM CONTINUED
      X=0.
      Y=0.
      Z=0.
            DO 35 I=6,31
      G=I
      U=U+S(I)
      V=V+G*S(I)
      W1=W1+1.
      X=X+G
      Y=Y+G*G
   35 Z=Z+S(I)*S(I)
      D1=W1*Y-X*X
      A1=(U*Y-X*V)/D1
      B1=(V*W1-X*U)/D1
      RMS1=SQRF(Z/W1)
      H=Z-A1*A1*W1-B1*B1*Y-2.*A1*B1*X
      RMS2=SQRF(H/W1)
      C1=60.*B1
      C2=A1+34.*B1
   40 IF (SENSE SWITCH 2) 41,420
   41 PRINT,RMS1,RMS2,C1,C2
      PRINT,
  420 IF (SENSE SWITCH 1) 42,142
   42 PUNCH,RMS1,RMS2,C1,C2
  142 J=0
   43 DO 48 I=1,38
      G=I
   44 S(I)=S(I)-A1-B1*G
      IF (SENSE SWITCH 2) 45,147
   45 PRINT,J,S(I)
  147 IF (SENSE SWITCH 4) 47,48
   47 PUNCH,J,S(I)
   48 J=J+1
      DO 2 K=1,4
    2 PRINT,
      GO TO 5
      END
```

TOTAL

D.3 COMPUTER SIMULATION PROGRAM

The program listed in this section was used to simulate the signal and the signal-processing system. (See section 6.2.) A block diagram of the program is given in Fig. 20.

The time required to run this program on the IBM 1620 computer was approximately 100 hours; however, this time did not have to be continuous. If Sense Switch 1 was turned on, the computer would punch out cards containing all of the useful results that had been computed up to that time. These cards could then be fed back into the machine at a later time. In this way, the 100 hours computing time was accumulated, for the most part, at night and on week ends.

A sample of the Computer Simulation program follows.

```
C COMPUTER SIMULATION PROGRAM
      DIMENSION H(40),AR(21),AS(38),SW(38,21),ARX(21),VRX(21),ARY(21)
      DIMENSION VRY(21),ASX(38),VSX(38),ASY(38),VSY(38),W(40),X(21)
      DIMENSION Y(21),RX(21),RY(21),SX(38),SY(38)
      IM=40
      NM=21
      LM=38
      KM=21
      DO 9 I=1,IM
    9 READ,H(I)
      DO 11 N=1,NM
   11 READ,AR(N)
      DO 13 L=1,LM
   13 READ,AS(L)
      READ,F,F2,T2
      READ,Z1,Z2,KZ
      IF(F)17,17,28
   17 DO 21 N=1,NM
      ARX(N)=0.
      VRX(N)=0.
      ARY(N)=0.
   21 VRY(N)=0.
      DO 26 L=1,LM
      ASX(L)=0.
      VSX(L)=0.
      ASY(L)=0.
   26 VSY(L)=0.
      GO TO 32
   28 DO 29 N=1,NM
   29 READ,ARX(N),ARY(N),VRX(N),VRY(N)
      DO 31 L=1,LM
   31 READ,ASX(L),ASY(L),VSX(L),VSY(L)
   32 FKZ=KZ
      V=SQRF(3.3326563E7*FKZ)
      U=4999.5*FKZ
      IM1=IM+1
      NM1=NM+1
      PI=3.1415926
      PI1=PI*.5
      PI2=PI/21.
      PI3=2.*PI/75.
      DO 46 L=1,LM
```

```
      DO 45 K=1,KM
      SWK=K-1
      SWLK=(L-1)*(K-1)
   45 SW(L,K)=(.5+.5*COSF(PI2*SWK))*COSF(PI3*SWLK)
   46 CONTINUE
      T1=IM+NM+9
      T3=T2+T1
      A=.33
      B=.59
   49 F=F+1.
      JF=F
      PRINT,JF
```

2

```
C COMPUTER SIMULATION PROGRAM CONTINUED
      DO 53 I=1,IM
   53 W(I)=0.
      DO 58 N=1,NM
      X(N)=0.
      Y(N)=0.
      RX(N)=0.
   58 RY(N)=0.
      T=1.
   60 DO 61 I=2,IM
   61 W(I-1)=W(I)
      DO 64 N=2,NM
      X(N-1)=X(N)
   64 Y(N-1)=Y(N)
      ZT=0.
      DO 74 K=1,KZ
      Z=Z1*Z2
      IF(Z-B)69,70,70
   69 Z=Z+A
   70 Z1=Z2
      Z2=Z
      NZ=Z*1.E8
      Z=NZ
   74 ZT=ZT+Z
      W(IM)=(ZT-U)/V
      X(NM)=0.
      DO 78 I=1,IM
      IM2=IM1-I
   78 X(NM)=X(NM)+H(I)*W(IM2)
      IF(X(NM))83,83,85
   83 Y(NM)=-1.
      GO TO 86
   85 Y(NM)=1.
   86 IF(T-T1)88,80,80
   80 DO 81 N=1,NM
      NM2=NM1-N
      RY(N)=RY(N)+Y(NM)*Y(NM2)
   81 RX(N)=RX(N)+X(NM)*X(NM2)
   88 T=T+1.
      IF (SENSE SWITCH 3) 82,84
   82 JT=T
      PRINT, JT
   84 CONTINUE
      IF(T-T3)60,60,90
```

```
 90 RX1=RX(1)*.0001
    RY1=RY(1)
    DO 98 N=1,NM
    RX(N)=RX(N)/RX1
    ARX(N)=ARX(N)+RX(N)
    VRX(N)=VRX(N)+(RX(N)-AR(N))**2
    RY(N)=SINF(PI1*RY(N)/RY1)*10000.
    ARY(N)=ARY(N)+RY(N)
 98 VRY(N)=VRY(N)+(RY(N)-AR(N))**2
```


C COMPUTER SIMULATION PROGRAM CONTINUED

```
      DO 101 L=1,LM
      SX(L)=0.
 101  SY(L)=0.
      DO 111 L=1,LM
      DO 105 K=2,KM
      SX(L)=SX(L)+RX(K)*SW(L,K)
 105  SY(L)=SY(L)+RY(K)*SW(L,K)
      SX(L)=(10000.+2.*SX(L))/75.
      ASX(L)=ASX(L)+SX(L)
      VSX(L)=VSX(L)+(SX(L)-AS(L))**2
      SY(L)=(10000.+2.*SY(L))/75.
      ASY(L)=ASY(L)+SY(L)
 111  VSY(L)=VSY(L)+(SY(L)-AS(L))**2
      IF(SENSE SWITCH 2)113,120
 113  PRINT,RX1,RY1
      DO 116 N=1,NM
      NTAB=N-1
 116  PRINT,NTAB,RX(N),RY(N)
      DO 119 L=1,LM
      LTAB=L-1
 119  PRINT,LTAB,SX(L),SY(L)
 120  IF(F-F2)121,131,131
 121  IF(SENSE SWITCH 1)122,49
 122  PUNCH,F,F2,T2
      PUNCH,Z1,Z2,KZ
      DO 125 N=1,NM
 125  PUNCH,ARX(N),ARY(N),VRX(N),VRY(N)
      DO 127 L=1,LM
 127  PUNCH,ASX(L),ASY(L),VSX(L),VSY(L)
      PRINT,
      PRINT,F,F2,T2
      GO TO 135
 131  PUNCH,0.,F2,T2
      PUNCH,Z1,Z2,KZ
      PRINT,
      PRINT,0.,F2,T2
 135  PRINT,Z1,Z2,KZ
      PRINT,
      DO 144 N=1,NM
      ARX=ARX(N)/F
      ARY=ARY(N)/F
      VRX=SQRF(VRX(N)/F)
      VRY=SQRF(VRY(N)/F)
      IF(F-F2)143,142,143
 142  PUNCH,ARX,ARY,VRX,VRY
 143  NTAB=N-1
 144  PRINT,NTAB,ARX,ARY,VRX,VRY
      PRINT,
```

```
      DO 153 L=1,LM
      ASX=ASX(L)/F
      ASY=ASY(L)/F
      VSX=SQRF(VSX(L)/F)/AS(L)
```

4

```
C COMPUTER SIMULATION PROGRAM CONTINUED
      VSY=SQRF(VSY(L)/F)/AS(L)
      IF(F-F2)152,151,152
  151 PUNCH,ASX,ASY,VSX,VSY
  152 LTAB=L-1
  153 PRINT,LTAB,ASX,ASY,VSX,VSY
      FVSX=0.
      FVSY=0.
      DO 154 L=11,30
      FVSX=FVSX+.05*SQRF(VSX(L)/F)/AS(L)
  154 FVSY=FVSY+.05*SQRF(VSY(L)/F)/AS(L)
      PRINT,
      PRINT, FVSX, FVSY
      STOP
      END
```

```
C DATA FOR COMPUTER SIMULATION PROGRAM
C H(I) NEXT TEN CARDS
 4.0463063E-02 -.21109917      2.4860613E-07 -.52083049
-.40434399     -.46204016     -.77802933     -5.1404096E-07
-.54630318      .13955609      .17048281     -.99998148
 4.6108997E-07 -3.3561187     -3.2113635     -4.7972268
-11.575174     -1.4725131E-06 -32.110496      61.544267
 61.544267     -32.110496     -1.4725131E-06 -11.575174
-4.7972268     -3.2113635     -3.3561187      4.6108997E-07
-.99998148      .17048281      .13955609     -.54630318
-5.1404096E-07 -.77802933     -.46204016     -.40434399
-.52083049      2.4860613E-07 -.21109917      4.0463063E-02
C AR(N) NEXT TEN CARDS
 10000.000     -.25521402     -3094.1803     -.36289696
-1801.3094     -.72864953     -501.72699     -2.9739641
 210.65958     -5.8054740      242.76102      16.444171
 29.214253      3.8847207     -74.478626     -3.3146357
-50.744705     -10.362919      7.3988346     -8.8327196
 9.0940393      1.6463153      2.5638795      1.1505103
 .29097677      .57754945     -1.1877550E-02  .27485701
 .23565760      .16557374      .29605178      .12468219
 .15563592      8.3742613E-02  2.7678368E-02  3.8857877E-02
-8.7503395E-03  9.2514949E-03 -3.5466145E-03  3.3990395E-04
C AS(L) IN TABLE 6.2
C Z1, Z2, KZ ON NEXT CARD
.75326499 .90037117 5
```

23

TOTAL 23

Acknowledgment

My first thanks must go to Dr. H. I. Ewen who, in 1957, aroused my interest in radio astronomy and suggested the deuterium-line search to me. Dr. Ewen also made a generous contribution to the initial financing of my thesis work.

Also, I would like to thank my supervisor, Professor Jerome B. Wiesner, for encouraging me to undertake this research as a doctoral thesis, being ever so helpful in obtaining technical and financial support, and, through his interest and quality of leadership, being a constant source of inspiration for my work. It is fortunate for me that he was present at the Massachusetts Institute of Technology long enough to fulfill the first two functions, and that his presence was not required for the third.

Many people have given encouragement and helped through technical discussions concerning various aspects of this research work. I would especially like to thank Dr. R. Price of Lincoln Laboratory, M.I.T., Professor Amar G. Bose, Professor Henry J. Zimmermann, and Professor Alan H. Barrett of M.I.T., Professor A. E. Lilley of Harvard College Observatory, and Dr. F. D. Drake, Dr. D. S. Heeschen, and Dr. T. K. Mennon of the National Radio Astronomy Observatory.

I am thankful to the founders and staff of the National Radio Astronomy Observatory for providing the excellent observing facilities and supporting help. My stay at Green Bank, West Virginia, was one of the most pleasant and stimulating periods of my life.

The facilities of the Computation Center, M.I.T., were used for part of this work. I appreciate the programming assistance provided by Mr. D. U. Wilde at M.I.T., and by Mr. R. Uphoff at Green Bank.

References

1. W. B. Davenport and W. L. Root, Random Signals and Noise (McGraw-Hill Book Company, New York, 1958); see especially p. 182.

2. J. S. Bendat, Principles and Applications of Random Noise Theory (John Wiley and Sons, Inc., New York, 1958); see especially Chapter 3.

3. U. Grenander and M. Rosenblatt, Statisical Analysis of Stationary Time Series (John Wiley and Sons, Inc., New York, 1957); see especially p. 129.

3a. Ibid., pp. 153-155.

4. J. T. Tou, Digital and Sampled-Data Control Systems (McGraw-Hill Book Company, New York, 1959); see especially pp. 444-464.

4a. I would like to thank M. J. Levin of Lincoln Laboratory, M.I.T., for pointing out this technique to me.

5. J. H. Van Vleck, The Spectrum of Clipped Noise, Report No. 51, Radio Research Laboratory, Harvard University, July 21, 1943.

6. J. J. Faran and R. Hills, Correlators for Signal Reception, Technical Memo No. 27, Acoustics Research Laboratory, Harvard University, September 1952.

7. J. F. Kaiser and R. K. Angell, New Techniques and Equipment for Correlation Computation, Technical Memo No. 7668-TM-2, Servomechanisms Laboratory, M.I.T., December 1957.

8. C. R. Green, Measurement of Polarity Coincidence Correlation Functions Using Shift Register Elements, U.S. Naval Ordnance Laboratory Report No. 4396, December 17, 1956.

9. B. P. Veltmann and H. Kwakernaak, Theorie und Technik der Polaritats – Korrelation fur die Dynamische Analyse Niederfrequenter Signale und Systeme, Regelungstechnik, Vol. 9, No. 9, pp. 357-364, September 1961.

10. P. Jespers, P. T. Chu, and A. Fettweis, A New Method for Computing Correlation Functions, International Symposium on Information Theory, Brussels, Belgium, September 3-7, 1962.

11. R. B. Blackman and J. W. Tukey, The Measurement of Power Spectra (Dover Publications, Inc., New York, 1958); see especially pp. 95-100.

12. J. D. Kraus, Antennas (McGraw-Hill Book Company, New York, 1950); see especially p. 194.

13. C. L. Dolph, A Current Distribution for Broadside Arrays which Optimizes the Relationship between Beam Width and Side-Lobe Level, Proc. IRE 34, 335-348 (June 1946).

14. Reference Data for Radio Engineers (published by Federal Telephone and Radio, New York, 1956).

15. J. A. McFadden, The Correlation Function of a Sine Wave Plus Noise after Extreme Clipping, IRE Transactions, Vol. IT-2, pp. 66-67, June 1956.

16. H. B. Dwight, Tables of Integrals and Other Mathematical Data (Macmillan Company, New York, 3rd edition, 1957).

17. J. A. McFadden, Two Expansions for the Quadvariate Normal Integral, Biometrika 47, 325-333 (1960).

18. D. E. Norgaard, The Phase-Shift Method of Single-Sideband Signal Reception, Proc. IRE 44, 1735-1743 (December 1956).

19. D. G. C. Luck, Properties of Some Wideband Phase-Splitting Networks, Proc. IRE 37, 147-151 (February 1949).

20. R. S. Burington and D. C. May, Handbook of Probability and Statistics (Handbook Publishers, Sandusky, Ohio, 1953).

21. J. F. Kenney and E. S. Keeping, Mathematics of Statistics (D. C. Van Nostrand Company, Princeton, N.J., 2d edition, 1951).

22. J. Cohen and T. Orhaug, Measurement of Output Characteristics of a Radiometer, Internal Report No. 1, National Radio Astronomy Observatory, Green Bank, West Virginia, June 1962.

23. I. S. Shklovsky, Cosmic Radio Waves (Harvard University Press, Cambridge, Mass., 1960).

24. I. S. Shklovsky, Astr. Zhur. 29, 144 (1952).

25. G. G. Getmanzev, K. S. Stankevitch, and V. S. Troitsky, Detection of Monochromatic Radio Emission of Deuterium from the Center of the Galaxy on a Wavelength of 91.6 mc, Doklady Akad. Nauk S.S.S.R., Vol. 103, pp. 783-786, February 1955.

26. G. J. Stanley and R. Price, An Investigation of Monochromatic Radio Emission of Deuterium from the Galaxy, Nature 177, 1221-1222 (June 30, 1956).

27. R. L. Adgie and J. S. Hey, Intensity of the Radio Line of Galactic Deuterium, Nature 179, 370 (February 1957).

28. R. L. Adgie, An Attempt to Detect the 327 MC/S Line of Galactic Deuterium, Paris Symposium on Radio Astronomy (Stanford Press, Stanford, Calif., 1958); pp. 352-354.

29. L. Heller, Theories of Element Synthesis and the Abundance of Deuterium, Astron. J. 126, 341-355 (September 1957).

30. W. A. Fowler, Nuclear Clues to the Early History of the Solar System, Science, Vol. 135, No. 3508, pp. 1037-1045, March 23, 1962.

31. W. A. Fowler, J. L. Greenstein, and F. Hoyle, Nucleosynthesis during the Early History of the Solar System, Geophys. J. Roy. Astron. Soc., Vol. 6, No. 2, pp. 148-220, 1962.

32. S. Weinreb, The Detection of UHF Radiation from Deuterium in Interstellar Space, S.B. Thesis, Massachusetts Institute of Technology, June 1958.

33. S. Chandrasekhar, Radiative Transfer (Oxford University Press, London, 1950).

34. G. B. Field, Excitation of the Hydrogen 21-cm Line, Proc. IRE 46, 240-250 (March 1952).

35. J. P. Hagen, A. E. Lilley, E. F. McClain, Absorption of 21-cm Radiation by Interstellar Hydrogen, Astrophys. J. 122, 361-375 (November 1958).

36. C. A. Muller, 21 cm Absorption Effects in the Spectra of Two Strong Radio Sources, Astrophys. J. 125, 830-834 (May 1957).

37. B. G. Clark, V. Radhakrishnan, and R. W. Wilson, The Hydrogen Line in Absorption, Report No. 3, California Institute of Technology Radio Observatory, Pasadena, California, 1961.

38. J. A. Galt, C. H. Slater, and W. L. H. Shuter, An Attempt to Detect the Galactic Magnetic Field Using Zeeman Splitting of the Hydrogen Line, Mon. Not. Roy. Astron. Soc., Vol. 120, pp. 187-192, 1962.

39. R. D. Davies, C. H. Slater, W. L. H. Shuter, and P. A. T. Wild, A New Limit to the Galactic Magnetic Field Set by Measurements of the Zeeman Splitting of the Hydrogen Line, Nature 187, 1088-1089 (September 24, 1960).

40. J. G. Bolton and J. P. Wild, On the Possibility of Measuring Interstellar Magnetic Fields by 21-cm Zeeman Splitting, Astrophys. J. 125, 296 (1957).

41. D. A. MacRae and G. Westerhout, Table for the Reduction of Velocities to the Local Standard of Rest (published by the Observatory, Lund, Sweden, 1956).